EFFECT OF Bi INCORPORATION ON THE OPTICAL, ELECTRICAL AND THERMAL PROPERTIES OF *a*-Se-Te AND *a*-Ge-Te GLASSY ALLOYS

by

Ambika

A THESIS SUBMITTED IN FULFILLMENT OF THE REQUIREMENTS
FOR THE DEGREE OF

DOCTOR OF PHILOSOPHY

IN

PHYSICS

JAYPEE UNIVERSITY OF INFORMATION TECHNOLOGY
WAKNAGHAT
JULY 2009

CERTIFICATE

This is to certify that the thesis entitled "**EFFECT OF Bi INCORPORATION ON THE OPTICAL, ELECTRICAL AND THERMAL PROPERTIES OF *a*-Se-Te AND *a*-Ge-Te GLASSY ALLOYS"** which is being submitted by ***Ms. Ambika*** in fulfillment for the award of Degree of **Doctor of Philosophy** in **Physics** by **Jaypee University of Information Technology,** is the record of candidates own work carried out by her under my supervision. This work has not been submitted partially or wholly to any other University or Institute for the award of this or any other degree or diploma.

Date: September 18, 2009

Dr. P B Barman
Supervisor
Department of Physics
JUIT, Waknaghat

Dedicated to my parents……..

Acknowledgements

I would truly like to acknowledge all those people who are collaborated directly or indirectly with my research and made this thesis possible.

First and foremost I am deeply grateful to my supervisor, **Dr. P. B. Barman**, for his continuous guidance, encouragement and wholehearted supervision, throughout the progress of the work. He provided me smooth and rewarding research life with his valuable co-operation, enthusiasm and encouragement.

I extend my warm and sincere thanks to Prof. (Dr.) S. C. Katyal (Head, Department of Physics), Dr. S. K. Khah, Dr. Pankaj Sharma, Dr. Vineet Sharma, Mr. Dheeraj Sharma and Dr. Ishu Sharma (my senior) for consistent support.

I truly thank to JUIT authorities especially **Dr. Y. Medury**, and **Brig. (Retd.) Balbir Singh** for providing me every kind of financial and administrative assistance during entire course.

I would like to express my deep sense of gratitude and indebtedness to my Husband, Parents and primarily my Brother for their complete association and unflagging love during my research work. I would also like to thank my friend Sangeeta Thakur for her support, encouragement and helpful discussions at every moment of my work.

Finally, for the completion of this work, I thank to the almighty **God** for fulfilling my desire to complete this study under **HIS** kind blessings.

Date: September 14, 2009 ***(Ambika)***

Abstract

This thesis work is concerned with the effect of Bi incorporation on the optical, electrical and thermal properties of a-Se-Te and a-Ge-Te chalcogenide (ChG) glassy alloys. Glassy alloys and their thin films prepared and studied are:

I. $Se_{85-x}Te_{15}Bi_x$ (x = 0, 1, 2, 3, 4, 5)

II. $Ge_{20}Te_{80-x}Bi_x$ (x = 0, 1.5, 2.5, 5.0)

Melt quenching technique has been used for the growth of glassy alloys. Thin films of prepared samples were deposited using thermal evaporation technique. X-ray diffraction technique has been used to know the nature (amorphous or crystalline) of bulk and deposited films. The optical properties have been estimated by analyzing the transmission and reflection spectra obtained from ultraviolet-visible-near infrared spectrometer. Swanepoel's method has been used to determine refractive index and extinction coefficient. Optical band gap has been calculated using Tauc extrapolation. The various electrical measurements on the thin films including both the dark and photoconductivity measurements at different temperatures were carried out in a metallic sample holder under a vacuum ~ 10^{-3} mbar throughout the measurements. In order to measure the thermal properties of a-Se-Te-Bi Differential Scanning Calorimetric technique (DSC) has been used whereas in case of a-Ge-Te-Bi system Differential Thermal Analysis (DTA) method has been employed. Some of the physical parameters have also been estimated for both of these series.

The thesis has been divided into six chapters;

General introduction of amorphous semiconductors and their classification is described in chapter I. A brief introduction of general properties of ChG has also been incorporated.

Various models applicable to ChG, their applications, motivation and objective of the thesis have also been included.

Chapter II describes the experimental techniques used for the preparation of glasses, deposition of thin films, characterization of bulk and thin films for X-ray diffraction, optical, electrical and thermal properties.

Chapter III contains experimental observations and general discussion of various parameters related to optical properties of *a*-$Se_{85-x}Te_{15}Bi_x$ and *a*-$Ge_{20}Te_{80-x}Bi_x$ thin films. Optical parameters have been determined from their normal incidence transmission and reflection spectra.

In chapter IV, effect of Bi addition on electrical properties *a*-$Se_{85-x}Te_{15}Bi_x$ and *a*-$Ge_{20}Te_{80-x}Bi_x$ thin films has been studied. The *I-V* characteristics have been discussed qualitatively alongwith dark and photoconductivity measurements as a function of temperature.

Chapter V deals with the thermal properties of both of these series. An estimation of physical parameters like density, molar volume *etc*. of both *a*-Se-Te-Bi and *a*-Ge-Te-Bi glassy alloys have also been included in this chapter.

Finally, chapter VI deals with the summary and overall conclusion of the work.

List of Publications

1. **Ambika Sharma**, P. B. Barman *"Calorimetric and optical study of amorphous* $Se_{85-x}Te_{15}Bi_x$ *glassy alloy*". **Thin Solid Films** 517 (2009) 3020

2. **Ambika Sharma**, P. B. Barman *"Effect of Bi incorporation on glass transition kinetics of* $Se_{85-x}Te_{15}$ *glassy alloy"* **Journal of Thermal Analysis and Calorimetry** 96 (2009) 413

3. **Ambika**, P. B. Barman *"Theoretical prediction of physical parameters of GeTeBi glassy alloy"*. **Journal Ovonic Research** 3 (2007) 21.

4. **Ambika**, P. B. Barman *"Theoretical prediction of physical parameters of GeTeBi glassy alloy (Part II)"* **Journal Ovonic Research** 3 (2007) 44.

5. **Ambika**, P. B. Barman *"Effect of Bi incorporation on defect state density in* $Se_{85-x}Te_{15}Bi_x$ *thin films".* **Physica B** 404 (2009) 1591.

6. **Ambika Sharma**, P.B. Barman *"Transient photoconductivity of a-*$Se_{85-x}Te_{15}Bi_x$ *thin films"* **Asian Journal of chemistry** (accepted) 2009.

7. **Ambika**, P. B. Barman *"Study of physical parameters of a-*$Ge_{20}Te_{80-x}$ Bi_x *glassy system*". **Defects and Diffusion** 293 (2009) 107.

8. **Ambika**, P. B. Barman *"An optical study of vacuum evaporated* $Se_{85-x}Te_{15}Bi_x$ *chalcogenide thin films"* **Physica B** (2009) doi:10.1016/j.physb.2009.06.147

9. **Ambika**, P. B. Barman *"An optical study of vacuum evaporated* $a\text{-}Ge_{20}Te_{80-X}Bi_x$ *chalcogenide thin films"* **Applied Physics B** (accepted) 2009.

Conferences (National/International)

10. **Ambika Sharma,** P. B. Barman, *"Theoretical prediction of physical parameters of GeTeBi glassy alloy"* **ICCMP** Abstract Book (2007) 115.

11. **Ambika Sharma,** P. B. Barman, *"Effect of Bi incorporation on defect state density in* $Se_{85-x}Te_{15}Bi_x$ *thin films".* **ICSAM** Abstract Book (2009).

12. **Ambika Sharma,** P. B. Barman *'Transient photoconductivity of* $a\text{-}Se_{85-x}Te_{15}Bi_x$ *thin films"* AMRP Abstract Book 2009.

13. **Ambika Sharma,** P. B. Barman *"Determination of optical band gap of amorphous* $\boldsymbol{Ge_{20}Te_{80-X}Bi_x}$ *thin films using their transmission and reflection spectra"* ICMOM Abstract Book 2009.

Contents

List of Figures

List of Tables

CHAPTER 1

Introduction

1.1 Introduction

Solids are a particular state of condensed matter characterized by strong interaction between the constituent particles (atoms, molecules). They are considered as materials with viscosities exceeding $10^{14.6}$ Poise. Solids can be found or prepared either in an ordered (crystalline) state or in a disordered (non-crystalline) state. A crystal is a regular three dimensional design and is a consequence of the regular arrangement of atoms, ions or molecules of which it is built up. When this periodicity extends throughout a single piece of material one calls it a single material. A polycrystalline material is composed of tiny crystals. The periodicity of the structure in the polycrystalline materials is interrupted at grain boundaries. The size of grains in which the structure is periodic may vary from macroscopic dimension to a size much larger as compared to the size of the pattern unit. When the size of the grains become comparable to the size of the pattern unit, one can no longer speak of the crystals; one then speaks of non-crystalline, amorphous or vitreous solids.

The amorphous state is the state of a solid that has become disordered. The main feature of the structure of matter in the amorphous state is the absence of long range order. The macro particles have no regular and definite arrangement of atoms and lack the distinct structure with definite symmetry elements inherent in the crystalline solids. A substance in the amorphous state has short range order within the limits of one or several unit cells (ordering of the structure in a range 10-15 Å). Beyond the limits of unit cell, the order is as a rule violated. Each unit cell differs from the preceding one in its position in space. The cell displacement directions are statistically disturbed. Amorphous solids like crystalline solids can be insulators, semiconductors or in some even be superconductors.

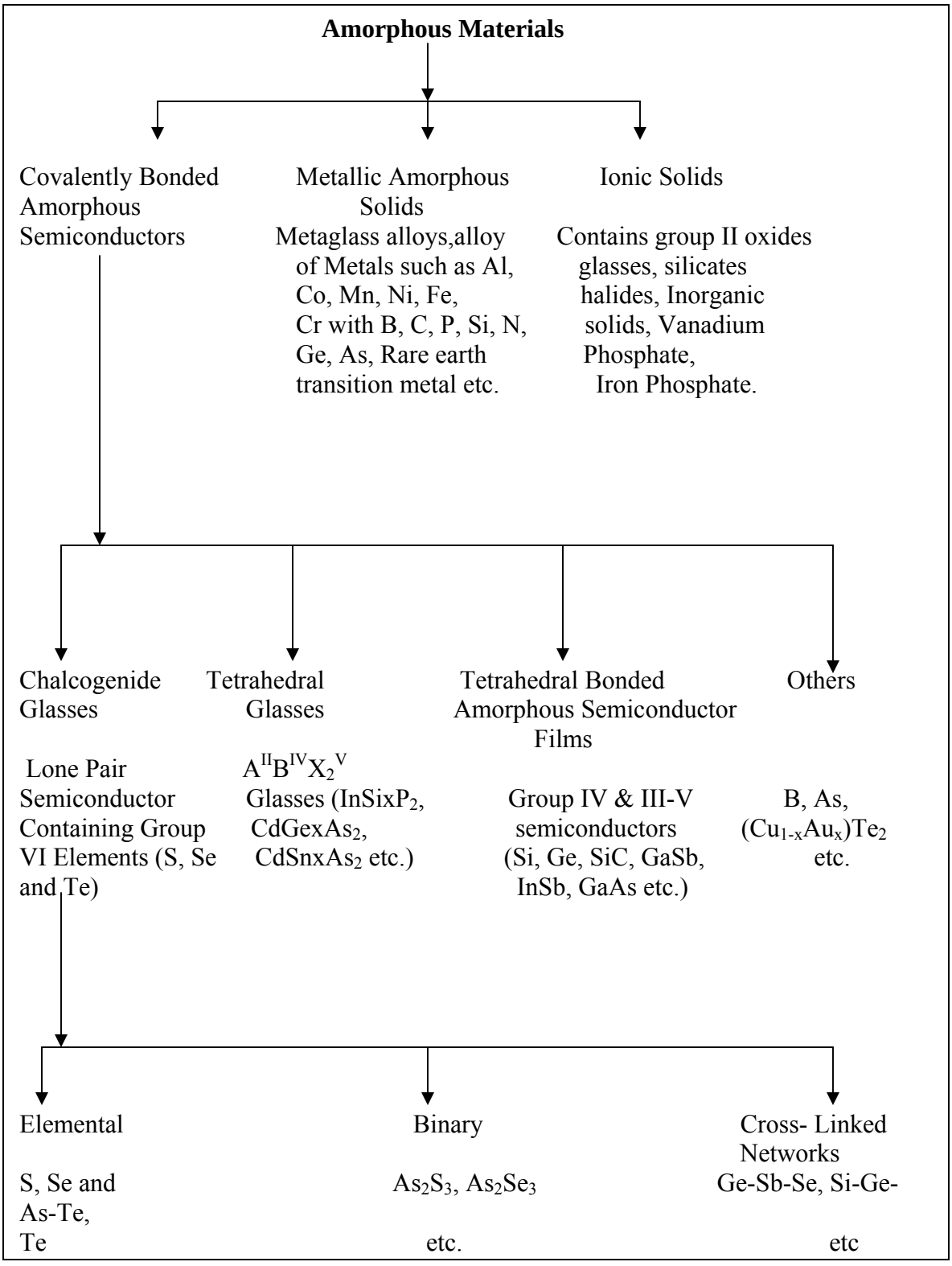

Table 1.1 Classification of amorphous materials

It was Ioffe [1] who first pointed out that basic electronic properties of a solid are determined from the character of bonds between nearest neighbours rather than by long range order. B.T Kolomiets [2] while working on glasses observed that these glasses behave similar to intrinsic crystalline semiconductors. The chemical bond approach enabled Mooser and Pearson [3, 4] to predict many of the semiconducting properties of amorphous materials. On the basis of difference in their chemical bonding, amorphous materials can be classified into three major categories followed by their sub categories and are shown in table 1.1.

1.2 Structure of Amorphous Solids

The key features of atomic arrangement in a perfect crystal and an amorphous material are shown in figure 1.1. The solid spheres represent the equilibrium position about which the atoms oscillate. In the crystalline structure, there exists a translational periodicity; almost all the bond lengths and bond angles are identical, independent of the atom's position in the solid. This results in long-range order throughout the solid. In amorphous solids there are slight variations in the bond lengths and bond angles. These slight variations serve to dissolve the spatial periodicity of the structure for distances greater than few atomic radii. The amorphous structure therefore exhibits short-range order rather than long-range order characteristic of crystalline states. This type of disorder is called topological disorder. In some cases, the disorder in the amorphous semiconductors makes it impossible to satisfy the bonding requirement for the atom. This leads to the formation of dangling bonds which has significant influence on the physical and electronic properties of these materials. Other forms of disorder include spin disorder, compositional disorder (for compound materials) and vibrational disorder.

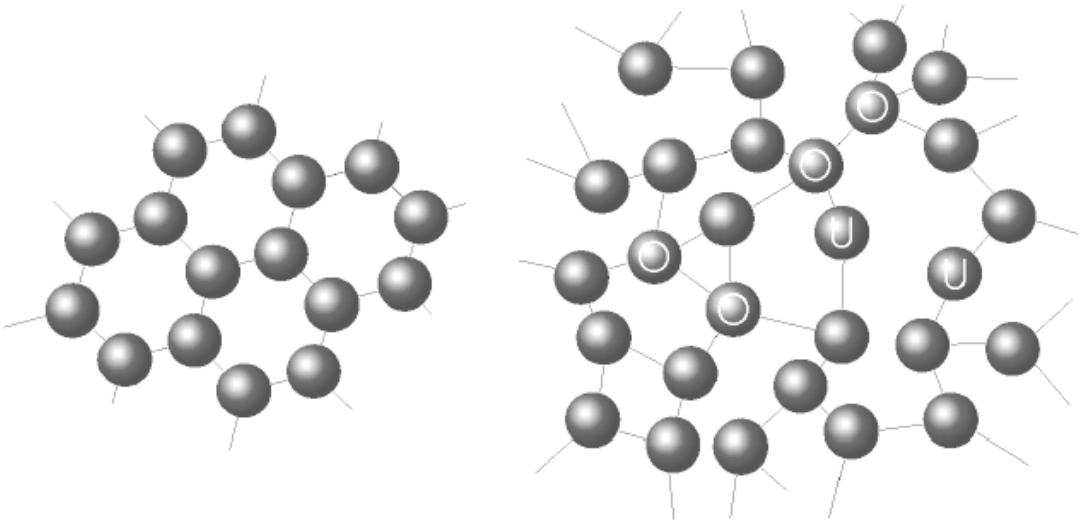

Figure 1.1: Comparison of the atomic arrangements in (a) a perfect crystal and (b) an amorphous semiconductor. The atomic structure shown here is three-fold coordinated, with the atoms labeled with U are under- and atoms labelled with O are over-coordinated.

Despite lacking long-range spatial order, the amorphous solid still has a high degree of short range order. Generally the valence requirements are satisfied for individual atoms and each atom is normally bonded to the same number of nearest neighbours. Hence it can be said that no solid is strictly "amorphous" in the sense of completely lacking in any type of definable order [5, 6].

1.3 Band Models for Amorphous Semiconductors

The key feature to understand the electronic properties of the materials is the knowledge of their electronic band structure. In case of crystalline semiconductors, sophisticated theoretical models are available for their structure. In case of a semiconductor, theories of band structure are crude and qualitative because long range periodicity is absent. Different models have been proposed to explain the electrical and optical properties of

non-crystalline semiconductors in terms of 'states in gap', which are normally due to defects *i.e*. the presence of strained and weak bonds. For a rigid network, the conduction (or valence) band differs from that in a crystal in having a 'tail' of states localized in the sense of Anderson [7] and any charge carriers created in these states will be localized on some weak, strained or dangling bonds. These localized states are inevitable in the amorphous materials. The localized states being separated from the extended states by an energy known as mobility edge [8]. Electronic energy states of a semiconductor consist of delocalized states like valence and conduction bands, commonly known as extended states and the localized states like tails and dangling bond states. The extended states are due to short range order and the tail states are due to translational and compositional disorder which is assumed to cause fluctuations of the potential of sufficient magnitude such that they give rise to localized states extended from the conduction and valence bands in the gap. The extended states are quantum mechanical states of motion in which electron may be found anywhere in space with equal probability. A single model can not describe the essential features of all amorphous materials. So, various models and even their modifications have been proposed to give appropriate understanding of the vital features of these semiconductors. To describe the properties of amorphous materials, three basic models are given below.

1.3.1 CFO Model / Mott - CFO Model

For alloy glasses which contains compositional as well as potential disorder, the 'CFO' model was put forward by Cohen, Fritzsche and Ovshinsky [9] shown in figure 1.2. They investigated the tails of localized states pulled out of the conduction and valence band by the disorder and some overlap between these tails. Such overlapping states would pin the

Fermi level. The principal concept of this model was the existence of mobility edges, identical with the critical energies 'E_c' and 'E_v', introduced earlier by Mott [10], also known as Mott – CFO Model. The character of wave function changes at 'E_c' and 'E_v', separating localized states from extended states. In extended states, the electron and hole mobility drops sharply as compared to high density states, so called 'mobility edges'. It also defines mobility gap i.e. E_c - E_v, which contains only localized states.

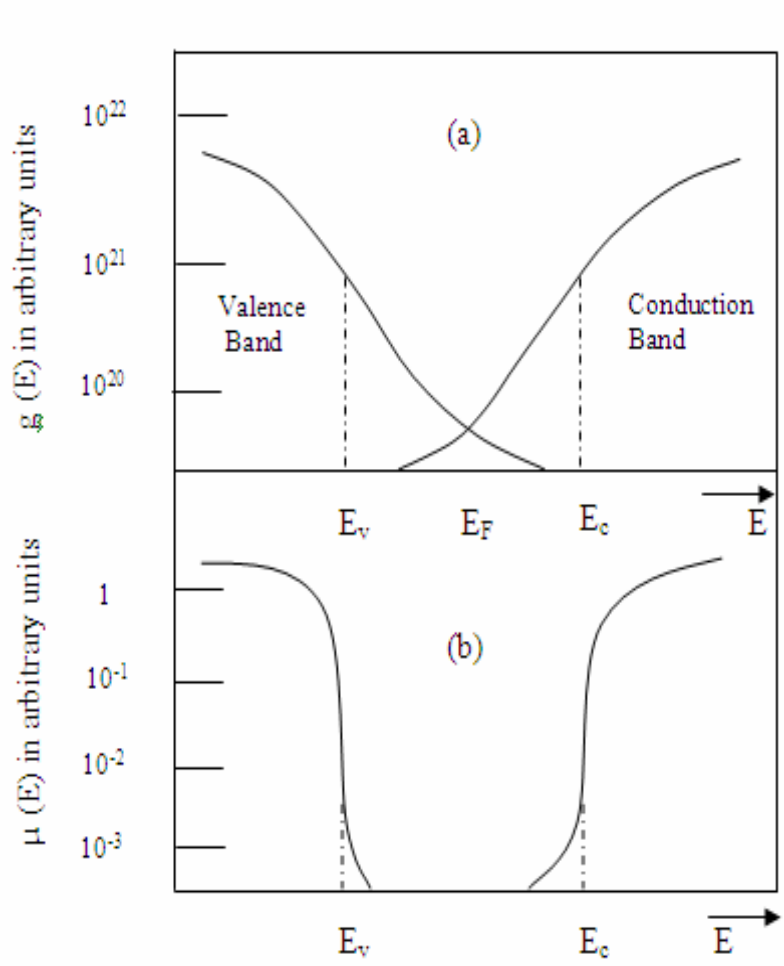

Figure 1.2 Sketch of (a) the partial densities of states of the valence and conduction bands and (b) the electron and hole mobility, respectively.

1.3.2 Davis – Mott Model

This model was proposed by Davis and Mott [11] and band model is shown in figure 1.3. According to this model the mobility edges for electron and holes lie again at 'E_c' and 'E_v'. A strong distinction is made between localized states which originate from lack of long range order and others which are due to defects in the structure. The defect states form longer tails but of insufficient density to pin the Fermi level, but the authors [11] proposed a bend of compensated levels near the gap centre in order to pin the Fermi level. Thermally assisted hopping may also take place in these ranges.

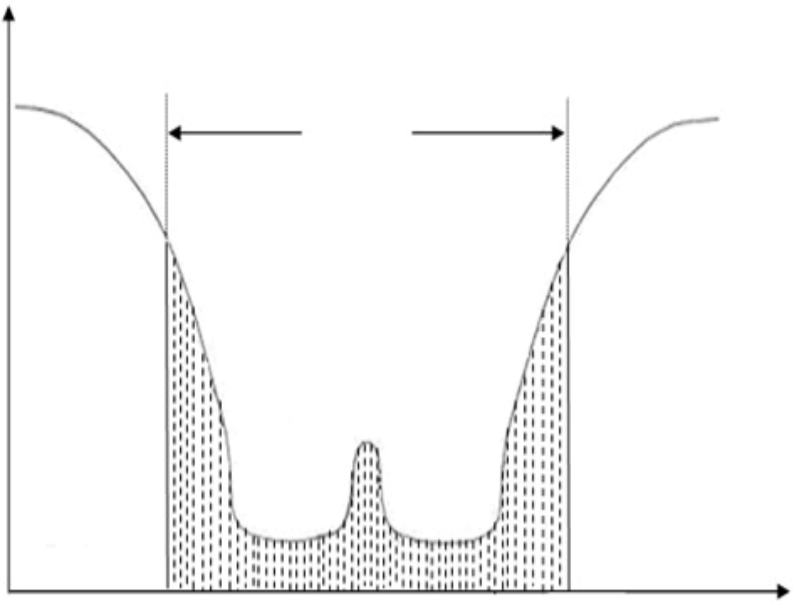

Figure 1.3 Sketch of Mott and Davis Model.

1.3.3 Mott, Davis and Street Model

This model is a further amendment of Mott and Davis model. According to Mott, Davis and Street model the centre band further splits into two levels forming donor and acceptor bands as shown in figure 1.4. According to Mott [12], the bands of localized states originate due to the dangling bonds.

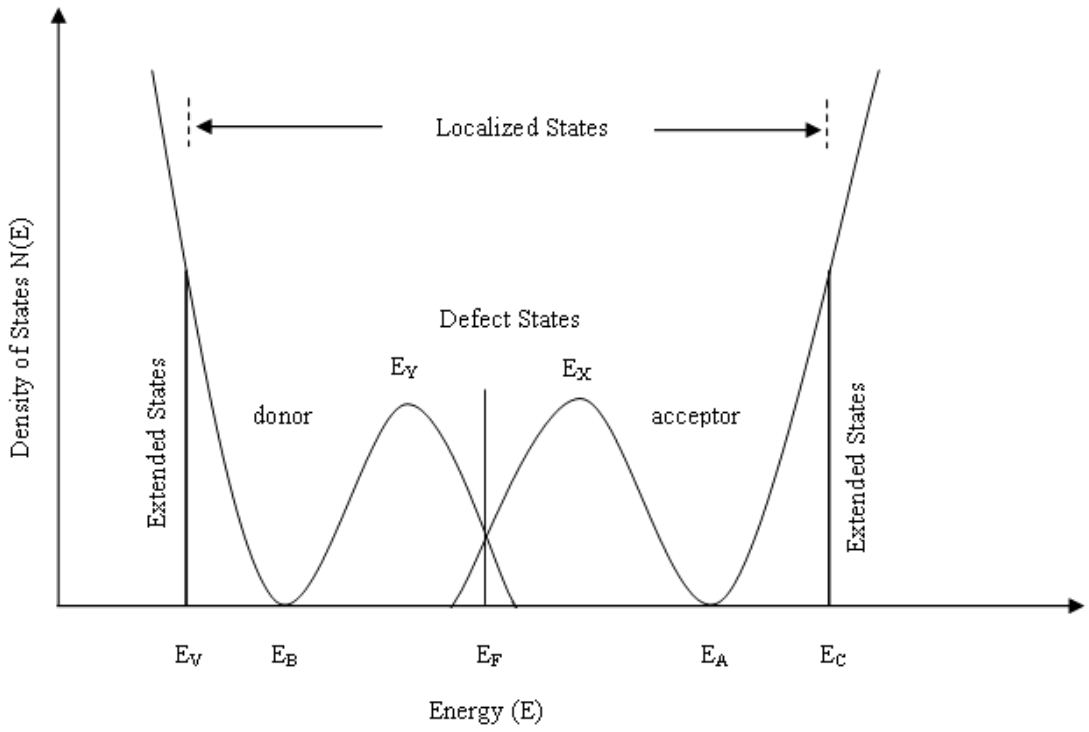

Figure 1.4 Sketch of Mott, Davis and Street Model.

These bonds can take zero, one or two electrons and are therefore, designated as D^+, D^0 and D^- states respectively. The dangling bond energy levels depend mainly on the lattice distortion and the energy level involved. In actual case, two electrons are shared in a chemical bond between atoms. In certain configuration, the atoms are not able to share the electrons and the bond breaks. Because of this unstable situation, the dangling bond emerges out. If a dangling bond is singly occupied i.e. D^0, it is neutral indicating an electron spin resonance signal. If an additional electron is attracted by the dangling bond; thus providing a lone pair designated as D^-, indicating that there will be no ESR signal and when the bond even loses the single electron it will be D^+ giving rise to a hole representing a bond without any spin. The model is based on the assumption that only paired states *i.e.* D^+ and D^- are preferred in chalcogenide glasses.

1.4 Defect States in Amorphous Semiconductors

In amorphous semiconductors, defect is defined as a departure from the fully coordinated random network. One type of point defect concerns the atomic coordination, which occurs due to either under or over – coordination. 'Under coordinated defects' are simply known as dangling bonds or broken bonds. A neutral dangling bond normally contains one electron but under certain conditions (*e.g.* chemical or electronic doping), the electronic occupancy can be changed to create negatively or positively charged dangling bonds. Photoluminescence study [13], photoconductivity measurements [14] and pinned Fermi level gives the evidences that chalcogenide glasses contain high concentration of defect states. Paramagnetism study at lower temperature [15] and absence of ESR signal shows the absence of unpaired electrons which is the characteristic feature of broken bonds. In amorphous chalcogenides, the electron – phonon coupling causes the network to relax to a new equilibrium state at a lower total energy. The addition of an electron into a dangling bond *i.e*. spin pairing of electron at a defect centre, may cause a change in the bonding which lowers the electronic correlation energy, U_c by an amount U_r. Now the effective correlation energy for two spin paired electrons at a same site is given by

$$U_{eff} = U_c - U_r = U_c - \frac{\lambda^2}{c} \qquad (1.1)$$

where, λ is the electron – phonon coupling constant and the force constant c is related to phonon frequency as $\omega = (c/m)^{1/2}$ which is taken to be constant. U_{eff} is negative if $U_c < U_r$, *i.e.,* for strong electron - lattice coupling. This spin pairing defect is called the negative U defect. This idea proposed by Anderson [16] was first applied to defect in amorphous chalcogen by Mott and Street [17] and later by Kastner et al. [18]. These defects are often called as charged-dangling bond (CDB) as the defect of the dangling

bond is charged due to pairing of electrons and holes. The feature of CDB in a-Se can be presented by a model as shown in figure 1.5.

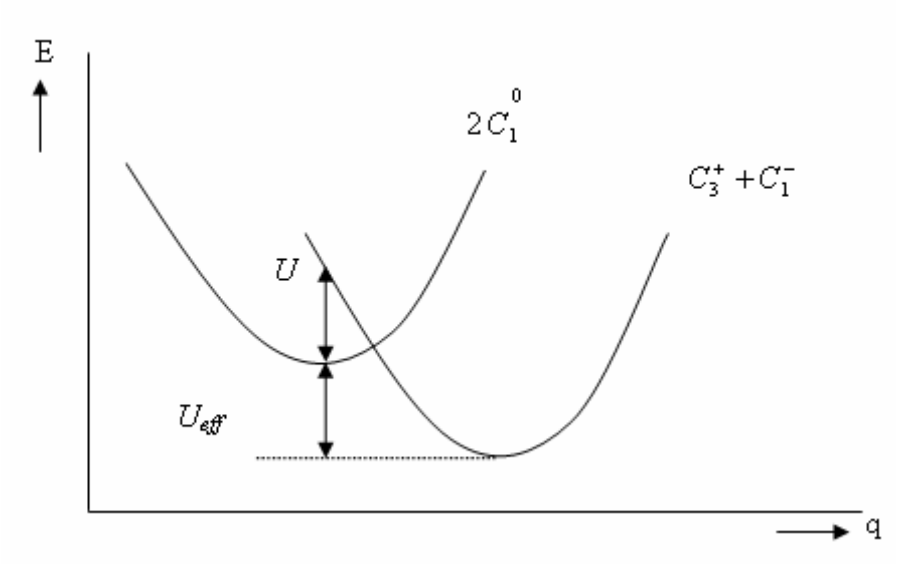

Figure 1.5 Configuration-coordinate diagram for the formation of a $D^+(C_3^+)$ - $D^-(C_1^-)$ pair

The structure of Se is two fold coordinated and is believed to consist mostly of chains. The dangling bond will contain an unpaired electron if electron – phonon interaction is not strong and is written as C_1^0 . However, electron pairing should occur at C_1^0 centre due to low atomic coordination resulting in a high degree of network flexibility (strong electron – phonon interaction). There are also non-bonding pπ orbitals at chalcogen atom (Se or S) and hence the transfer of an electron from one C_1^0 centre to another produces a negatively charged C_1^- (electron spin paired) and a three-fold-coordinated positively-charged dangling bond C_3^+(hole spin paired). The reaction $2C_1^0 = C_1^- + C_3^+$, is thus exothermic with an effective negative correlation energy. Using configuration coordinate diagram, this process is illustrated in figure 1.5. Thus the neutral C_1^0 is unstable and $2C_1^0$

transform into a pair of C_1^- and C_3^+, which is called a valence – alteration pair (VAP) by Kastner et al [18].

1.5 Chalcogenide Glasses

Chalcogenide glasses are the chains of random lengths and random orientations formed by bonding of chalcogen elements sulphur (S), selenium (Se) and tellurium (Te) and alloys containing these chalcogen as the major constituents. Systematic research on chalcogenide glasses started at the middle of the twentieth century. Chalcogenide glasses have been of enormous interest for infrared optics since 1950 [19]. In 1968, Ovshinsky [20] made an outstanding discovery. He observed the memory and switching effects exhibited by certain chalcogenide films when subjected to an electrical field. The structure of a glass is very important because many properties depend on it. In 1978 Popescu [21] and in 1979 Phillips [22] demonstrated that in many non crystalline solids an 'ordering at not too large scale but more extended than the short range order' must be admitted in order to explain the first sharp diffraction peak (FSDP). Thus the concept of medium-range order or intermediate-range order was born. The glass structure consists of covalently bonded molecules, as opposed to the ionic bonding of other glasses and these are weakly bound via a combination of covalent and vander Waal like attraction [23, 24]. The amorphous chalcogenide field continued to develop both from fundamental and applications point of view. New phenomena were discovered, new applications are emerged. The recent discovery of intermediate, self-organized phases in chalcogenides and other glasses [25, 26] will have high impact not only in glass science but also in many other fields of research *viz*. protein folding, thin-film gate dielectrics and high-temperature superconductivity. The freedom allowed in the preparation of glasses in

varied composition brings about changes in their short range order and thus results in variation of their physical properties. Therefore, it is possible to tailor their various properties as desired, for technological applications. They have well defined niches in passive and active applications like grating fabrication, phase change optical disk, glass waveguide for IR evanescent wave sensor, photoinduced waveguide, fiber fabrication, fiber amplifiers and lasers, IR micro lens arrays, optical switching, optical computing, regeneration, efficient femtosecond devices *etc*. [27-34] and many of which have been realized or anticipated but still a lot of work is needed for complete understanding of these materials.

1.6 Se-Te Glassy System / $Se_{85}Te_{15}$ System

Selenium is an element from the group VI column of the periodic table. The elements in this column are referred to as chalcogens. All elements of the chalcogen family have six electrons in their outermost shell and can accommodate up to eight electrons. The outermost shell consists of two subshells, called *s*-type and *p*-type subshells. The *s*-type states can hold two electrons, while *p*-states have six allowed states. Selenium has atomic number Z = 34, implying that it has twenty eight inner core electrons and six valance electrons in the outer most shell. The two s-electrons form a lone pair (L P) and do not participate in bonding. The remaining four electrons reside in the p-subshell. Two of the four p-state electrons usually form a lone pair and are sometimes referred to as nonbonding (N B) states. The remaining two electrons are available for covalent bonding to other atoms. This configuration results in two-fold coordination bonding and has an optimal bond angle of 105° and represents the lowest energy configuration for selenium. Chalcogens generally exhibit divalent bonding and thus form chain-like structures.

However, if trigonally bonded atoms, for example those from Group IV or V are added to the structure, they cross-link with the divalent chains to attain three dimensional stability in the amorphous alloy. It was assumed that the amorphous form of Se would consist of a mixture of the rings and chain formations of trigonal and monoclinic allotropes. However, structural investigation of a-Se and its alloys indicates a "random chain model" with all the atoms in a two-fold coordinated chain structure. The angle between two adjacent bonding planes is defined as the dihedral angle, denoted by φ. The concept of dihedral angle φ is explained in figure 1.6 which shows a selenium random chain model.

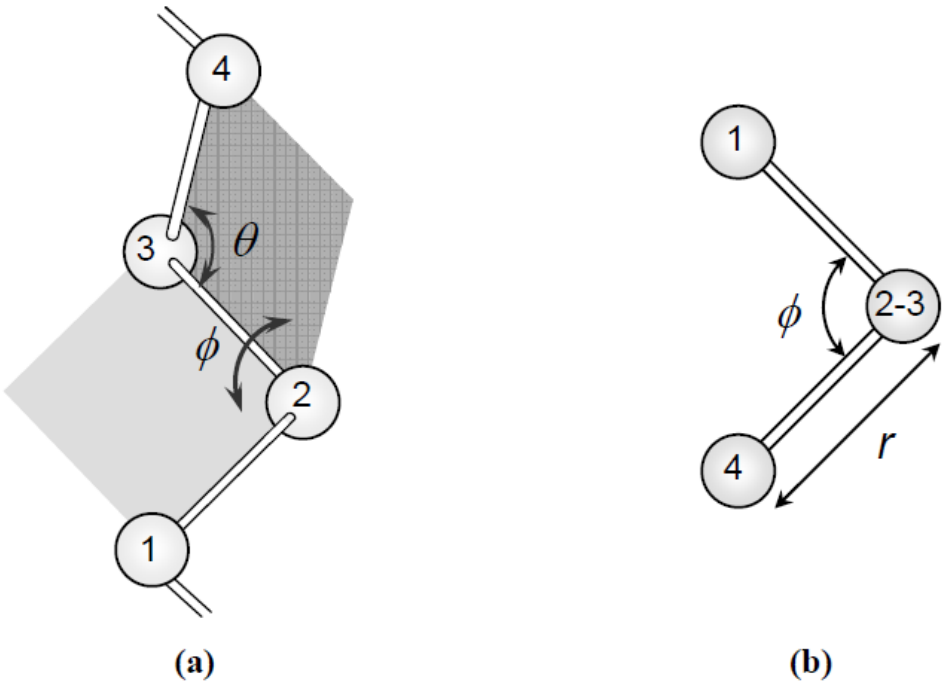

Figure 1.6: Definition of dihedral angle φ in selenium random chain model. (a) The definition of dihedral angle formed between two planes of atoms 123 and 234. (b) Looking down on the bond joining atoms 2 and 3 [37].

In this example, atoms labelled 1, 2, and 3 form one bonding plane and atoms 2, 3, and 4 from the second bonding plane. The angle between these two planes is the dihedral angle which is further illustrated in figure 1.6 (b) by looking down the bond that connects atoms 2 and 3. The magnitude of the 22 dihedral angle φ in the random chain model remains constant but its sign changes randomly [35, 36].

In the amorphous form of selenium, the dihedral angle changes its sign randomly, leading to ring-like and chain-like segments. If + or – is used to indicate the relative phase of the dihedral angle φ, then a sequence of + – + – represents a ring-like and a sequence of ++++ or – – – – represents a chain-like structure. A structure of amorphous selenium shown in figure 1.7 can be characterized by +++ – + – + – – –. Only local molecular order within the selenium chain has been assumed in this model and it has been used successfully to explain the vibrational spectra of a-Se to account for the presence of various Se_8-like spectral features in the infrared absorption and Raman scattering spectra. Other structural studies also support this random chain model [38, 39]. The structure of amorphous solids is not completely random and there is a degree of order at least between the individual atoms. Though each individual atom in the solid tends to fulfil its valency requirements, but all the atoms can not satisfy their individual requirements due to lack of periodicity in the amorphous structure. An important property of chalcogenide glasses is that these materials contain thermodynamically derived charged structural defects, called valence alternation pairs (VAP). These defects correspond to some of the chalcogen atoms being over and under coordinated [40-42]. Figure 1.8 depicts the bonding configurations possible for *a*-Se. The first column in the figure consists of notations representing the bonding configurations. In this column, *C* stands for

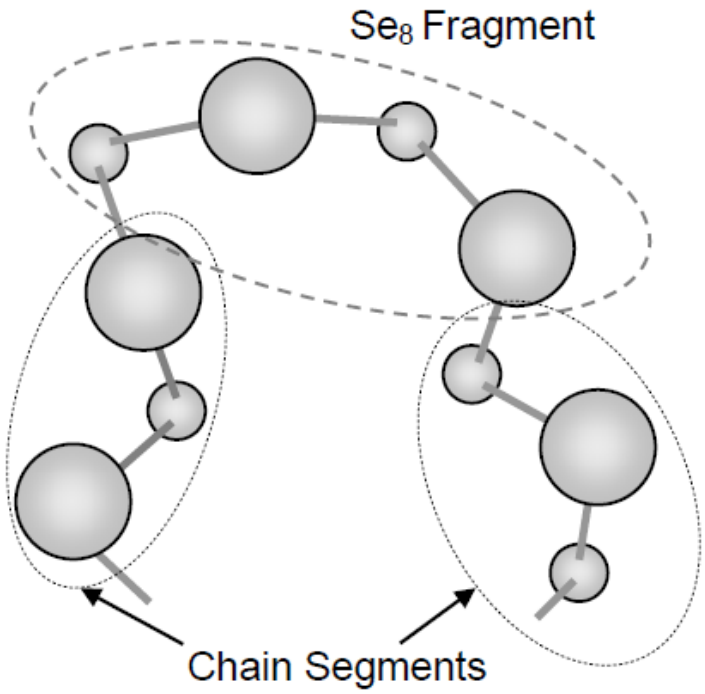

Figure 1.7: Random chain model of amorphous selenium depicting chain-like and ring-like segments [37].

chalcogenides and the subscripts indicate coordination number and the superscripts represent the polarity. The energy of the non-bonding lone pair is taken to be zero. The energy per electron of any bonding orbital σ is taken as $-E_b$ regardless of the nature of the bond. Since anti-bonding orbitals lie at a slightly higher energy level as compared to the energy depth of the bonding orbitals, the per electron anti-bonding orbital energy is $E_b + \Delta$, where $\Delta > 0$ and is called anti-bonding repulsive energy. Whenever an additional electron is placed on an atom, there is an increase in energy due to electronic correlation U_c. The first state shown in figure 1.8 (a) represents the two-fold coordinated structure, C^0_2 which has overall energy $-2E_b$. In this configuration, two of the p-state electrons form a lone pair (LP) in the non-bonding state, and the rest of the two electrons reside in

bonding states. The next lowest energy configuration is trigonally coordinated atom, C^0_3 shown in figure 1.8 (d). Formation of this type of defect costs the anti-bonding repulsive energy Δ. Another electrically neutral defect is the chain end, represented as C^0_1 in figure 1.8 (b). In this configuration, three p-shell electrons are in non-bonding state and one electron is in the bonding state available for bonding. Since this configuration lacks a second bond, this defect provides the system the energy of the second bond. Unpaired non-bonding and anti-boding electrons can be detected using experimental techniques. The absence of electronic spin resonance (ESR) signal eliminates the existence of these types of defects in amorphous selenium [43, 44]. Kastner, Adler, and Fritzsche [40] studied the absence of ESR signal and proposed that the neutral defect C^0_3 is unstable and would transform into positively and negatively charged centers (VAPs), C_1^- and C_3^+ respectively. The defect generating reaction can be written as

$$2C^0_2 \rightarrow C_1^- + C_3^+ \qquad (1.2)$$

The one- fold C_1^- and three- fold coordinated C_3^+ defects are shown in the figure 1.8 (c) and (e) respectively. If a pair of these defects is in close proximity, then they are called intimate valence alternation pairs (IVAP). The formation of these under - and over coordinated atoms is energetically more favourable, as the singly bonded defects are relatively unstable. Moreover the total energy of the system is lowered by the transformation provided the electron correlation energy U_c is less than 2Δ. For example, a chain end C^0_1 can lower its energy by approaching the lone pair on a normally coordinated C^0_2 atom and generate an IVAP. The diffusion of the resulting IVAP pair away from each other can further reduce the Gibbs free energy of the solid. An example

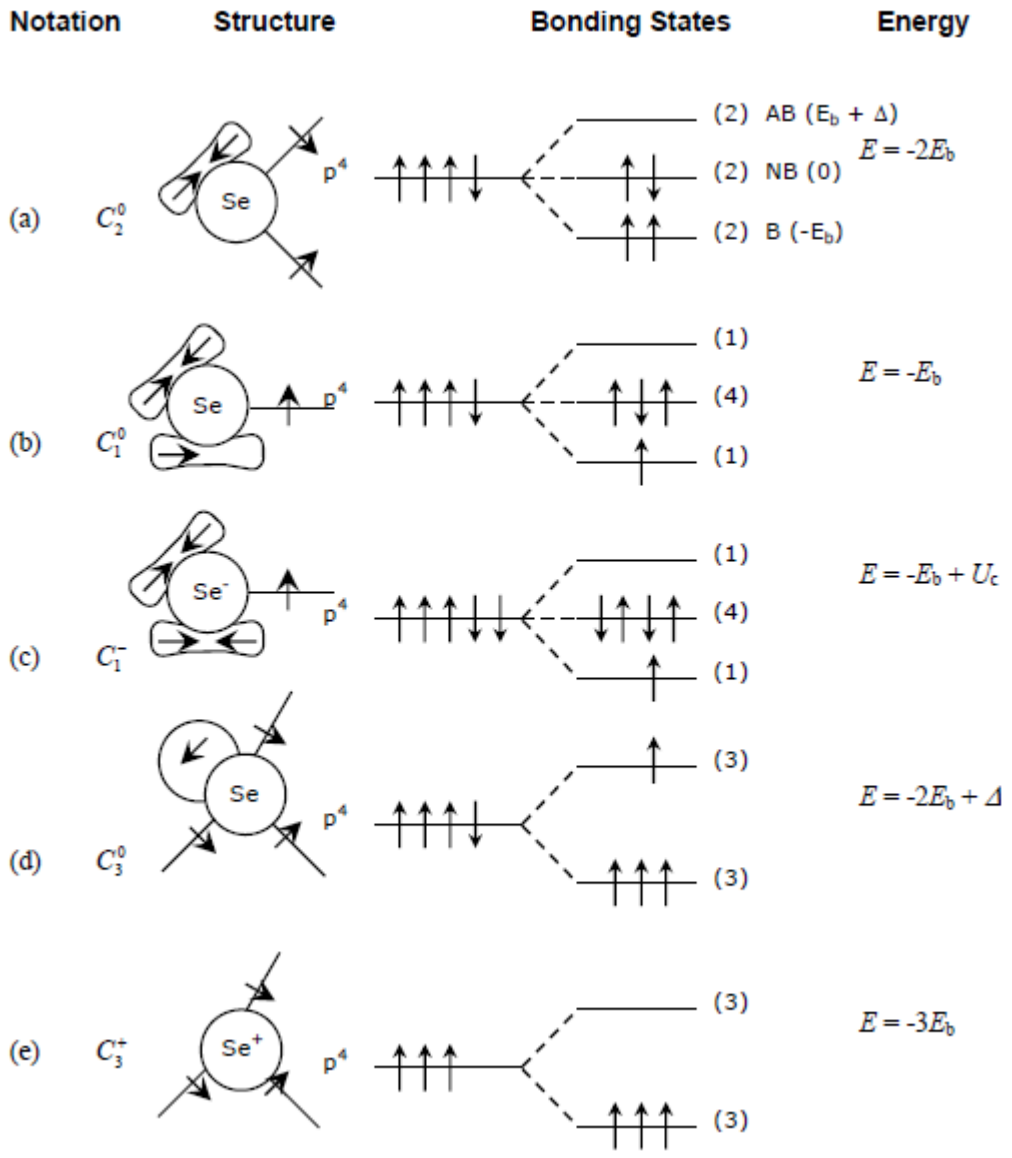

Figure 1.8: Bonding configurations and structure of selenium atoms. Solid straight lines represent boding orbitals, lobes represent lone-pair (non-bonding) orbitals, and circles represent antibonding orbitals.

of the reaction given by equation 1.2 is shown in figure 1.9. A bond between trignonally coordinated defect, C^0_3 and a two-fold coordinated atom, C^0_2 is broken. An electron from a trigonally coordinated atom can transfer bonded defect, resulting in an IVAP as shown

in the figure 1.9 (b). The overall material remains neutral despite the presence of large number of positive and negative charged defects. The defect centers, C_1^- and C_3^+ are in close proximity to each other and hence an approaching carrier "sees" IVAP centers as neutral defects. Many photoelectric properties of *a*-Se and its alloys can be qualitatively explained by using concepts based on VAP- and IVAP-type defects and on the inter-conversions between the normally bonded (two-fold coordinated) Se atoms and these defects. The physics of such processes has been extensively discussed in the literature [45, 46]. Their existence and the possible defect reactions that can occur in the structure have led to many important predictions and have provided much insight in to the behaviour of chalcogenide semiconductors. For example, the linear dependence of the steady state photoconductivity on the light intensity in *a*-Se has been interpreted via photoinduced IVAP - type centers [47]. As for as the commercial utility of *a*-Se is concerned, it has a wide range of technological applications. It is used in digital xerography where the film-based detector consists of a photographic film sandwiched between two fluorescent screens. It is used in digital radiography and as photoconductors in high definition TV pick up tubes. Besides the wide commercial/device applications like switching memory, xerography *etc*., Se also exhibits a unique property of reversible transformation [48]. This property makes it very useful in optical memory devices but pure Se has also some shortcomings like short life time and low sensitivity. Binary alloys of amorphous selenium with tellurium have been widely studied in both vacuum deposited amorphous films and vitreous bulk form due to their electrophotographic applications such as photoreceptors in photocopying and laser printing. The average

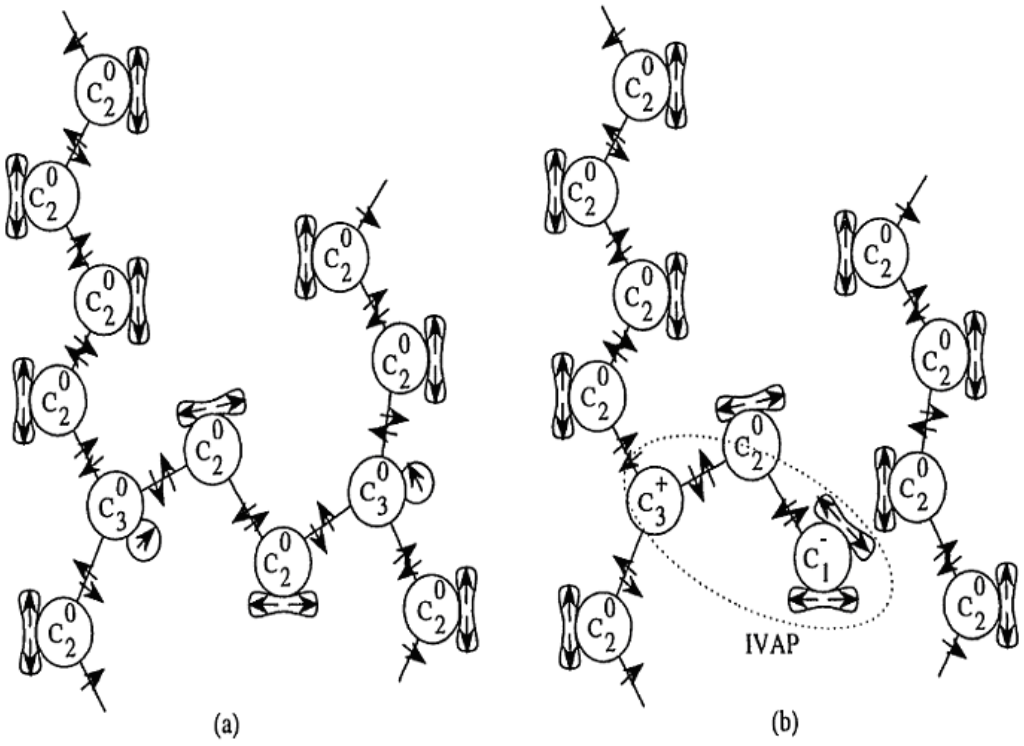

Figure 1.9: In amorphous selenium, (a) C_3^0 defects cross-link the divalent chains and (b) dissolve to form and IVAP.

coordination number of Se is two. Neutron diffraction studies of $Se_{1-x}Te_{1-x}$ glasses (x = 0-40 at. %) shows that Te has short range order and is mainly substitutional with the average coordination number Z is kept almost constant; $Z \approx 2$ [49]. EXFAS (extended X-ray absorption fine structure) measurements [50] have validated above conclusions even in liquid $Se_{1-x}Te_x$ mixtures upto $x < 50$ at %. Although Te enters the structure by an isoelectronic substitution so that its coordination remains two, there will be nonetheless changes in van der Waals bonds or interchain secondary bonds, because the Te atom is larger than the Se atom and has more electrons in its orbital (both Se and Te have same crystal structure, trigonal which consists of chains that are held together by Vander Waals bonds and the Van der Waal interaction in Te crystals is stronger than in Se crystals).

One can therefore argue an increase in secondary bonding between chains as more Te is added to the glass. Stronger secondary bonding and the increase in average chain mass with Te addition lead to an increase in the glass transition temperature T_g. The addition of Te will also increase the concentration of charged valence alteration pair (VAP) type defects [51], so that it may be argued that the increase in T_g is partly due to Se_3^+ and Te_3^+ type defects connecting neighbouring chains and limiting molecular mobility.

1.7 Ge-Te Glassy System / $Ge_{20}Te_{80}$ System

In the solid state Ge-Te alloy can exist either in amorphous or crystalline form. It is established that the atomic distribution and bonding nature in a- Ge-Te alloy are different from those of crystalline Ge-Te compound. The first coordination number for *a*- Ge-Te estimated from the experimental radial distribution function (RDF) lies between 3 and 4. Therefore it can be supposed that (i) Ge atoms might be four fold and Te atoms two fold coordinated, or (ii) Ge is three fold coordinated, while some Te atoms are three fold and others are two fold coordinated. Concerning the atomic structure of amorphous Te- rich germanium tellurides, these assumptions are also considered. For example, it was shown by Betts *et. al.* [52] that experimental RDF of $Ge_{17.5}Te_{82.5}$ amorphous alloy could be described by both 3(Ge) – 3(Te) and 4(Ge) - 2(Te) models. However it is supposed that amorphous $GeTe_2$ structure with fourfold coordination of Ge and two fold coordination of Te is most stable in the alloys containing less than 33 at.% of Ge. In opposite, after investigation of amorphous Ge-Te films in a wide concentration interval by different methods, a possibility of formation of amorphous compounds at either $Ge_{50}Te_{50}$ or $Ge_{33}Te_{67}$ composition was ruled out [53]. The existence of strong covalent bonding in a-Ge-Te has been proven by photoemission measurements by Fukui [54]. Moreover, the

covalency in amorphous phase was shown to be stronger than in crystalline phase. From the experimental structure factors and pair correlation functions of Ge-Te alloys as investigated by I. Kaban et.al. [55], one may guess that amorphous Ge-Te alloys are a random mixture of Ge and Te atoms and Ge-Te bonds are formed statistically when Ge is added. On the other hand, it can be supposed that Te- rich Ge-Te amorphous alloys are chemically ordered on the microlebel and some structural units with strong Ge-Te bonds are distributed among Te atoms. If the last assumption is correct than the question concerning the composition of these structural units arises. Recent investigations of crystallization behaviour of amorphous Ge-Te alloys under heat treatment [56] have helped us to choose a plausible model. It was established that $Ge_{20}Te_{80}$ composition alloy shows single- stage amorphous-to- crystalline transformation due to simultaneous formation of Ge-Te and Te crystallites, whereas the alloy containing 15 at.% Ge exhibits two-stage transformation due to segregation of Te and subsequent formation of GeTe crystallites. Obviously this difference in the crystallization of the Ge-Te alloys is explained by differences in their atomic structures. We suppose that all Ge atoms in $Ge_{20}Te_{80}$ composition alloy are bonded with Te atoms with stiochiometry $GeTe_4$. On the other hand the alloy between $Ge_{20}Te_{80}$ and pure Te contain $GeTe_4$ tetrahedra as structural units and Te atoms distributed among them.

To check this assumption, the experimental data for amorphous $Ge_{20}Te_{80}$ and $Ge_{15}Te_{85}$ alloys were modelled by means of the Reverse Monte Carlo (RMC) technique with 20,000 atoms. The following constraints were used during the simulation. For the $Ge_{20}Te_{80}$ composition it was supposed that (i) no Ge-Ge distances shorter than 3.5 Å occur in the alloy ; (ii) every Ge atoms has four Te neighbours between 2.4 and 3.24 Å ;

(iii) 50% of the Te atoms had no Ge neighbour in the first coordination shell, so that $GeTe_4$ tetrahedra were forced to share Te atoms. At the end of simulation, 98.4 % Ge atoms had 4 Te nearest neighbour at the distance of ~ 2.5 Å and 49.9 % Te atoms had no Ge neighbour in the first coordination sphere. For the $Ge_{15}Te_{85}$ composition it was assumed that minimum Ge-Ge distance is of 3.5 Å and every Ge atoms has four nearest Te neighbours at distances between 2.4 and 3.24 Å, the rest Te atoms have no Ge neighbour in first coordination sphere. At the end of simulation 96% of Ge atoms were with four Te atoms at the distance of ~ 2.7 Å. For a covalently bonded network constrained by bond stretching (α) and bond bending (β), Phillips [22, 57] suggested that the glass forming tendency will be optimized when the number of constraints per atom (N_c) is equal to the degree of freedom (N_d). Enumeration of α and β constraints for three dimensional network showed that the condition is satisfied when the mean coordination number < r > of a network acquires a critical value $< r > = 2.4$. To explain the strong glass forming property of some chalcogenide system, Phillips stated that the covalent bonding in glasses may be optimized when the average coordination number $< r > = 2.4$. When, $N_c < N_d$, the unconstrained glass is floppy in nature. At this stage the connectivity of the glass is diluted. Here the average coordination number is nearly two. Network has begun to fall apart into disconnected chain segment. On adding cross-linking bonds at random, the number of such floppy modes (whose number per atom, f is $N_d - N_c$) decreases and it extrapolates to zero at average coordination number of 2.4 corresponding to $Ge_{20}Te_{80}$ composition. This transition is a new glassy phase also called 'intermediate phase', which is strictly a topological phase. The phase has no special symmetry, but it does have a characteristic connectivity. This glassy phase is not an equilibrium phase *i.e.*

it is not a true phase in the sense of equilibrium thermodynamics. Two transitions define the limits of an intermediate phase that separates the floppy from the stressed rigid phase. It has lead to a structure based classification of glasses in terms of their elastic response *i.e.* floppy-intermediate-stressed rigid. Thus when $N_c = N_d$, the network is rigid and yet stress free but for $N_c > N_d$, the glass network is rigid and stressed.

1.7.1 General Properties of Ge-Te System

In tetrahedral semiconductors (Si, Ge, III-V compound etc.), bonding band forms the valence band and antibonding bands forms the conduction band, but the situation is quite different in chalcogenide glasses. In chalcogenide glasses, the valence band (σ - bonding) originates from lone-pair (LP) electron states whereas the conduction band arises from antibonding (σ*) states. Ge in four fold coordination has hybridized sp^3 orbitals which split into bonding (σ) and antibonding (σ *) states. In solid, these molecular states are broadened into bands. Thus in tetrahedral semiconductor, bonding bands forms the valence band and antibonding bands form the conduction band. In Te on the other hand, s-state lie well below the p-states and need not be considered. Te is normally two fold coordinated because only two of the p-states are utilized for the bonding and leaves one non-bonding electron pair. These unshared or lone pair electrons form a band near the original p-state energy as shown in figure 1.10. σ and σ* bands split symmetrically. Both σ and lone pair bands are occupied. Thus bonding band is no longer the valence band (VB); this role is played by lone pair band. Here lone – pair band determines the conduction properties and thus these materials might appropriable be called as Lone Pair semiconductors. In both cases, a filled state is pulled out of the σ band and an

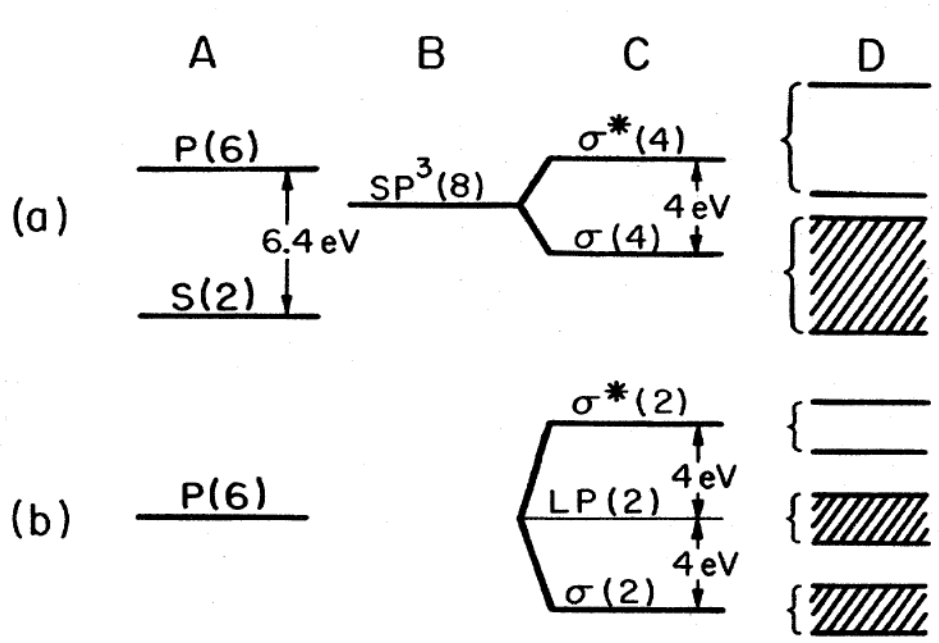

Figure 1.10: Bonding in (a) Ge and (b) Se. (A) atomic states, (B) hybridized states, (C) molecular states, (D) broadening of states into bands in the solids.

unoccupied state forms σ^* band. In tetrahedral materials, these produce localized states in the gap. Considering Coulombic interaction and correlation, one estimates that a donor is formed near the gap centre and acceptor above it. In chalcogenide materials, the lone pair band lies in the energy region between the σ and σ^* bands. The occupied state from σ bands falls into the lone pair bands and the unoccupied state probably forms acceptors above the lone pair bands. It is also possible, particularly at a high concentration of dangling bonds that the unoccupied state lie within the lone pair band.

1.8 Effect of Metallic Additives

Earlier work by Kolomiets and co-workers [58, 59] on amorphous semiconductors suggested that the electrical properties of chalcogenide glasses are comparatively insensitive to composition variations and presence of impurities. This is explained by

Mott [60] using his 8 - N rule. According to this rule, impurities in these glasses are coordinated in such a way that covalent bonding requirements are satisfied, therefore they do not form donors and acceptors. However, some experiments show that certain impurities can cause significant changes in the behaviour of chalcogenide glasses. The concept of charged dangling bonds and valence alteration pairs [61, 62] have been used by several workers to explain the behavior of chalcogenide glasses. It is postulated that the impurities may either destroy the dangling bond centers of one sign or form charged centers which are compensated by centers of opposite sign. Under such circumstances, activation energy may either increase or decrease. The addition of certain elements to a glass can alter the density of valence alteration centers [63]. The defect-chemistry in lone pair semiconductors is governed by the quite unusual inter-conversion property of the valence-alteration centers. At equilibrium, the valence-alteration centers reduce the influence of foreign atoms on the conductivity in two ways: (i) they retard the occurrence of charged additives and (ii) they increase in number such that their concentration always exceeds that of charged additives. Consequently, the valence-alteration centers remain the source of charge carriers. They are allowed to establish equilibrium by annealing the chalcogenide glass near glass-transition temperature or by adding third element, *i.e*. additive to the base melt. It is interesting to note from the experimental investigations that the metal atoms are mostly three - fold coordinated in glassy selenides such as As-Se-Ag, Ge-Se-Ag and Ge-Se-In systems [64-66]. Chalcogenide bulk glasses exhibiting n-type conduction were first prepared by quenching the melts of a mixture of Ge, Se and Bi_2Se_3 or Bi by Tohge et. al. [67]. They noticed that Seebeck coefficient 'S' is negative, suggesting the electrons are dominant carriers in these glasses ($Ge_{20}Bi_{10}Se_{70}$). Thin films

of $Ge_{20}Bi_xSe_{70-x}Te_{10}$ (x = 7, 9, 11, 13) were studied for their switching properties [68] and it was observed that films with $x \geq 9$ exhibited electronic switching. These amorphous semiconductors with tailored properties have a potential for thermoelectric and photovoltaic device application. To explore the possibility of such applications, it is necessary to obtain these materials in thin film form and to understand their physical properties. Some attempts have been made to prepare and study the properties of Bi-Ge-Se [69] and Bi-Ge-Se-Te [70, 71] thin films. Study of the electronic structure of p-type and n-type amorphous Ge-Se-Bi films and the density of states in the conduction band as well as that in the valence band has been investigated by inverse-photoemission and ultraviolet photoemission spectroscopy by Matsuda et. al. [72]. It was found that, with increasing Bi content, the conduction band minimum approaches the Fermi level, while the valence band maximum remains unchanged with respect to the Fermi level. Thus it was concluded that the mixture of Ge-Se and Bi-Se anti-bonding orbits compose the conduction band of the Ge-Se-Bi system. The origin of the n-type conduction in the high Bi concentration is attributed to this conduction band which appears just above the Fermi level. Carrier type reversal (p to n) has been observed Pb-Ge-Se-Te glasses at 8 at. % of lead. Electrical properties are found to exhibit notable change at $p \rightarrow n$ transition threshold [73]. Effect of annealing rate on the crystallization process in $Ge_5Bi_{18}Se_{77}$ thin films and a detailed analysis of the structural properties has been presented by Rajagopalan et al. [74]. Bhat et al. [75] proposed a consistent approach to understand the mechanism of three-fold coordinated Bi doping in Ge–Se glasses by carrying out specific heat (C_p) measurement in $Ge_{20}Se_{70-x}Te_{10}Bi_x$ system for $0 \leq x \leq 11$. The two softening temperatures exhibited by heat treated samples are explained on the basis of ‘microscopic

phase separation'. The minimum in 'configurational heat capacity' at x = 7.5 is related to be a feature of chemical threshold. Effect of Sn content on the electrical and optical properties of Ge-Se-Sn glasses is studied by Fadel et. al. [76]. Optical properties of amorphous Ge-Se-Tl investigated by Aziz et. al. [77] concluded that optical band gap decrease with increase in tail width with the increase of Tl content. Effect of Ag on the $Ge_{15}Se_{85}$ glassy alloy on ac-conductivity was investigated by Fouad et al. [78] and found the conductivity to be temperature dependent. The effect of both; the chalcogenide composition and the nature of the chemical bonding of Ge-Se-Ag samples are analyzed using a simple consideration based on coordination number. Electrical transport properties of amorphous $Se_{78-x}Te_{22}Bi_x$ films have been carried out by Khan et al. [79]. By alloying Bi to Se-Te base alloy, dark conductivity increases. Effect of Cu on the structure of Ge-Se is studied by Tecklenburg et al. [80]. They suggested that presence of Cu extinguishes the photoconductivity effect exhibited by Ge-Se_2. Density of defects increases with addition of Cu. Cu affects the defects (Ge-Ge bonds) but does not affect the Ge-Se_2 chain. Photoconductivity in $Se_{90}Ge_{10-x}In_x$ (x = 2, 4, 6, 8, 10) as studied by Singh et. al. [81] found that the conductivity is thermally activated process and activation energy is found to decreases with increasing intensity. Electrical and optical system on Pb modified amorphous Ge-Se-Te film was carried out by Pattanaik et al. [82] and they observed p to n type conduction was by the addition of 9 at. % lead. Activation energy and optical gap decreases with the addition of Pb content. Space charge limited conduction on $Se_{78-x}Te_{22}Bi_x$ ($0 \leq x \leq 4$) thin films has been studied by Khan et al. [83]. The density of states $N(E_F)$, calculated by fitting the data to the theory of SCLC assuming uniform distribution of localized state, increases with increasing Bi concentration. Effect

of Bi addition to Ge-Se on the ac-conductivity is studied by Singh et. al. [84]. The value of ac-conductivity decreases at low concentration of Bi (4 at. %) and increases at higher concentration of Bi (10 at. %) and the frequency exponent value decreases as the temperature increases. Electrical properties of amorphous $Se_{70}Ge_{30-x}M_x$ (x = 0, 5); (M = Ag, Cd, Pb) thin films have been investigated by Afifi *et. al.* [85]. They found that increase in conductivity with Pb is higher than that of Cd which in turn is higher than that of Ag. I-V curves of the investigated samples were analysed typically for a memory switch. In $(Ge_{20}Se_{80-x})_{1-x}Sn_x$ glassy alloys, the dc conducting measurements at high electric field have been studied. Non-ohmic behavior is observed. Experimental data confirms the presence of SCLC in this glassy material [86]. A peculiar role of Sn as an impurity in $Ge_{20}Se_{80-x}$ is studied. Saffarini et al. [87] used DSC to establish the heat capacity jump, ΔC_p at T_g [$\Delta Cp = C_{pl} - C_{pg}$, C_{pl} is C_p value of super cooled liquid and C_{pg} is of glassy state] for Ge-Se-In glasses and concluded that ΔC_p possess a local minimum in the vicinity of $< r > \approx 2.4$ (where $< r >$ is coordination number) *i.e.* minimum fragility. Thus strongest thermodynamic character is reached at about $< r > \approx 2.4$ or glass forming liquid has a minimum crystallization tendency by virtue of having reduced accessible structural or configurational reordering in the super cooled region. Thin amorphous chalcogenide films from the $GeSe_x$ (x = 1-5), $(GeSe_4)_{100-y}Ga_y$ and $(GeSe_5)_{100-y}Ga$ (Tl, B)$_y$ (y = 5, 10, 15, 20) systems have been prepared by thermal evaporation and characterized with respect to their internal stress using a cantilever technique [88]. The correlations between the stress, the composition and the structure of the films were investigated. The obtained results were related with some structural and mechanical parameters of the glasses like mean coordination number, number of constrains per atom,

density, compactness etc. With the addition of Ag in the Ge-Se glassy alloy, refractive index is found to increase with the subsequent decrease of optical band gap [89]. Effect of Bi impurity on the ac-conductivity of $Ge_{20}Se_{80}$ glassy alloy has been studied by Singh *et al.* [90]. The value of ac-conductivity decreases at low concentration of Bi (4 at. %) but increase for higher Bi content (10 at. %). DC conductivity and switching phenomenon of $Se_{80}Te_{20}$-xGe_x amorphous system has been investigated by Afifi *et al.* [91]. The observed switching phenomenon for these compositions was of memory type. Electrical measurements on $(Ge_{20}Se_{80})_{100-x}Cu_x$ has also been carried out by Thakur *et al.* [92]. They showed that value of dark conductivity and photoconductivity increases and activating energy decreases upto 1 at. % of Cu addition to $Ge_{20}Se_{80}$ glassy alloy. Photosensitivity increases and decay time constant decreases upto 1 at. % of Cu addition. With the further increase of Cu concentration (> 1 at. %), reverse trend takes place. Effect of In incorporation on the optical properties of $Se_{90}Ge_{10-x}In_x$ (x = 2, 4 and 6) thin films have been reported by Pandey *et al.* [93]. Authors have observed from optical transmission measurements that optical band gap decreases with In content while refractive index and real dielectric constant decreases with increasing wavelength. Marquez et al. [94] studied the optical dispersion and absorption of Ag-photodoped $Ge_xSb_{40-x}S_{60}$ chalcogenide glass thin films. The film thickness and optical constants, determined by envelope method and dispersion of linear refractive index of Ag-photodoped chalcogenide film is analyzed in terms of Wemple-DiDomenico oscillator model. Effect of Te on the Ge-Se glassy alloy has been studied by Sharma et al. [95, 96]. They found that optical gap decreases with increase of Te. With the increase in thickness, optical gap decreases. Pre-exponential factor of Arrhenius equation for the isothermal crystallization of Se-Ge, Se-In and Se-Te

chalcogenide glasses has been reported by Mehta et al. [97]. They observed the Meyer-Neldel rule between pre-exponential factor and activation energy of crystallization in these systems. Thermal stability and percolation threshold of $Ge_xSe_{100-x-y}Fe_y$ (y = 2, 4, 6) glasses as determined by DSC and DTA technique have been discussed by Saffarini et al. [98]. They observed that the maximum stability of network is just obtained if the percolation threshold limit is reached. The overall mean bond energies and their correlation with Tg have been investigated. Thermal stability and crystallization kinetics of $As_{14}Ge_{14}Se_{72-x}Sb_x$ glasses are studied using DSC by Dahshan [99]. The values of T_g and peak temperature of crystallization (T_p) are found to be dependent on heating rate and antimony content. They found that thermal stability decreases with increase of Sb content. Thermal properties of $GeSe_2$-As_2Se_3-CdSe glasses were investigated by DSC measurements. The dependence of T_g and thermal stability on glass composition were discussed by Zhao et al. [100]. Optical and thermo-mechanical properties of new Ge-Ga-Se-AgI glasses are studied by Roze et. al. [101]. They found that the possibility of shaping and drawing these glasses give them a great interest in ion exchange experiments to achieve gradient of refractive index. Thermally and optically induced irreversible changes in the optical gap and refractive index were investigated for sulphur rich and sulphur poor Ge-As-S system by Kincl et al. [102]. They found that with illumination, optical gap decreases and refractive index increases. The influence of light illumination on the optical parameters of Ge-Sb-Te thin films is studied by spectral ellipsometry in visible ranges of light. It was found that illumination of films leads to the decrease of refractive index. With the increase of Ge content, optical gap increases [103]. Glasses and glass-ceramics based on $GeSe_2$-Sb_2Se_3 and halides for far infrared transmission have

been studied by Calvez et al. [104]. They showed that shaped glass ceramics are still transparent and show improved mechanical properties. Seedek et. al. [105] studied the effect of laser irradiation on the electronic structure of a-$Ge_{36}Se_{64}$ films by detecting variation of bond length (r) and coordination number (CN). Variation of r and CN values induced by subsequent annealing of thin films has also been reported. Singh et. al. [106] and has shown that with the addition of Pb content to $Ge_{20}Se_{80}$ system, ac-conductivity and static permittivity increases. Effect of annealing on the optical and electrical properties of a-$Ge_{30}S_{10}Se_{60}$ thin films has been investigated by Aly et. al. [107]. Annealing at $T \leq Tg$ results in the slight increase in optical gap and dark activation energy, where as for $T > Tg$, optical gap and dark activation energy decreases with further increase of annealing temperature. Nano phase separation (observed by SEM, supported by XRD) and effect on the properties of Ge-As-Se chalcogenide glasses has been carried out by Xia et. al. [108]. They established that nano phase separation becomes more intensive when $< r > > 2.64$.

1.9 Selection of the Problem

Being a glass, chalcogenides are versatile platform mainly for optical devices. Main motivation of this thesis work is to carry out and expand the range of certain properties (mainly optical, electrical and thermal) of multicomponent chalcogenide glasses by the alteration of their chemical compositions. One of the most important properties of any amorphous solid is its optical properties. There are two reasons for this, (i) optical properties of crystalline semiconductor are well studied, so the optical properties of amorphous semiconductors can easily be related and compared. (ii) Optical properties are directly related to the structural and electronic properties of solids and hence very

important in device application. So, a detailed knowledge of some important and related parameters can provide huge information on material about their structure and optoelectronic behavior. These measurements give valuable information regarding the defect states and other mechanism responsible for electrical conductivity and photoconductivity behavior of alloy. These materials exhibit unique physical properties that make them good candidates for several potential applications such as infrared transmission and detection, threshold and memory switching *etc*. [109-110]. The addition of third element as an impurity has a pronounced effect on the optical, electrical and physical properties. Though some scattered literature is available on the Se-Te-Bi and Ge-Te-Bi system, but many features of these compounds still remain unexplored. There is no report on the detailed study of optical, electrical, thermal and physical properties of these systems in the literature to the best of our knowledge. In view of all these observations, we proposed to study the role played by metallic bismuth, belonging to group III of periodic table on Se-Te and Ge-Te glassy alloys in this thesis. The first system under investigation is $Se_{85-X}Te_{15}Bi_x$ (x = 0, 1, 2, 3, 4, 5) and second system is $Ge_{20}Te_{80-x}Bi_x$ (x = 0, 1.5, 2.5, 5.0). The aim of this study is to undertake a systematic investigation of these systems and to lighten some new features of their optical, electrical, thermal and physical behavior.

1.10. Outline of thesis

General introduction of amorphous semiconductors along with their classification is described in chapter I. Different band models for amorphous semiconductors are also discussed. A brief introduction of general properties of chalcogenides has been included. This section also includes the basic properties of Se-Te and Ge-Te glassy alloys.

Chapter 2 describes the experimental techniques used for the preparation of bulk glasses, cleaning of substrate, deposition of thin films and characterization of bulk and thin films for X-ray diffraction. Method for optical studies of thin films using UV-Vis-NIR transmission and reflection spectra has been included. This section also includes the technique for electrical and thermal measurements. Density measurement of bulk glasses has also been incorporated.

Chapter 3 describes the effect of Bi incorporation on the optical properties of $Se_{85}Te_{15}$ and $Ge_{20}Te_{80}$ glassy alloys. In the former Bi is incorporated by the simultaneous replacement of Se, whereas later includes the Bi incorporation by the replacement of Te. UV-Vis-NIR spectroscopy (transmission and reflection spectra) has been used for the analysis of optical properties. The refractive index and film thickness are calculated by using envelope method proposed by Swanepoel. The dispersion parameters E_d, E_0 and n_0 are discussed in terms of WDD model. The optical absorption in the given system seems to be of non direct type and the optical band gap is determined in the strong absorption region by using Tauc's extrapolation method. The behaviour of optical band gap is interpreted in terms of cohesive energy and electronegativity difference of the atoms involved. The dielectric constants and optical conductivity are determined for the system and they are found to follow the similar trend as that of refractive index.

In chapter 4 the electrical properties of $Se_{85-x}Te_{15}Bi_x$ and $Ge_{20}Te_{80-x}Bi_x$ glassy systems are studied. *I-V* characteristics are recorded and the conduction mechanism is studied qualitatively in the samples. The study of dark and photoconductivity of $Se_{85-x}Te_{15}Bi_x$ and $Ge_{20}Te_{80-x}Bi_x$ thin films as a function of temperature reveals that the conduction is through an activated process with single activation energy. Activation energy for

photoconduction is found to be much smaller than its value for dark conduction. Intensity dependent photoconductivity has also been studied and it shows the existence of bimolecular recombination in the thin films. The values of σ_{Ph}/σ_d and n_σ are calculated for the studied thin films at absolute temperature (303 K) within the intensity range 20-1085 lux. The transient photoconductivity measurements for investigating thin films at room temperature and 1035 lx intensity shows that the photocurrent rises in a monotonic manner up to a steady state value, and after cessation of illumination, it follows a non-exponential decay. An increase in the differential lifetime is also observed with time (for all compositions) as well as with the increase in the Bi concentration.

In chapter 5, the effect of Bi incorporation on the thermal and physical properties of $Se_{85}Te_{15}$ and $Ge_{20}Te_{80}$ glassy systems are studied. Differential scanning calorimetric technique (DSC) has been employed for thermal studies of $Se_{85-x}Te_{15}Bi_x$ chalcogenide glasses. On the other hand differential thermal analysis (DTA) technique has been employed to study the thermal behaviour of $Ge_{20}Te_{80-X}Bi_x$ glassy alloy. The DSC and DTA curves are analyzed for T_g, T_c and T_m. The glass transition temperature has been found to increase due to Bi addition. The specific heat capacity and change in heat capacity at glass transition is also evaluated and has been found that both the parameters decreases with increasing Bi concentration. Various physical parameters such as density, molar volume, number of atoms per unit volume, lone pair electrons and mean bond energy are also calculated and there behaviour with increasing Bi concentration is also investigated.

Finally Chapter 6 deals with the summary and overall conclusion of the work.

References

1. Ioffe A F 1951 *Bull. Acad. Sci. USSR* 15 447.

2. Kolomietes B T 1964 *Phys. Stat. Solidi* (b) **7** 359 713.

3. Mooser E and Pearson W B 1956 *Phys Rev* 101 1608.

4. Mooser E and Pearson W B 1960 *Progresses in semiconductors V* (London: Butterworth).

5. Marshall J M 1983 "Carrier Diffusion in Amorphous Semiconductors", *Report on Progress in Physics* 46 1235-1282.

6. Polischuk B T 1994 "*Interrupted Field Time-of-Flight Photoconductivity Technique and its Applications to Amorphous Semiconductors*", Ph.D. Thesis, University of Saskatchewan 21-22.

7. Anderson P W 1958 Phys. Rev. 109 1492.

8. Mott N F 1967 Adv. Phys. 16 49.

9. Cohen M H, Fritzsche H and Ovshinsky S 1969 Phys. Rev. Lett. 22 1065.

10. Mott N F 1966 Phil. Mag. 13 989.

11. Davis E A and Mott N F 1970 Phil. Mag. 22 903.

12. Mott N F 1971 Phil. Mag. 24 911.

13. Bhat N A, Sangunni K S and Rao K S R K 2003 J. Non-Cryst. Solids 319 192.

14. Sharma I, Tripathi S K, Monga A and Barman P B 2008 J. Non-Cryst. Solids 354 3215.

15. Marshall J M and Owen A E 1971 Phil. Mag. 24 1281.

16. Anderson P W 1975 Phys. Rev. Lett. 34 953.

17. Street R A and Mott N F 1975 Phys. Rev. Lett. 35 1293.

18. Kastner M, Adler D and Fritzsche F 1976 Phys. Rev. Lett. 37 1504.

19. Hilton A R 1970 J. Non-Cryst. Solids 2 28.

20. Ovshinsky S R 1968 Phys. Rev. Lett. 21 (20) 1450.

21. Popescu M 1978 Proc. Intern. Conf Amorphous Semiconductors '78' Pardubice, Czechoslovakia 1 185.

22. Phillips J C 1979 J. Non-Cryst. Solids 34 153.

23. Elliott S R 1986 J. Non-Cryst. Solids 81 71.

24. Yamane M and Asahara 2000 Glasses for photonics (Cambridge: University press).

25. Wang F, Mamedov S, Boolchand P, Goodman B and Chandrasekhar M 2005 Phys. Rev. B 71 174201.

26. Chakravarty S, Georgiev D G, Boolchand P and Micoulaut M 2005 J. Phys.: Condens. Mat. 17 L1.

27. Zakery A 2002 J. Phys. D: Appl. Phys. 35 2909.

28. Taeed V G, Baker N J, Fu L, Finsterbusch K, Lamont M R E, Moss D J, Nguyen H C, Eggleton B J, Choi D Y, Madden S and Luther-Davies B 2007 Optics Express 15 9205.

29. Trnovcona V, Furar I and Lezal D 2007 J. Non-Cryst. Solids 353 1311.

30. Lyubin V, Klebanov M, Feigel A and Sfez B 2004 Thin Solid Films 459 183.

31. Babeva Tz., Dimitrov D , Kitova S and Konstantinov I 2000 Vacuum 58 496.

32. Ganjoo A, Jain H, Yu C and Pantano C G 2006 J. Non-Cryst. Solids 352 584.

33. Fu L B, Fuerbach A, Littler I C M and Eggleton B J 2006 Appl. Phys. Lett. 88 081116.

34. Lankhorst M H R 2005 Nat. Mater. 4 347.

35. Lucovsky G. 1979 “Physics of Selenium and Tellurium”, ed. by Gerlach E and Grosse P, Springer-Verlag, New York.

36. Lucovsky G, and Galeener F L 1980 “Intermediate Range Order in Amorphous Solids”,*Journal of Non-Crystalline Solids* 35-36 1209-1214.

37. Kasap S O 1991 “Photoreceptors: The Selenium Alloys”, *Handbook of imaging materials*, ed. by Diamond A S, Marcel Dekker Inc., New York, 329-372.

38. Meek P E 1977 “Structural Interpretations of the Vibrational Spectra of Models of Amorphous As and Se”, *Proceeding of the Symposium on the structure of Non-Crystalline Solids*, ed. by Gaskell P H, Taylor and Francis Ltd., London 235-237.

39. Robertson J 1983 “Electronic Structure of Amorphous Semiconductors”, *Advances in Physics* 32 361-452.

40. Kastner M, Adler D and Frutzsche H 1983 “Valence-Alternation Model for Localized Gap States in Lone-Pair Semiconductors”, *Physical Review Letters* 37 1504-1507.

41. Kastner M “Amorphous and Liquid Semiconductors”, *Seventh International Conference on Amorphous and Liquid Semiconductors*, ed. by Spear W E University of Edinburgh, Edinburgh 504 1977.

42. Adler D 1977 “Amorphous Semiconductors”, *Scientific American* **236** 36-48

43. Abkowitz M 1967 “Changes in the Photoelectric Properties of Glassy Chalcogenides Induced by Chemical Doping, Irradiation, and Thermal History”,

Journal of Chemical Physics 46 4537.

44. Agarwal S C 1973 "Nature of Localized States in Amorphous Semiconductors: A Study by Electron Spin Resonance", *Physical Review B* **7** 685-691.
45. Elliot S R 1984 Physics of Amorphous Materials (New York: Longman).
46. Elliot S R 1986 "A Unified Model for Reversible Photostructural Effects in Chalcogenide Glasses", *Journal of Non-Crystalline Solids* 81 71-98.
47. Carles D, Lefrancois G and Larmagnac J P 1984 "A Model for Steady-State Photoconductivity in Amorphous Selenium", *Journal of Physics Letters* 45 L901-L906.
48. Tanaka K 1989 Phys. Rev. B 39 1270.
49. Bellisent R and Tourand G 1980 *Journal of Non-Crystalline Solids* 35-36 1221.
50. Tamura K, Inui M, Yao M, Endo H, Hosokawa S, Hoshino H, Katayama Y, Maruyama K 1991 J. Phys.: Condens. Mat. 3 7495.
51. Springett B E 1988 Phosphorous and Sulpher 38 341.
52. Betts F, Bienenstock A, Keating, D T 1972 J P de Neufville, *Journal of Non-Crystalline Solids* **7** 417.
53. Nath P, Suri S K, Chopra K L 1975 Phys. Stat. Solidi (a) 30 771.
54. Fukui K 1992 J. Phys. Soc. Jpn. 61 1084.
55. Kaban I, Halm Th, Hoyer W, Jovari P and Neuefeind J 2003 *Journal of Non-Crystalline Solids* 326-327 120.
56. I Kaban, E Dost, W. Hoyer.
57. Phillips J C 1981 J. Non-Cryst. Solids 44 17.
58. Kolomiets B T 1976 Thin Solid Films 34 1.

59. Kolomiets B T and Raspopova E M 1973 J. Non-Cryst. Solids 11 350.

60. Mott N F 1969 Phil. Mag. 19 835.

61. Kastner M 1972 Phys. Rev. Lett. 28 355.

62. Elliot S R 1977 Phil. Mag. 36 1291.

63. Kastner M 1978 Phil. Mag. B 37 127.

64. Dejus R J, Susman S, Volin K J, Montague D G and Price D L 1992 J Non-Cryst. Solids 143 162.

65. Benmore C J and Salmon P S 1993 J. Non-Cryst. Solids 156-158 720.

66. Saffarini G 1999 Phys. Stat. Soli. B 213 261.

67. Tohge N, Yamamoto Y, Minami T and Tanaka M 1979 Appl. Phys. Lett. 34(10) 640.

68. Rahman S and Sastry G S 1992 Mat. Sci. Eng. B 12 219.

69. Kumar S, Kashyap S C and Chopra K L 1986 J. Non-Cryst. Solids 85 100.

70. Rahman S, Muralidhar K V and Sastry G S 1993 Phys. Chem. Glasses 34 176.

71. Rahman S and Kumar K S 1996 Phys. Chem. Glasses 37 76.

72. Matsuda O, Ohba T, Murase K, Ono I, Grekos P, Kouchi T, Nakatake M, Tamura M, Namatame H, Hosokawa S and Taniguchi M 1996 J. Non-Cryst. Solids 198-200 688.

73. Murugavel S and Asokan S 1998 Phys. Rev. B 58 4449.

74. Rajagopalan T and Reddy G B 1999 Thin Solid Films 353 254.

75. Bhat N A and Sangunni K S 2000 Solid State Commun. 116 297.

76. Fadel M, Sedeek K and Hegab N A 2000 Vacuum 57 307.

77. Abdel-Aziz M M, El-Metwally E G, Fadel M, Labib H H and Afifi M A 2001

Thin Solid Film 386 99.

78. Fouad S S, Bekheet A E and Farid A M 2002 Physica B: Condensed Matter 322 163.

79. Khan M A M, Zulfequar M and Husain M 2003 J. Mater. Sci. 38 549.

80. Tecklenburg M M J, Larsen E, Lita B and Qadir D I 2003 J. Non-Cryst. Solids 328 40.

81. Singh S, Sharma R S, Shukla R K and Kumar A 2004 Vacuum 72 1.

82. Pattanaik A K and Srinivasan A 2004 Semicond. Sci. Technol. 19 157.

83. Khan M A M, Zulfequar M and Husain M 2005 Physica B 366 1.

84. Singh G, Sharma J, Thakur A, Goyal N, Saini G S S and Tripathi S K 2005 J. Optoelectron. Adv. Mater. 7(4) 2069.

85. Afifi M A, Fadel M, El-Metwally E G and Shakra A M 2005 Vacuum 77 259.

86. Singh R, Tripathi S K, Kumar S 2006 J. Non-Cryst. Solids 352 3230.

87. Saffarini G and Saiter J M 2004 J. Mater. Sci. 39 6141.

88. Popov C, Boycheva S, Petkov P, Nedeva Y, Monchev B and Parvanov S 2006 Thin Solid Films 496 718.

89. Thakur A, Singh G, Saini G S S, Goyal N and Tripathi S K 2007 Optical Materials 30 565.

90. Singh G, Goyal N, Saini G S S and Tripathi S K 2007 J. Non-Cryst. Solids 353 1322.

91. Afifi M A, Hegab N A, Atyia H E and Farid A S 2007 Journal of Alloys and Compounds doi: 10.1016/j.jallcom.2007.09.011.

92. Thakur A, Saini G S S, Goyal N and Tripathi S K 2007 J. Non-Cryst. Solids 353

1326.

93. Pandey V, Tripathi S K and Kumar A 2007 Physica B: Condensed Matter 388 200.

94. Marquez E, Gonzalez J M, Bernal-Oliva1 A M, Wagner T and Garay R J 2007 J. Phys. D: App. Phys. 40 5351.

95. Sharma P and Katyal S C 2007 Thin Solid Films 515 (20) 7966.

96. Sharma P and Katyal S C 2007 Mater. Lett. 61 4516.

97. Mehta N and Kumar A 2007 J. Mater. Sci. 42 490.

98. Saffarini G, Saiter J M and Matthiesen J 2007 Mater. Lett. 61 432.

99. Dahshan A 2008 J. Non-Cryst. Solids 354 (26) 3034.

100. Zhao D, Zhang X, Wang H, Zeng H, Ma H, Adam J L and Chen G 2008 J. Non-Cryst. Solids 354 1281.

101. Roze M, Calvez L, Ledemi Y, Ma H L, Lucas J and Zhang X H 2008 J. Optoelectron. Advance. Mater. 10 141.

102. Kincl M and Tichy L 2008 Mater. Chem. Phys. 110 322.

103. Pamukchieva V and Szekeres A 2008 Optical Material 30 1088.

104. Calvez L, Ma H L, Lucas J and Zang X H 2008 J. Non-Cryst. Solids 354 1123.

105. Sedeek K, Adam A, Balboul M R, Wahab L A and Makram N 2008 Mater. Res. Bull. 43 1355.

106. Singh G, Goyal N, Saini G S S and Tripathi S K 2008 Physica B:Condensed Matter 403 599.

107. Aly K A, Abousehly A M, Osman M A and Othman A A 2008 Physica B:Condensed Matter 403 1848.

108. Xia F, Baccaro S, Wang W, Pilloni L, Zang X, Zeng H and Chem G 2008 J. Non-Cryst. Solids 354 (12-13) 1137.

109. Saffarini G and Saiter J M 2004 J. Mater. Sci. 39 6141.

110. Savage J A 1985 Infrared Optical materials and their antireflecting coatings (London: A. Hilger).

CHAPTER 2

Experimental

2.1 Introduction

This chapter deals with the techniques used for the preparation and characterization of bulk samples and their corresponding thin films. A short theory background has been given in each case along with the reason for using that particular technique.

2.2 Bulk Glass Fabrication

Glass formation has been discussed for a long time from the view point of thermodynamics, kinetics and structural properties. The most convenient and conventional technique for the bulk glass formation is melt quenching. During quenching of molten material, the glass forming ability depends on viscosity of melt as the amorphous solid is formed by continuous hardening (increase in viscosity). On cooling, viscous liquid does not provide the atomic mobility necessary for forming crystallites. Glass formation from the rapid cooling melts requires prevention of the nucleation and growth process which is responsible for crystallization. The extent of glass forming region is slightly dependent on the quenching rate or the amount of material used in sample preparation. Amorphous materials can be prepared by several other techniques such as thermal quenching of melts, glow discharge, RF sputtering, chemical vapour deposition and sol-gel processes, but melt quenching was widely used technique to get bulk sample. The advantage of melt quenching technique over other techniques is the large flexibility of compositions. Since quenching of melt does not require stoichiometry among constituents, the preparation of glasses with a wide variety of compositions consisting of sometimes up to ten kinds of constituents at various ratios from a few to several ten of percent is possible.

In this experimental work melt quench method has been used to grow various samples of chalcogenide glasses. Chalcogenide glasses can be prepared by elemental precursors like S, Te, Se, Ge, As, Ga *etc*. and from compound precursors like sulphides and selenides. For obtaining high quality glasses, 5N pure raw materials are used. Prior to batching and melting, quartz ampoules (with outer diameter = 1.0 cm, inner diameter = 0.8 cm), were etched with chromic acid. The degreasing of these ampoules has been done by using tri-chloro-ethylene (TCE), acetone and methanol followed by thorough wash with double distilled water and then heat treated in vacuum for eight hours in order to remove adsorbed water and inorganic contaminants. First materials are weighed in batch of 4 g according to their atomic weight percentages followed by sealing of these materials in an evacuated (~ 10^{-4} Pa) quartz ampoule. Resulting chalcogenide glass melts have high vapour pressure at the melting temperature and so melting is carried out in a properly sealed system. Thus, after batching, the quartz ampoule is sealed off by an oxy fuel burner, while being evacuated to a vacuum ~ 10^{-4} Pa. For melting, the sealed ampoule is transferred to an electric furnace and heated gradually in steps at a heating rate of 3-4 ^{o}C / min to the melting temperature in order to prevent explosion due to high vapour pressure of the batch components. Melting temperature is maintained for 24 hours to make the melt homogeneous. The quenching was done in ice cold water to get the glassy alloys.

In case of $Se_{20}Te_{80-x}Bi_x$ the temperature of the furnace is raised to 300^{o}C for two hours, so that the Se (T_m = 217 ^{o}C) and Bi (T_m = 271 ^{o}C) diffuse into the rest of the constituents. The temperature is then raised to 600 ^{o}C, so that the Te (T_m = 450 ^{o}C) thoroughly mixes with other constituents. For $Ge_{20}Te_{80-x}Bi_x$, the temperature step is given at 300 ^{o}C (for Bi, T_m = 271 ^{o}C), at 500 ^{o}C (for Te, T_m = 450^{o}C) and finally 1000 ^{o}C, so that the Ge (T_m =

938 ^{o}C) thoroughly mixes with other constituents. The quenching was done in ice-cold water to get the glassy alloys. To ensure homogenization of viscous melts, the melt is agitated by rocking the quartz ampoule.

2.2 Thin Film Deposition

Development of techniques of producing and studying thin films, lead to better understanding of their optical, electrical, photoelectrical properties. There is an appreciable dependence of film properties on the condition of formation of thin films. Among the factors which are liable to influence the properties of thin films are; rate of deposition, velocity of impinging atoms, structure and condition of target surface, history of film between deposition and examination etc. Lack of information on these and many other variables which may determine the nature of film makes difficult to compare the results of various workers. Thin films of the materials can be prepared using various techniques; physical and chemical. Physical methods are vacuum evaporation, electron-beam evaporation, flash evaporation, RF sputtering, multi-source evaporation, ion beam evaporation, laser beam evaporation, resistive evaporation *etc*. Some chemical methods which essentially depend on electrical separation of ions, thermal effect or thermal growth are (i) anode electrolytic deposition (ii) chemical bath deposition (iii) cathode electrolytic deposition (iv) chemical vapour deposition and (v) plasma-enhanced chemical vapour deposition *etc*. The increasing use and study of thin films are in part due to the rapid strides which have been made in vacuum techniques. In the present work, thermal deposition in vacuum by resistive heating method is used. This is the most commonly used technique adopted for deposition of metals, alloys and also many compounds. The primary requirement for this method is a high vacuum deposition

system at a pressure of about 10^{-4} Pa or even less. The attainment of low pressure necessary for the production and study of films has been so facilitated that rapid progress has been made possible. Most widely used method of depositing films, particularly for use in optical system, is that of thermal evaporation. Prior to deposition of thin films, it is essential to clean the surface of the substrate because thin films readily adhere to a clean insulating surface. Tendency for the films to crack and peel increases, if the surface is contaminated with foreign impurities since the adhesion of the films is degraded. Cleaning of the substrate is done in three steps: (i) soap solution cleaning and (ii) cleaning with acetone (vapour cleaning) and (iii) with methanol. Soap solution cleaning basically involves scrubbing the substrate in the soap solution, then rinsing it thoroughly with double distilled water. This procedure is repeated 3 - 4 times for cleaning single substrate. Soap solution cleaning is used to remove any visible oil, grease and dust impurities. Vapour cleaning procedure is mainly used to remove the organic impurities, which are present on the surface of substrate. Acetone vapour is used for the removal of organic impurities. For the removal of inorganic impurities, methanol is used. After all this cleaning the substrates are subjected to dry in vacuum oven at a temperature approximately 110 ^{o}C and then put into deposition chamber. Fine powder of the material which has to be deposited is put into the flash cleaned molybdenum (Mo) boat. Flash cleaning is done by passing a heavy current through the boat so as to make it white hot or incandescent for a short period. Then the system was evacuated to a base pressure of 10^{-4} Pa. A shutter was incorporated in between the source and the substrate so that no vapor stream of the material can reach the substrate directly prior to attaining the required deposition conditions. After establishing the required source temperature, substrate

temperature and vacuum in the chamber, the shutter was removed to start the deposition of film on the cleaned substrate. When the required film thickness was obtained the shutter was brought back to the original position. Thin films were kept in the deposition chamber in the dark for 24 h to attain thermodynamic equilibrium as stressed by Abkowitz et al. [1]. The vacuum evaporation process was carried out in a coating system (HINDHIVAC model 12A4D India). The rate of evaporation of deposited thin films and thickness of the films deposited has been measured by thickness monitor (Model DTM-101). For the electrical measurements, indium electrodes were deposited using a mask so that the desired electrode gap is left for the deposition of thin films between the electrodes. Thin films of the required sample were deposited on to the electrode gap by passing low voltage and high current through the molybdenum (Mo) boat containing the material. These films of the glassy alloys are used to make the necessary electrical measurements. The films thus deposited are kept in the deposition chamber in dark for 24 hours so that the deposited films attain thermodynamic equilibrium before making any measurements on them. The deposition parameters are kept identical for all alloys (binary, ternary and quaternary) to make the analysis and comparison of the various properties, parameters and change in them under identical conditions.

2.3 Characterization of Thin Films

2.3.1 X-Ray Diffraction

XRD is presently the most widely used technique to characterize the amorphous nature of bulk glasses and their thin films. The powder method was used to check the nature (i.e. amorphous or polycrystalline or crystalline) of the bulk samples. The bulk samples were crushed to fine powder with a pestle and mortar and then this powder was used for taking

XRD pattern. Philips PW 1710 X-ray diffractometer (Radiation used was Cu-Kα, λ = 1.540598 Å, 40 KV and 25 mA) was used to plot the XRD patterns of the samples. Data acquisition was made in the 2θ range from 5^o to 60^o with a step size of 0.05^o. Thin films of the bulk samples deposited on the microscopic glass slides were also characterized to check the crystalline or amorphous nature of the films.

2.3.2 Optical Characterization

No material is fully transparent in all optical frequencies and hence there always be some absorption in some region of the spectra. When light is incident on a thin film some of its energy is reflected, some is absorbed and rest is transmitted. Thin films are studied more accurately by acquiring transmission instead of absorption as was the case for bulk glasses. The normal incidence transmittance and reflectance spectra in the spectral range 700–2400 nm of films were obtained by a double beam ultraviolet–visible–near infrared spectrophotometer (Perkin Elmer Lambda-750). All measurements were performed at room temperature (300 K). The spectrophotometer is set with a slit width of 1 nm in the spectral range. Therefore, it is unnecessary to make slit width corrections because of a small slit width value in comparison with different line widths. Typical interference fringes were obtained and the signal is used to calculate the refractive index dispersion curves using Swanepoel's technique [2] which is based on the approach of Manificier et al. [3]. This technique additionally allows the calculation of thickness of deposited thin films, optical absorbance and absorption coefficient.

2.3.2 Electrical Characterization

To carry out the various electrical measurements on the thin films (dc and photoconductivity measurements) at different temperatures, a specially designed metallic

sample holder is fabricated in the laboratory. Stainless steel is used for making the sample holder to take care of surface currents and unwanted disturbances in the measurements of small currents (pA). It also helps to provide proper shielding to the thin film samples for the accurate current measurements during various experimental observations. At low and high temperature, stainless steel is highly durable and corrosion free. The sample holder is fitted with a Chromel-Alumel thermocouple through teflon tape. During different measurements, this thermocouple gives the exact temperature reading to which thin film is subjected. The junction of the thermocouple is placed on copper block very near to thin film so that the chance of error in the temperature measurement of thin film is very rare. A small circular glass window is installed in the sample holder directly above the space at which film is placed on the copper block. This copper block is connected to the base of the sample holder through a copper rod. By this arrangement, the temperature gradient is very small between the copper block and base of the sample holder. The light could be shone through out the

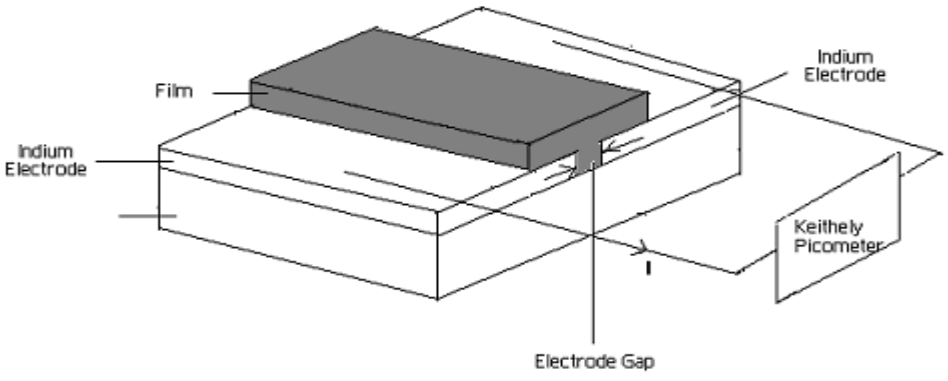

Figure 2.1 Circuit diagram showing electrode / films configuration

photoconductivity measurements on thin films. To cut off the IR part of the light, water in transparent petri dish is kept above the glass window while taking the various photoconductivity measurements. The Cu block from lower side is fitted with heater to anneal the films and to study their behaviour with rise in temperature. These heaters are connected to a variac through Teflon feed from outside the sample holder to vary the rate of heating. The rate is monitored through the display of the digital panel meter which is connected to the thermocouple. Predeposited thick indium electrodes on well-degassed Corning 7059 glass substrates have been used for the electrical contacts. A planar geometry of the film (length ~ 1.78 cm; electrode gap ~ 8×10^{-2} cm, shown in figure 2.1) is used for the electrical measurements. A dc voltage (0-300V) was applied across the sample and the resulting current was measured by a digital picometer (Keithley, model 6487). The intensity of light is measured using a digital Luxmeter (TES-1332). Photocurrent (I_{ph}) is measured after subtracting the dark current (I_d) from the current measured in the presence of light (I). The sample holder is connected to rotary vacuum pump to maintain a vacuum ~ 10^{-3} mbar throughout the measurements. The pressure inside the sample holder is measured by using a vacuum gauge that is connected to the sample holder. These measurements are also carried out in a vacuum ~ 10^{-5} mbar using an oil diffusion pump but the results are found to be same in both the cases. Thin films of the glassy alloys after deposition and attainment of the thermodynamic equilibrium on being characterized for their amorphous nature using XRD are mounted on the sample holder as mentioned earlier. Various electrical and photoconductivity measurements are carried out in the same sample holder in continuity without disturbing the particular film under investigation. The present measurements are found to be of the same nature in the

films deposited in different runs. Therefore, the conclusion of the present work will not be much affected by the surface effects, as most of the explanations given are qualitative in nature. The deposition parameters are kept almost identical in case of binary, ternary and quaternary systems so that a comparison of the results could be made for almost identical conditions. This confirms that the composition of the evaporated films is not very different from the corresponding glassy alloys prepared by quenching techniques.

2.3.3 Thermal characterization

All the amorphous solids are thermodynamically unstable and tend to relax towards a stable or metastable phase. The time scale on which these changes occur varies enormously is usually a sensitive function of temperature. A class of non-crystalline solids prepared from the liquid state is called glass. These are characterized by being structurally continuous with liquid state and are prepared by quenching the molten liquid to a temperature far below their equilibrium melting point without crystallizing and can remain in their metastable states indefinitely. When the temperature decreases from the liquid phase, some materials do not crystallize below their melting point, but they become a super cooled liquid. As the temperature keeps decreasing, glass transition occurs at a certain temperature, "T_g" below which they become glass. The thermal behaviour is recorded using Differential Scanning Calorimetric (DSC) or Differential Thermal Analysis (DTA) technique.

DSC / DTA is a technique for measuring the energy necessary to establish a nearly zero temperature difference between a substance and an inert reference material, as the two specimens are subjected to identical temperature regimes in an environment heated or cooled at a controlled rate. There are two types of DSC systems in common use (figure

2.2). In power-compensation DSC the temperatures of the sample and reference are controlled independently using separate, identical furnaces. The temperatures of the sample and reference are made identical by varying the power input to the two furnaces; the energy required to do this is a measure of the enthalpy or heat capacity changes in the sample relative to the reference.

In heat flux DSC, the sample and reference are connected by a low-resistance heat-flow path (a metal disc). The assembly is enclosed in a single furnace. Enthalpy or heat capacity changes in the sample cause a difference in its temperature relative to the reference; the resulting heat-flow is small compared with that in differential thermal analysis (DTA) because the sample and reference are in good thermal contact. The temperature difference is recorded and related to enthalpy change in the sample using calibration experiments.

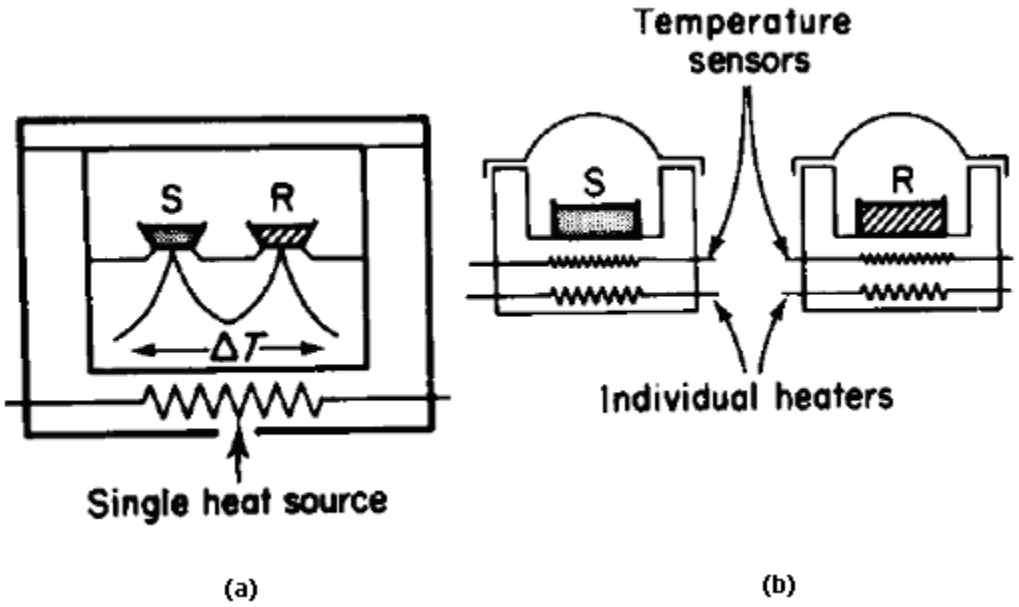

Figure 2.2 (a) Heat-flux DSC; (b) power-compensation DSC

For $Se_{85-x}Te_{15}Bi_x$ system is thermal behavior of the sample is recorded using Mettler Toledo Star^e DSC system. In each study approximately 10 mg bulk material is used. DSC runs are taken at four heating rates (5, 10, 15, 20 K min^{-1}) for each of the composition so as to get (T_g), (T_p) and (T_m) for the system. However in case of $Ge_{20}Te_{80-x}Bi_x$ system thermal behaviour is recorded using Shimadzu DTG-60. DTA has been performed for second series because of its more versatility than DSC at higher temperature.

References

1. Abkowitz M, Foley G M T, Markovics J M and Palumbo A C 1984 Optical Effects in amorphous Semiconductors (AIP Conf. Proc. vol 120) ed. Taylor P C and Bishop S G (New York: American Institute for Physics) 117.

2. Swanepoel R 1983 J. Phys. E : Sci. Instrum 16 1214.

3. Manificier J C, Gasiot J and Fillard J P 1976 J. Phys. E: Sci. Instrum 9 1002.

CHPTER 3

Effect of Bi incorporation on optical properties of Se-Te and Ge-Te glassy alloys

3.1 Introduction

There are numerous applications in science and technology for optical coatings, such as communication, sensing, imaging and display. So while designing and manufacturing the optical coatings and devices, it is essential to know the various parameters of the coating materials; such as refractive indices, absorption coefficients and optical band gap. In recent years, the optical memory effects in chalcogenide semiconducting films have been investigated and utilized for various applications. The chalcogenide vitreous semiconductors exhibits excellent optical properties like transmittance in the infrared region (in the wavelength regions 3-5 μm and 8-14 μm), continuous shift in the optical absorption edge and the variation in refractive index under the influence of light. These properties also have a very strong correlation with the corresponding chemical composition of chalcogenide, which explains the significant interest in these amorphous materials for the manufacture of filters, anti reflection coatings and in general, a wide variety of optical devices [1-3]. Due to their high refractive index (ranging between 2.0 and 3.5) and optical band gap lying in the sub-band gap region, chalcogenide glasses are used as core materials for optical fibres which is further used for transmission, especially when short length and flexibility is required [4-6]. Impurity effects in chalcogenide glasses have importance in fabrication of glassy semiconductors. These impurity atoms are supposed to satisfy all the valence requirements when they enter the glassy network and therefore not supposed to play the role of acceptors or donors. The effect of impurity atoms in chalcogenide glasses depends upon the composition of the glasses, the chemical nature of impurity, and the value of impurity concentration. Several authors [7-9] have reported the impurity effects in various chalcogenide glasses. Amorphous selenium has been investigated extensively due to its wide commercial applications. Its applications

like rectifiers, photocells, xerography and switching and memory etc. made it very attractive in the field of devices. Pure Se has short lifetime and low sensitivity. This problem can be overcome by alloying it with certain elements which in turn gives high sensitivity, high crystallization temperature and smaller aging effects [10, 11]. The substitution of Te for Se partly breaks up the Se_8 ring structure and increases the chain fraction. More recently it has been pointed out that Se-Te has some advantages over amorphous Se as for as their use in xerography is concerned [12]. The addition of third element expands the glass forming area and also creates compositional and configurational disorder in the system. The addition of impurities like Bi has produced a remarkable change in the optical and electrical properties of chalcogenide glasses. The conductivity of chalcogenide glasses changes from p to n type due to Bi addition [13-16]. An increasing concentration of Bi in Se-Te glassy alloy is responsible for the band tailing and broadening of valence band which is further known to reduce the width of optical band gap. One of the most advantageous characteristics of these materials is in 'phase change optical memory' technology. Phase change recording materials are designed to have at least two structural forms; amorphous and crystalline, which can coexist at room temperature. Phase change applications utilize differences in optical and electrical properties between the amorphous and crystalline phases of the same material. While optical storage applications utilize small differences (approximately 20 %) in the reflectivity [17], electronic applications utilize a large difference (a factor approximately 10^3) in electrical conductivity [18]. These materials can be optically switched between the amorphous and crystalline states by the energy contained in a laser beam. Infrared optical fibers operating at 2-12 μm wavelength region are required for infrared sensing applications such as radiometric thermometry and CO_2 laser power applications such as

laser surgery [19]. Te based chalcogenide glasses are used for such applications because their infrared absorption edges is located in a wavelength region above 12 μm [20]. However, only a few compositions such as Ge-Te and As-Te based glasses have been investigated as memory switching glasses [21-25]. Impurity effects in chalcogenide glasses have importance in fabrication of glassy semiconductors. These impurity atoms are supposed to satisfy all the valence requirements when they enter the glassy network and therefore do not play the role of acceptors or donors. The effect of impurity atoms in chalcogenide glasses depends upon the composition of the glasses, chemical nature of impurity and the value of impurity concentration. Several authors [26-28] have reported the impurity effects in various chalcogenide glasses. We have chosen $Ge_{20}Te_{80}$ as base composition which is just at the stiffness threshold with coordination number 2.4 and Bi as dopant. The composition $Ge_{20}Te_{80-x}Bi_x$ can be taken as phase separated glasses with glassy Bi_2Te_3 clusters embedded in the background matrix of $GeTe_2$ and Te chains or layers. As Bi concentration is increased in the binary alloy $Ge_{20}Te_{80}$, the Bi_2Te_3 clusters having tetradymite structure find themselves in a matrix of increased mechanical rigidity. These types of structural changes have a numerous effect on the optical parameters like refractive index and optical band gap.

An increasing concentration of Bi in Se-Te and Ge-Te glassy alloy is responsible for the band tailing and broadening of valence band which is further known to reduce the width of optical band gap. The aim of the present chapter is to study the effect of Bi incorporation on the optical properties of Se-Te and Ge-Te matrix. Various optical parameters are determined by using the transmission spectra for $Se_{85-x}Te_{15}Bi_x$ and, transmission and reflection spectra for $Ge_{20}Te_{80-X}Bi_x$ chalcogenide thin films.

3.2 Experimental Details

Bulk samples of $Se_{85-x}Te_{15}Bi_x$ and $Ge_{20}Te_{80-X}Bi_x$ alloys were prepared using melt quench technique as discussed in chapter 2. Thin films of the alloys were prepared by thermal evaporation technique [Vacuum coating unit HINDHIVAC 12A4D Model] at room temperature and base pressure of $\sim 10^{-4}$ Pa using a molybdenum boat. The thickness of the deposited films has been measured by thickness monitor (DTM-101). Amorphous nature of the bulk samples and thin films were confirmed by XRD technique. No prominent peak was observed in the bulk as well as in films. The normal incidence transmittance spectra has been taken for $Se_{85-x}Te_{15}Bi_x$ thin films in the spectral range 700–2400 nm and transmission and reflectance spectra in the spectral range 700–2400 nm for $Ge_{20}Te_{80-X}Bi_x$ thin films using a double beam ultraviolet–visible–near infrared spectrophotometer (Perkin Elmer Lambda-750). All measurements were performed at room temperature (300 K). Repeated characterizations on the thin films of same composition (grown at different times), were carried out and the results only varied within ± 1-2 %. All optical measurements were performed at room temperature (300 K).

3.3 Methods to determine optical properties

A light beam experiences both refraction and dispersion as it passes through some medium. Refraction occurs when the direction of light beam is bent at all interfaces and dispersion occurs when the degree of bending depends on the wavelength. The techniques used to calculate the optical parameters like refractive index (n), extinction coefficient (k), absorption coefficient (α), thickness of thin film (d) and optical band gap (E_g) are described below.

3.3.1 Refractive Index and Extinction Coefficient

The index of refraction (n) of a material is defined as the ratio of velocity of light in a vacuum (c) to the velocity of light in the medium (v) *i.e.* $c = n / v$. The magnitude of n or

the degree of bending will depend on the wavelength of light and this effect is graphically demonstrated by the familiar dispersion of a beam of white light. Not only does the index of refraction affect the optical path of light, but it also influences the fraction of incident light that is reflected at the surface. The refractive index is given by

$$n = c/v = \frac{\sqrt{\mu\varepsilon}}{\sqrt{\mu_0\varepsilon_0}} = \sqrt{\varepsilon_r\mu_r} \tag{3.1}$$

where μ and e are permittivity and permeability respectively. Phenomenon of refraction is related to electronic polarization of relatively high frequencies for visible light; thus the electronic component of the dielectric constant may be determined from the index of refraction. Since the retardation of electromagnetic radiation in medium results from electronic polarization, the size of the constituent atoms or ions have a considerable influence on the magnitude of this effect. Generally, the larger an atom or ion, the greater will be the electronic polarizability, the slower the velocity and greater the index of refraction. From the Maxwell's equations, the complex refractive index (n^*) related to complex dielectric constant can be resolved into real and imaginary components as It is customary to define n as the refractive index and k as the extinction coefficient or absorption index. This index is a function of the wavelength, so that two beams with different colours (or frequencies) travel at different speeds. The knowledge of accurate value of wavelength dependent refractive index of the thin films is very important from technological point of view. It yields fundamental information for the design and modelling of optical components and optical coating such as interference filters. There are various methods to estimate the optical parameters n and k but here we are concerned only with those which are applicable to thin films only. Since films are not self supporting, a suitable supporting substrate is used for deposition. This results in a system

consisting of three dielectrics namely air, film and substrate. It is also possible that both the film and substrate may be transparent or partly opaque to the incident light. Hence the methods will considerably depend on the optical nature of film. There are number of methods for the calculation of optical constants of thin films like depending on the mode used such as (i) both reflection and transmission (ii) only reflection (iii) only transmission as discussed below

(i) Reflection and Transmission Method

In this method both reflectance and transmittance are used to measure the optical constants separately. Reflectance (R) and transmittance (T) are measured at normal incidence. Transmittance is given by the relation

$$T = \frac{16 n_s (n^2 - k^2) \exp(-4\pi k d/\lambda)}{\{(n+1)^2 + k^2\}\{(n_s + n)^2 + k^2\}} \tag{3.2}$$

where n and n_s are the refractive indices of thin film and substrate respectively. d is the thickness of thin film. Further T and R are related by the following relation

$$T = (1 - R^2)\exp(-4\pi k d/\lambda) \tag{3.3}$$

Extinction coefficient can be determined from the variation of T with film thickness given by the relation

$$k = -\frac{2.303 * \lambda}{4\pi d}\log T \tag{3.4}$$

(ii) Reflection Method

In this case reflectance from an absorbing surface is measured at normal incidence. n and k are estimated roughly with the help of following relation

$$R = \frac{(n-1)^2 + k^2}{(n+1)^2 + k^2} \tag{3.5}$$

If $(n-1)^2 >> k^2$, then n can reasonably be determined from R. However a second measurement at another angle of incidence is necessary for evaluation of n and k.

(iii) Transmission Method

Transmission method which was basically proposed by J. C. Manificier [29] and extended by Swanepoel [30] is easiest to apply, if thin film does not show much localised absorption band in between interference extremes. Thin films show very low absorption so that interference fringes are visible. Film should have optical thickness high enough (> 400 nm) to yield a few interference extremes for visible and near infrared spectra. This method considers only transmission spectra of thin films for the calculation of optical parameters. Swanepoel's method has advantage due to its non-destructive nature and yields the dispersion relation over a large range of wavelength without any prior knowledge of film's thickness and no parameters have to be introduced. Consider a thin film having thickness d and complex refractive index $n^* = n - ik$, where n is the real part of the refractive index and k is the extinction coefficient. The index of the surrounding air is $n_a \approx 1$. The glass substrate is several orders of magnitude thicker than the film and has a refractive index s =1.51. All the multiple reflections at the three interfaces, (figure 3.1), are taken into account when calculating transmittance T. If the thickness d is uniform and comparable with wavelength of light which goes through the thin film,

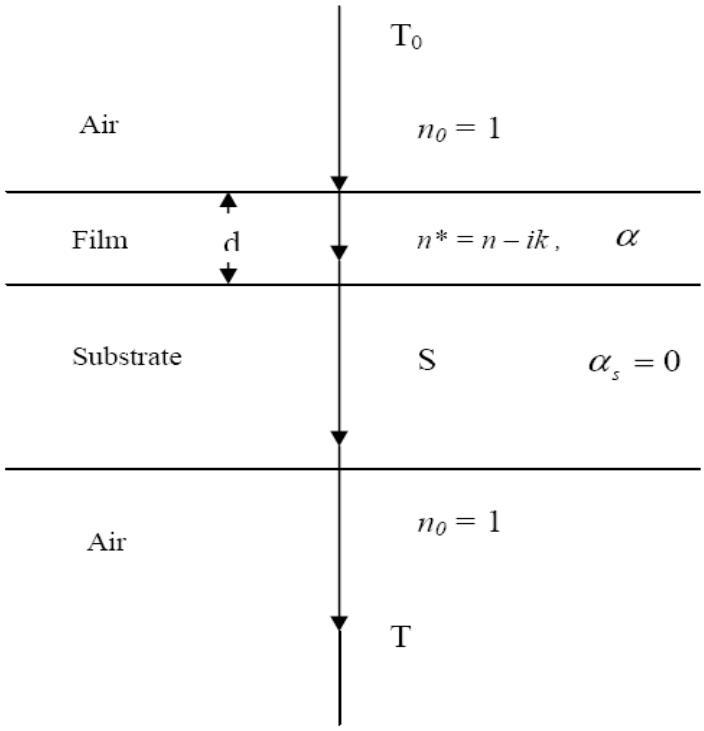

Figure 3.1 System of an absorbing thin film on a thick finite transparent substrate

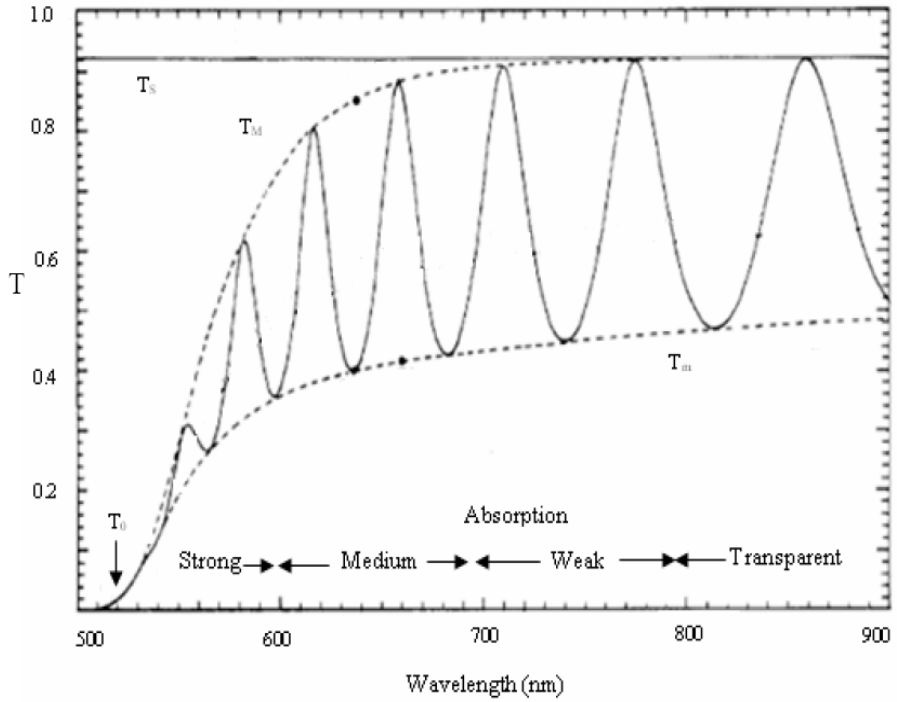

Figure 3.2 Different absorption regions in the transmission spectrum.

interference effect gives rise to a typical spectrum as shown in figure 3.2. Beginning at the long wavelength end and moving to shorter wavelength, we can divide the spectrum following Swanepoel [30] into different regions according to their transmission intensities. In the transparent spectral region of the film $\alpha \approx 0$, the transmission is determined by n and s through multiple reflections. In the region of weak absorption, α is small so the transmission starts to decrease. In the region of medium absorption, α is large and hence determines the overall transmission. In the region of strong absorption, the transmission decreases drastically almost exclusively due to the influence of α. In the transparent region, transmission fringe minima T_m can be used to calculate the refractive index of the film which is given by

$$n = \left[N + \left(N^2 - s^2\right)^{1/2}\right]^{1/2} \tag{3.6}$$

where

$$N = \frac{2s}{T_m} - \frac{(s^2+1)}{2} \tag{3.7}$$

In the region of weak and medium absorption, where $\alpha \neq 0$, transmittance decreases mainly due to the effect of absorption coefficient, α and eqn. (2) modifies to

$$N = \frac{2s(T_M - T_m)}{T_M T_m} + \frac{s^2+1}{2} \tag{3.8}$$

where T_M is the transmission maximum.

This optical characterization method provides values for refractive index of films at particular wavelengths where transmission spectra are tangential to their corresponding top and bottom envelops. A distinct advantage of using the envelopes of the transmission spectrum rather than only the transmission spectrum is that the envelopes are slow-

changing functions of wavelength (λ), whereas the spectrum oscillates rapidly with λ. In the strong absorption region, the transmittance decreases drastically due to the influence of α and the refractive index can be estimated by extrapolating the values of n calculated in the other regions of the spectrum. Thus we can evaluate the spectral dependence of the absorbance (x) and finally spectral dependence of absorption coefficient α. Therefore, we first apply Cauchy's formula [30] to estimate n

$$n = A + \frac{B}{\lambda^2} \tag{3.9}$$

where A and B are material dependent constants. Therefore, the resulting solid line of n in interference region is extrapolated onto the refractive index axis to obtain the value of n in strong absorption region [31] and then the value of absorbance can be calculated from

$$x = \frac{(n+1)^3(n+s^2)}{16n^2 s} T_0 \tag{3.10}$$

where T_0 represents the transmission in the region of strong absorption. In the region of weak and medium absorption using the transmission maxima, x can be calculated by

$$x = \frac{E_M - \left[E_M^2 - (n^2-1)^3(n^2-s^4)\right]^{0.5}}{(n-1)^3(n-s^2)} \tag{3.11}$$

where

$$E_M = \frac{8n^2 S}{T_M} + (n^2-1)(n^2-s^2) \tag{3.12}$$

The extinction coefficient also called absorption index is a measure of the fraction of light lost due to scattering and absorption per unit distance of the participating medium. The extinction coefficient (k) can be calculated using the relation

$$k = \frac{\lambda}{4\pi d} \ln(1/x) \tag{3.13}$$

where d is the thickness of the film.

3.3.2 Thickness of Film

Thickness of film can be determined from the envelope method proposed by Swanepoel [30]. If n_1 and n_2 are the refractive indices of two adjacent maxima or minima at wavelengths λ_1 and λ_2, then the thickness d of the film is given by

$$d_1 = \frac{\lambda_1 \lambda_2}{2(\lambda_1 n_2 - \lambda_2 n_1)} \tag{3.14}$$

3.3.3 Absorption Coefficient and optical band gap

An electronic transition between the valence and conduction bands in the crystal starts at the absorption edge which corresponds to the minimum energy difference between the lowest minimum of the conduction band and highest maximum of the valence band. If these extreme lie at the same point of the k-space then the transition is called direct. If this is not the case, the possible transitions are phonon assisted and are called indirect. In most of the amorphous compound semiconductors, the absorption curve appears similar. Optical absorption is characterized in terms of the absorption coefficient α. It is crucial to determine the absorption characteristics of glasses and thin films, especially when comes to optical materials in order to evaluate their potential applications. When light is incident on a thin film, some of its energy is reflected, some is absorbed and rest is transmitted. The optical absorption of thin films varies with thickness and wavelength and is a function of its physical and chemical structure. The absorption coefficient α measures the spatial decrease in intensity of a propagating beam of light due to progressive conversion

of the beam into different forms of energy. The values of absorption coefficient from the transmission spectra have been calculated using the equation.

$$\alpha = \left(\frac{1}{d}\right) \ln \frac{1}{x} \tag{3.15}$$

where *d* is the thickness of the film and *x* is the absorbance. The absorption coefficient of chalcogenide glasses is known to change rapidly for photon energies close to their band gap and for many glassy and amorphous non-metallic materials, the absorption edge can be divided into three regions;

(a) High absorption region ($\alpha = 10^4\ \text{cm}^{-1}$) which involves the optical transition between valence band and conduction band and determines the optical band gap. The absorption coefficient in this region is given by using Tauc relation [32]

(b) Spectral region with $\alpha = 10^2 - 10^4 cm^{-1}$ is called Urbach's exponential tail region in which absorption depends exponentially on photon energy and is given by.

$$\alpha h\nu = \alpha_0 \exp\left(h\nu / E_e\right) \tag{3.16}$$

where α_0 is a constant and E_e is interpreted as band tail width of localized states which generally represents the degree of disorder in amorphous semiconductor [33].

(c) The region $(\alpha \le 10^2 cm^{-1})$ involves low energy absorption and originates from defects and impurities.

The band gap is the energy difference between the lowest minimum of the conduction band and highest maximum of the valence band is called the band or forbidden gap or simply energy gap. When this energy gap is calculated using optical methods then it is called optical band gap. The optical band gap of most of the chalcogenide glasses varies in the range 0.7 to 3.0 eV [34]. By knowing the values of absorption coefficient, optical

band gap can be calculated by the method proposed by Tauc [32]. For different transitions from valence to conduction band the following relation is used;

$$\alpha h\nu = B(h\nu - E_g)^p \qquad (3.17)$$

where E_g is defined as optical energy gap and B is a constant related to band tailing parameter. In the above equation $p = 1/2$ for a direct allowed transition, $p = 3/2$ for direct forbidden transition, $p = 2$ for an indirect allowed transition and $p = 3$ for indirect forbidden transition. This relationship allows us to estimate the value of optical band gap by plotting $(\alpha h\nu)^{0.5}$ against $h\nu$. The value of E_g can be estimated by the intercept of the extrapolations to zero absorption with the photon energy axis $(\alpha h\nu)^{0..5} \rightarrow 0$

3.4 Results and Discussion

3.4.1 Optical properties of $Se_{85-x}Te_{15}Bi_x$ (x = 0, 1, 2, 3, 4, 5) system

3.4.1.1 Refractive index: WDD model

The transmission spectra of thin film samples under study are plotted in figure 3.3. The plot shows fringes due to interference at various wavelengths. A continuously oscillating maxima and minima at different wavelengths confirm the optical homogeneity of deposited thin films. According to Swanepoel's method, the envelope of the interference maxima and minima of transmission spectra can be used for deducing optical parameters *viz*. the values of the thickness (*d*), refractive index (*n*) and extinction of the thin films. The thickness of the films calculated from the transmission spectrum is reported in table 3.1. The variation of n and k with wavelength for different composition of $Se_{85-x}Te_{15}Bi_x$, glassy alloys is shown in figures 3.4 and 3.5 respectively. It is clear from figure that n decrease with increase in the wavelength.

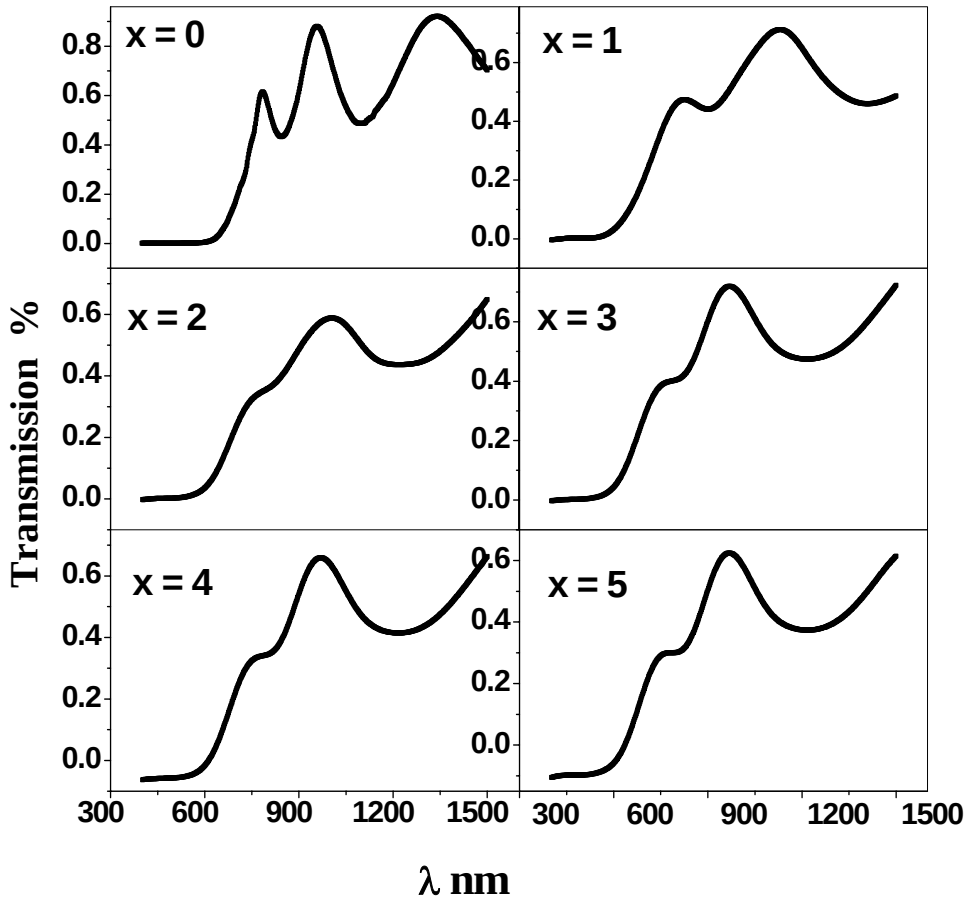

Figure 3.3 Plot of optical transmission versus wavelength for $Se_{85-x}Te_{15}Bi_x$ thin films.

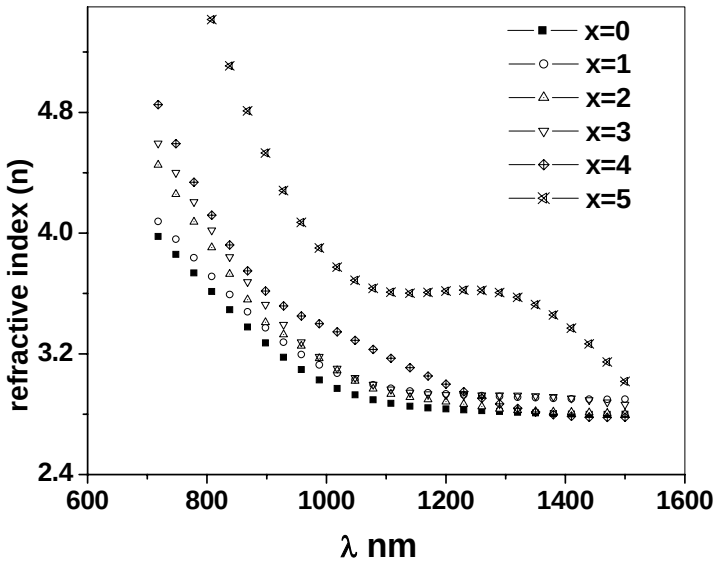

Figure 3.4 Plot of refractive index (n) versus λ (nm) for $Se_{85-x}Te_{15}Bi_x$ thin films.

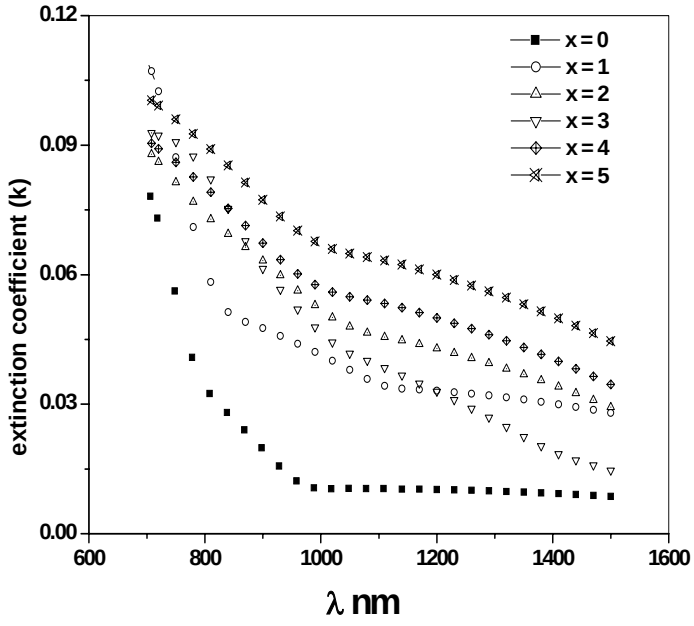

Figure 3.5 Plot of extinction coefficient (k) versus λ (nm) for $Se_{85-x}Te_{15}Bi_x$ thin films.

This behaviour is due to increase in transmittance and decrease of absorption coefficient with wavelength. The decrease in refractive index with wavelength shows the normal dispersion behaviour of the material. It is also evident from figure 3.4 that with the increase of Bi content n increases. This increase is related to the increased polarizability of the larger Bi atomic radius 1.46 Å compared to the Se atomic radius 1.16 Å [35]. The calculated value of n for thin films under study typically at 1100 nm is also stated in table 3.1. The spectral dependence of the refractive index has been analyzed in terms of Wemple-DiDomenico (WDD) model [36], which is based on the single effective oscillator approach having the expression

$$n^2 - 1 = \frac{E_d E_0}{{E_0}^2 - (h\nu)^2} \tag{3.18}$$

where $h\nu$ is the photon energy, E_0 is the single oscillator energy (also called average energy gap) and E_d is the dispersion energy which is a measure of average strength of the interband optical transitions. The oscillator parameters are determined by plotting refractive index factor $(n^2-1)^{-1}$ versus $(h\nu)^2$ and by fitting a straight line to the points as shown in figure 3.6. In figure 3.6, slope = $(E_0 E_d)^{-1}$ and the intercept on vertical axis $=(E_0 / E_d)$. The value of E_d and E_0 are calculated using these two relations and are listed in table 3.1 and table 3.2 respectively. The parameter E_d is related to other physical parameters by simple empirical relation proposed by WDD model *i.e.* $E_d = \beta N_c Z_a N_e$,where β is a two valued constant with either an ionic or covalent value ($\beta = 0.26 \pm 0.03 eV$ for ionic materials and $\beta = 0.37 \pm 0.04 eV$ for covalent materials), N_c is the effective *C. N.*

Table 3.1

Values of refractive index (n), extinction coefficient (k) and dispersion energy (E_d), are given at 1100 nm and static refractive index (n_0), band tailing parameter (E_e), and average thickness (d) for $Se_{85-x}Te_{15}Bi_x$ (x = 0, 1, 2, 3, 4, 5) thin films.

x	***n***	k	$\bar{d}_1$ (nm)	$\bar{d}_2$ (nm)	$E_d\,(eV)$	n_0	$E_e\,(eV)$
0	2.88	0.0104	445	439	15.16	2.58	0.28
1	2.90	0.0349	477	468	15.78	2.67	0.40
2	2.94	0.0460	456	464	15.95	2.72	0.47
3	2.98	0.041	497	488	16.06	2.76	0.56
4	3.18	0.054	470	464	16.20	2.79	0.69
5	3.62	0.0637	498	492	16.70	2.83	0.89

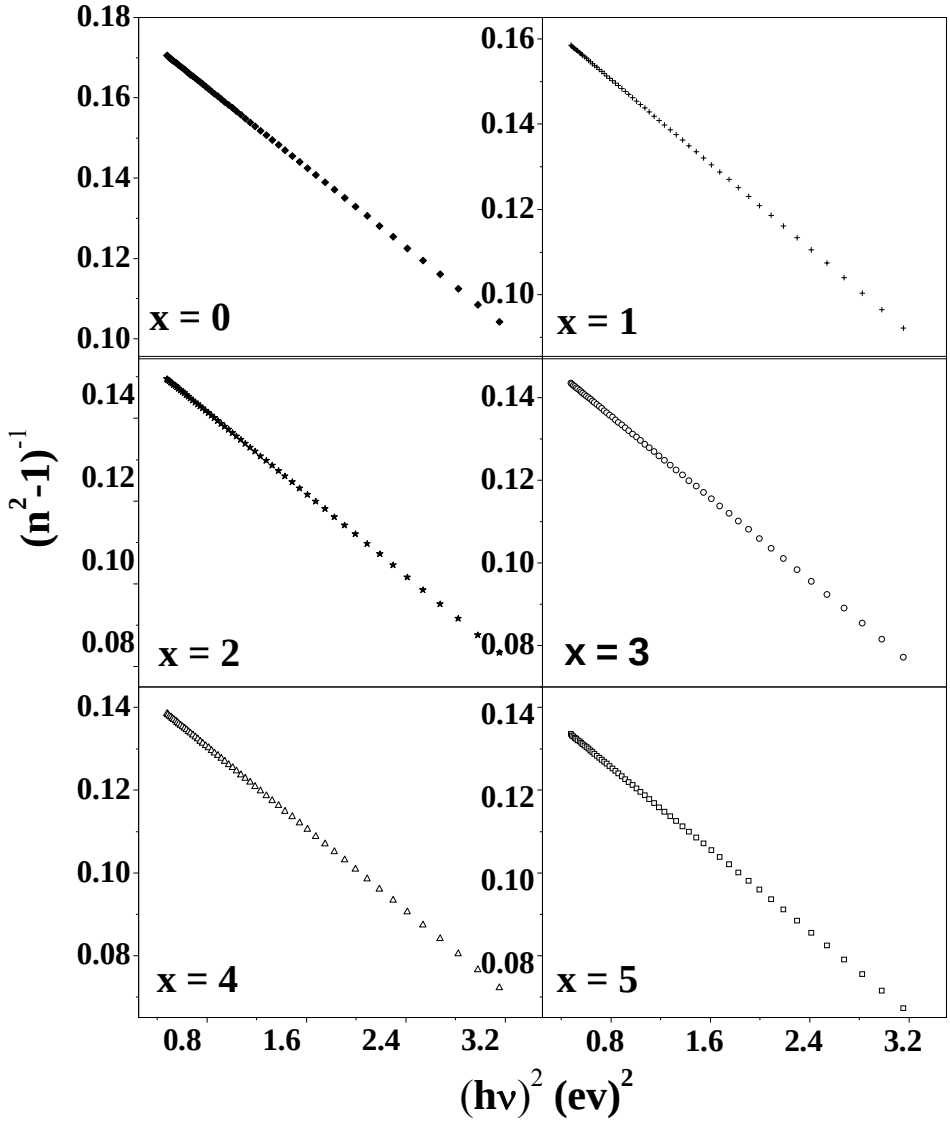

Figure 3.6 Plot of (n^2-1) versus $(h\nu)$ for $Se_{85-x}Te_{15}Bi_x$ thin films.

(coordination number) of the cation nearest neighbour to anion, Z_a is the formal chemical valance of the anion and N_e is the effective number of valence electrons per anion. The increase in the observed value of E_d with Bi content is only due to the increase in the value of N_c and N_e. The single oscillator energy E_0, also known WDD gap corresponds to the distance between centres of gravity of the valence and conduction band. It is therefore related to the average bond strength or cohesive energy of the system. The cohesive energy (CE), defined as stabilization energy of an infinitely large cluster of the material per atom is determined by summing the bond energies of the consequent bonds expected in the material. This behaviour is equivalent to assuming a simplified model consisting of non interacting electron pair bonds highly localized between adjacent pair of atoms. The cohesive energy (*CE)* of prepared bulk samples is evaluated using the relation [37]

$$CE = \sum \left(C_i D_i / 100 \right) \tag{3.19}$$

where C_i and D_i are the number of expected chemical bonds and energy of each bond respectively. The bond energy of heteropolar bonds is calculated by using Pauling method [38]. According to chemical bond approach (CBA) [39], atoms combine more favorably with atoms of different kind rather than with the same kind and the bonds are formed in the sequence of decreasing bond energies until all the available valences are satisfied. Consequently, bonds between like atoms will only occur if there is an excess of certain type of atoms. In the above mentioned system, Bi is expected to combine preferably with Se because the bond energy of Bi-Se (170.4 kJ/mol) bond is higher than that of Bi-Te (125.6 kJ/mol). This results in decrease of Se-Se (190.08 kJ/mol) bonds and

is further responsible for lowering the average bond energy and hence CE of the system. The excess Se-Se bonds and CE of the system is calculated and tabulated in table 3.2.

The value of static refractive index n_0 has been calculated by extrapolating $h\nu$ to zero in figure 3.6 and equation. (3.19) reduces to

$$n_0 = \left(1 + E_d / E_0\right)^{1/2} \tag{3.20}$$

The calculated values of static refractive index n_0, for films under investigation are stated in table3.1.

3.4.1.2 Absorption Coefficient and optical band gap

The absorption coefficient (α) of $Se_{85-x}Te_{15}Bi_x$ thin films can be calculated using the well-known relation (equation 3.15). The variation of $ln(\alpha)$ with $h\nu$ is shown in figure 3.7 and is found to increase with increase in photon energy. The optical band gap has been estimated from absorption coefficient data as a function of wavelength by using Tauc relation (equation 3.18). The graph between $(\alpha h\nu)^{1/2}$ and $h\nu$ for $Se_{85-x}Te_{15}Bi_x$ films is shown in the figure. 3.8. The non linear nature of the graph provides evidence that the transition in the forbidden gap is of indirect type. It is also evident from figure that optical band gap decreases with the addition of Bi content. This decrease in optical band gap may be correlated with the electronegativity difference of the elements involved. According to Kastner et.al [40], the valence band in chalcogenide glasses is constituted by lone pair p-orbital's contributed by the chalcogen atoms. These lone pair electrons will have a higher value of energies adjacent to electropositive atoms than those of electronegative atoms. Therefore the addition of electropositive elements to the alloy may raise the energy of lone pair states which is further responsible for the broadening of

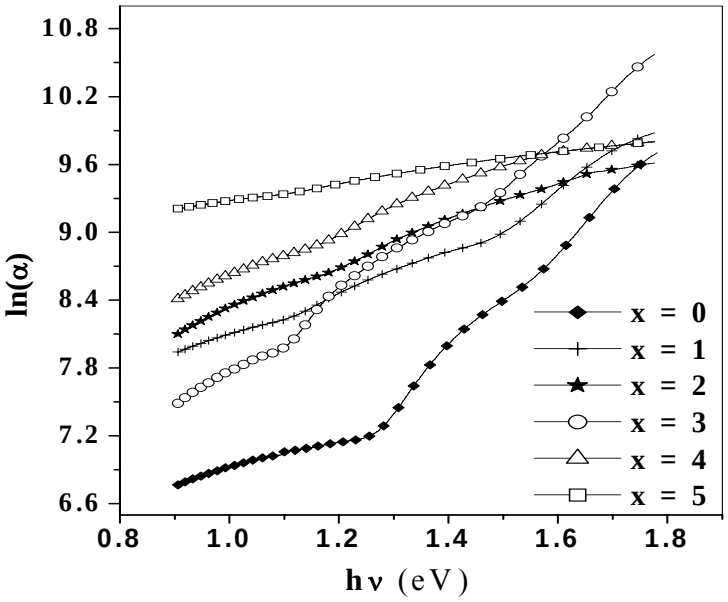

Figure 3.7 Plot of absorption coefficient (α) versus $h\nu$ for $Se_{85-x}Te_{15}Bi_x$ thin films.

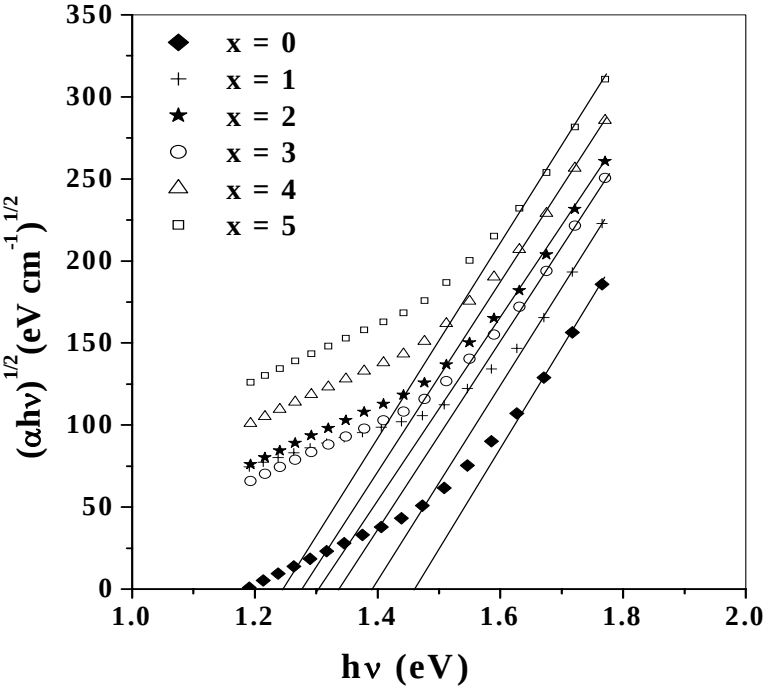

Figure 3.8 Plot of $(\alpha h\nu)^{1/2}$ and $h\nu$ for $Se_{85-x}Te_{15}Bi_x$ films.

valence band inside the forbidden gap. The electronegativities of Se, Te and Bi are 2.4, 2.1 and 2.0 respectively. Since Bi is less electronegative than Se, the substitution of Bi for Se may raise the energy of some lone pair states and hence broaden the valence band. This leads to band tailing and hence shrinking of the band gap. It is also evident from table 3.1 that band tailing parameter E_e increase with increasing Bi content, which may be due to the formation of structural defects like unsatisfied bonds. The concentration of these defects also increases with Bi content. Therefore isolated centers of these defects can only introduce localized states at or near the band edges leading to an increase in the band tailing width. The value of band gap decreases from 1.46 to 1.24 eV as the Bi content is increased from 0 to 5 at. % in the Se-Te glassy alloy. The optical band gap is a bond sensitive property [41]. Thus a decrease in optical band gap may also be explained on the basis of average bond energy of the system as explained earlier. Moreover the value of optical band gap E_g can be approximated using the oscillator energy value according to the relation $E_g = E_0/2$. The values are in good agreement with that derived from Tauc's extrapolation. The value of optical band gap for thin films under study is stated in table 3.2.

The dielectric constant of *a*-$Se_{85-x}Te_{15}Bi_x$ thin films is calculated with the help of refractive index and extinction coefficient. Real dielectric constant is calculated from the relation $\varepsilon_r = n^2 - k^2$ while the imaginary dielectric constant can be calculated from relation $\varepsilon_i = 2nk$. The variation of both real and imaginary dielectric constants with energy for thin films under consideration is shown in figure 3.9 and 3.10 respectively.

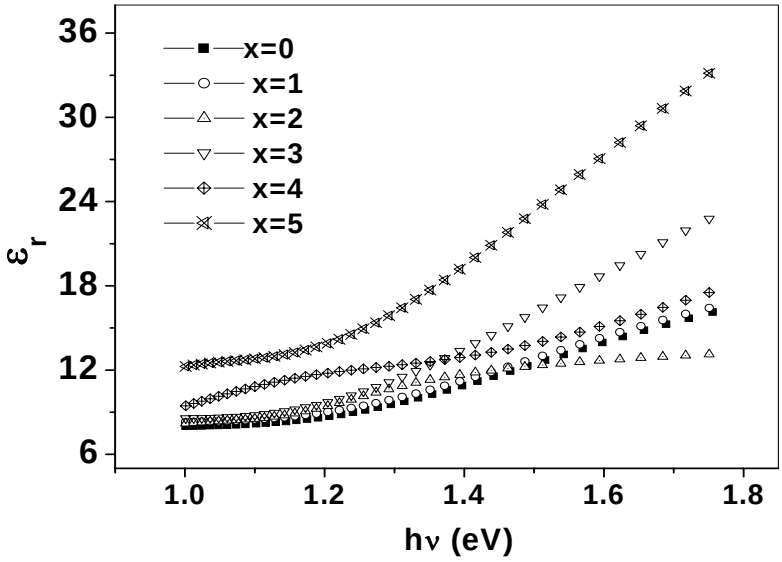

Figure 3.9 Plot of real part of dielectric constant ε_r versus hυ (eV) for $Se_{85-x}Te_{15}Bi_x$ films.

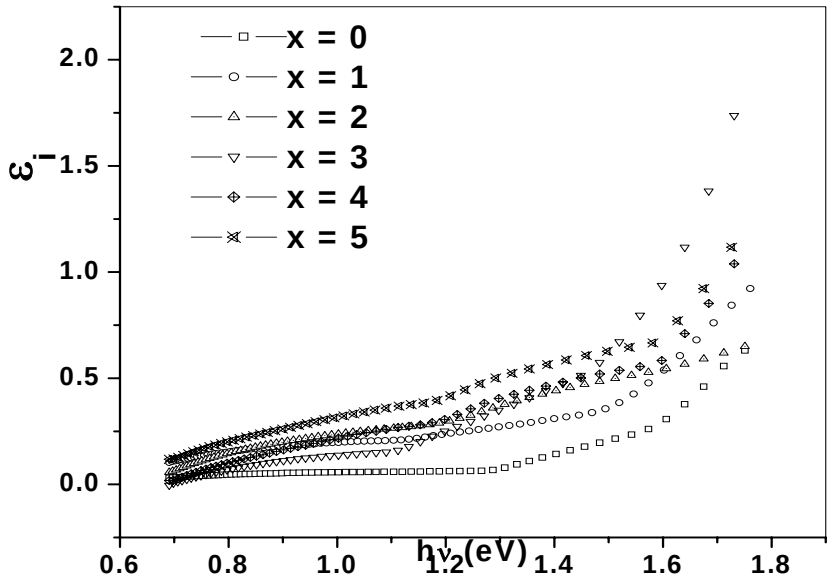

Figure 3.10 Plot of imaginary part of dielectric constant ε_i versus hυ (eV) for $Se_{85-x}Te_{15}Bi_x$ films.

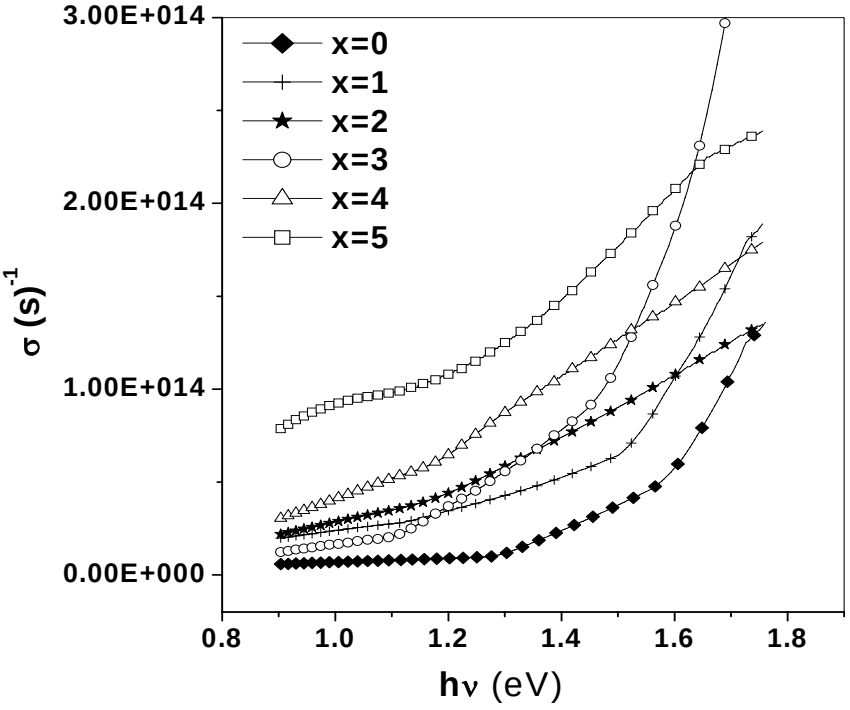

Figure 3.11 Plot of optical conductivity (σ) versus hυ (eV) for $Se_{85-x}Te_{15}Bi_x$ films.

Table 3.2

Excess Se-Se bonds, cohesive energy (CE), oscillator strength (E_0), and optical band gap (E_g), dielectric constant (ε_r), dielectric loss (ε_i) and optical conductivity *(σ)* are given at 1100 nm for $Se_{85-x}Te_{15}Bi_x$ (x = 0, 1, 2, 3, 4, 5) thin films.

x	Excess Se-Se bonds	$CE\ (eV)$	$E_0\ (eV)$	$E_g\ (eV)$	ε_r	ε_i	$\sigma \times 10^{12} (s^{-1})$
0	140	2.76	2.68	1.46	8.29	0.06	8.74
1	135	2.70	2.57	1.39	8.41	0.20	33.5
2	130	2.63	2.49	1.33	8.64	0.27	40.7
3	125	2.56	2.42	1.30	8.88	0.24	39.6
4	120	2.50	2.39	1.27	10.11	0.34	62.5
5	115	2.43	2.38	1.24	13.10	0.46	107.3

For *a*-$Se_{85-x}Te_{15}Bi_x$ thin films the variation of both, real and imaginary dielectric constants with energy follows the same trend as that of refractive index and extinction coefficient. The optical conductivity (σ) is determined using the relation [42], $\sigma = \alpha nc/4\pi$ where '*c*' is the velocity of light, 'α' is absorption coefficient and '*n*' is refractive index. Optical response is most conveniently studied in terms of optical conductivity. It has the dimensions of frequency which are valid only in Gaussian system of units. The optical conductivity directly depends on the absorption coefficient and refractive index and is found to increase sharply for higher energy values. This sharp increase in (σ) is attributed to large absorption coefficient and refractive index for these values. The plots of optical conductivity versus wavelength for *a*-$Se_{85-x}Te_{15}Bi_x$ thin films are given in figure 3.11. The variation of $\varepsilon_r, \varepsilon_i$ and σ (at λ = 1100 nm) with Bi at. % is given in table 3.2.

3.4.2 Optical properties of $Ge_{20}Te_{80-X}Bi_x$ (x = 0, 1.5, 2.5, 5.0) system

3.4.2.1 Behavior of Refractive Index: WDD Model

The transmission and reflection spectra of thin film samples under study are plotted in figure. 3.12. It is clear from figure that a red shift occurs in the interference free region with the Bi addition. Such shift in the spectrum of studied composition is a consequence of compositional dependence of the optical band gap and it also gives an enhanced value of refractive index. The optical absorption coefficient (α) is one of the important parameter and strongly depends upon transmittance (*T*) and reflectance (*R*). α is evaluated by using the relation [43]

$$\alpha = \frac{2.303}{d}\log\left(\frac{1-R}{T}\right), \qquad (3.21)$$

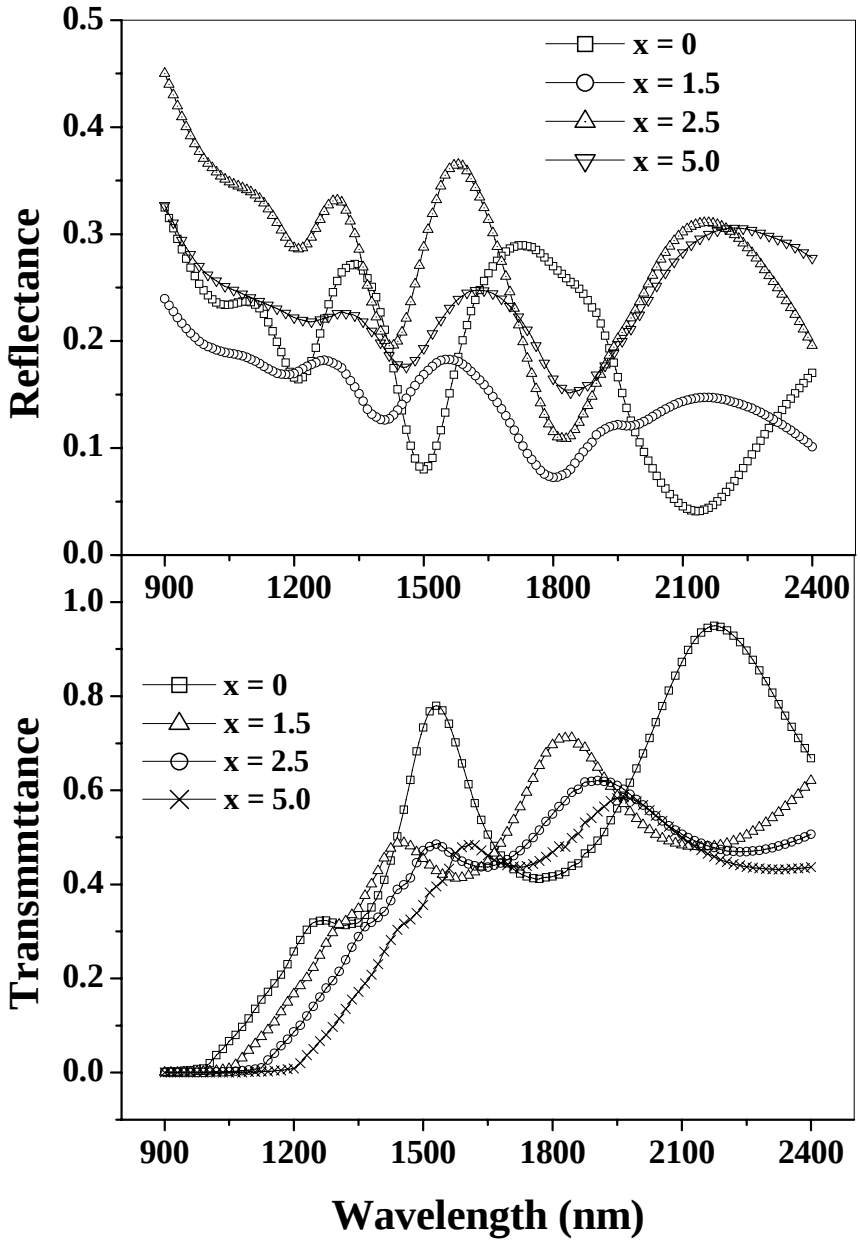

Figure 3.12 Plot of optical transmission and reflection versus wavelength for $Ge_{20}Te_{80-X}Bi_x$ (x = 0, 1.5, 2.5, 5.0) thin films.

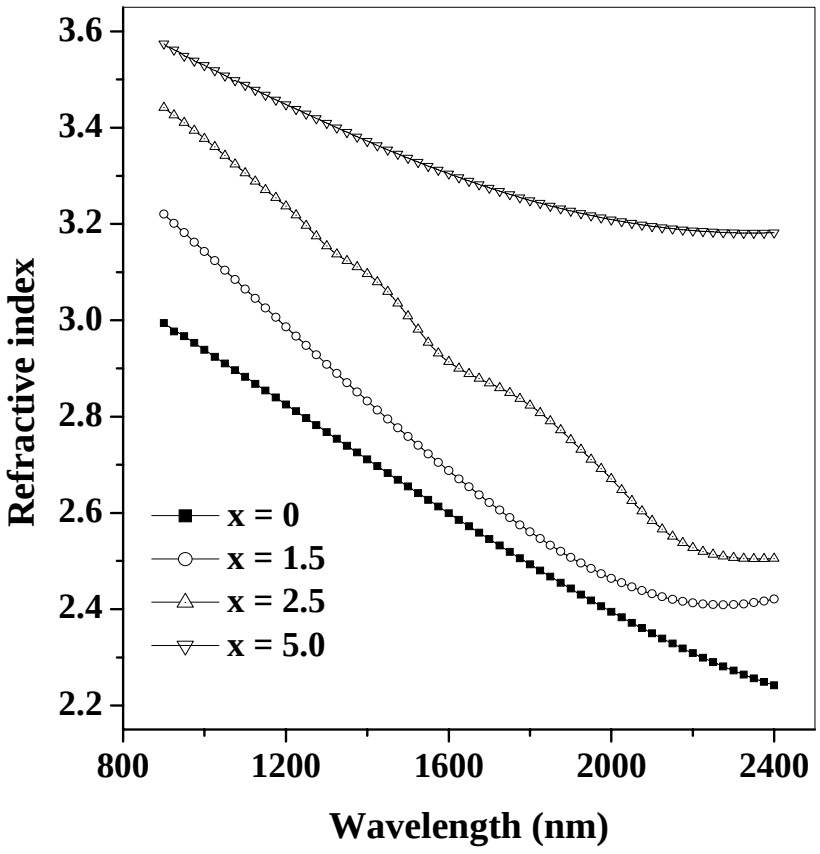

Figure 3.13 Plot of refractive index (n) versus λ (nm) for $Ge_{20}Te_{80-X}Bi_x$ (x = 0, 1.5, 2.5, 5.0) thin films.

where d is the film thickness ($d \approx 500$ nm for all the samples with an uncertainty of ± 20%). α has been found to be of the order of 10^4 cm^{-1}. For air as first medium with refractive index = 1 and considering the film as second medium which is highly absorbing in nature, the refractive index (n) has been calculated using the relation [43]

$$R = \frac{(n-1)^2 + k^2}{(n+1)^2 + k^2} \tag{3.22}$$

where k is extinction coefficient and has been calculated using $k = \lambda\alpha/4\pi$ [43]. It has been observed that both n and k decreases with increasing wavelength which further indicates the normal dispersion behavior of the films under study. It is also evident from figure 3.13 that with the increase of Bi content n increases. High refractive index values are beneficial for most of the technological applications as it leads to compact circuit designs. This increase in n is related to the increased polarizability of the larger Bi atomic radius (1.46 Å) compared to the Te atomic radius (1.36 Å). The larger the atomic radius of the atom, larger will be its polarizability and consequently according to Lorentz - Lorentz relation [44], larger will be refractive index. Since in our system less polarized atom Te is replaced by more polarized atom Bi, the refractive index of the system increases. The results are also justified with a clear red shift observed in the optical absorption edge as shown in figure 3.12. The calculated value of n, k and α for thin films under study typically at 1100 nm is shown in table 3.3. The spectral dependence of the refractive index has been analyzed in terms of Wemple-DiDomenico (WDD) model [36], which assumes that the properties of $Ge_{20}Te_{80-X}Bi_x$ thin films at high frequency could be treated as a single oscillator having the expression

$$n^2 - 1 = \frac{E_d E_0}{{E_0}^2 - (h\nu)^2}, \tag{3.23}$$

Table 3.3

Values of coordination number (m), refractive index (n), extinction coefficient (k), dielectric constant (ε_r), dielectric loss (ε_i) and optical conductivity *(σ)* are given at 1100 nm and static refractive index (n_0), for $Ge_{20}Te_{80-x}Bi_x$ thin films.

x	m	**n**	k	ε_r	ε_i	$\sigma \times 10^{12}(s^{-1})$	n_0	ε_∞
0	2.4	2.88	0.0031	8.29	0 .018	2.42	2.27	5.15
1.5	2.415	3.06	0.0046	9.36	0.028	3.87	2.40	5.76
2.5	2.425	3.31	0.0070	10.96	0.046	7.04	2.56	6.55
5.0	2.45	3.49	.01051	12.18	0.070	10.25	3.06	9.33

where $h\nu$ is the photon energy, E_0 is the single oscillator energy (also called average energy gap) and E_d is the dispersion energy which is a measure of average strength of the interband optical transitions. The oscillator parameters are determined by plotting refractive index factor $(n^2-1)^{-1}$ versus $(h\nu)^2$ and by fitting a straight line to the points as shown in figure 3.14. In figure 3.14, slope = $(E_0E_d)^{-1}$ and the intercept on vertical axis $=(E_0/E_d)$. The value of E_d and E_0 are calculated using these two relations and are listed in table 3.4. The parameter E_d is related to other physical parameters by simple empirical relation proposed by WDD model i.e. $E_d = \beta N_c Z_a N_e$, where β is a two valued constant with either an ionic or covalent value ($\beta = 0.26 \pm 0.03eV$ for ionic materials and $\beta = 0.37 \pm 0.04eV$ for covalent materials), N_c is the effective coordination number of the cation nearest neighbour to anion, Z_a is the formal chemical valance of the anion and N_e is the effective number of valence electrons per anion. The increase in the observed value of E_d with Bi content is only due to the increase in the value of N_c, which is calculated by using the relation $N_c = 0.01(aN_{Ge} + bN_{Te} + cN_{Bi})$, where N_{Ge}, N_{Te} and N_{Bi} are the coordination number for Ge, Te and Bi and *a, b, c* are their at. % respectively. The value of N_c for the system under investigation is found to increase from 2.40 to 2.45 as shown in table 3.3. The single oscillator energy E_0, also known WDD gap corresponds to the distance between centers of gravity of the valence and conduction band. It is therefore related to the bond energy of different chemical bonds present in the system. Moreover E_0 can also be used to estimate an approximate value of optical energy gap (E_g) by using an empirical relation proposed by Tanaka [45], i.e; $E_o \approx 2 \times E_g$.

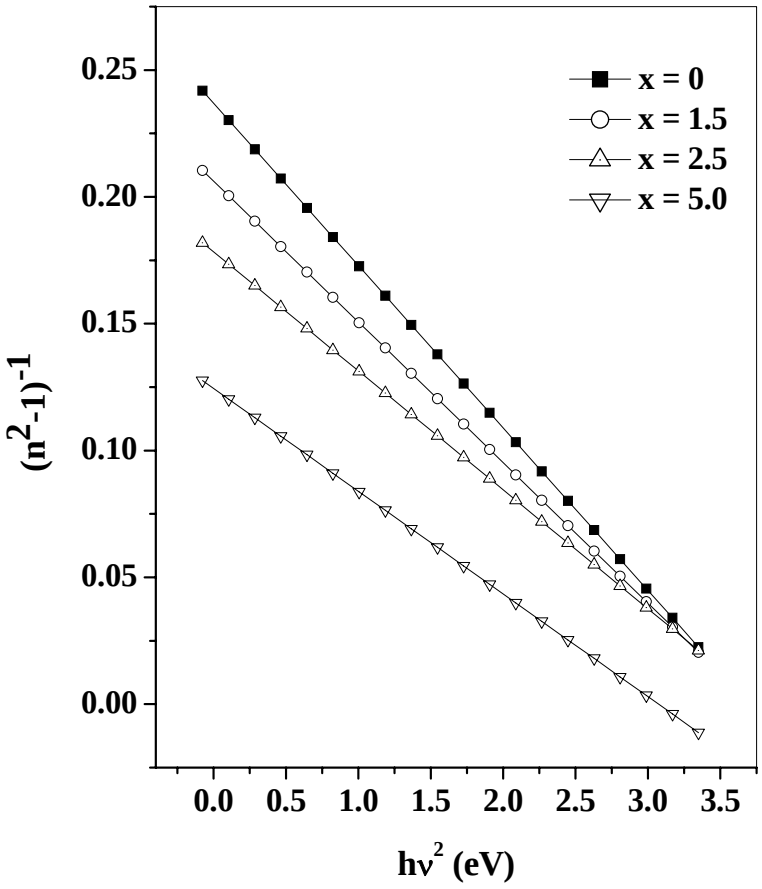

Figure 3.14 Plot of $(n^2 - 1)$ versus $(h\nu)$ for $Ge_{20}Te_{80-X}Bi_x$ (x = 0, 1.5, 2.5, 5.0) thin films.

It is clear from table 3.4 that values obtained by using the above relation are in good agreement with that obtained by using Tauc's extrapolation method. Similar results have also been reported earlier by various other researchers [46, 47].

The value of static refractive index n_0, has been calculated by extrapolating $h\nu$ to zero in figure 3.14 and equation (3.24) reduces to

$$n_0 = \left(1 + E_d / E_0\right)^{1/2} \qquad (3.24)$$

The calculated values of n_0, for films under investigation are found to increase with Bi content. The high frequency dielectric constant (ε_∞) have been calculated from the relation $\varepsilon_\infty = (n_0)^2$ and are reported in table 3.3. The dielectric constant (ε_r) and dielectric loss (ε_i) has been determined from the relation $\varepsilon_r = n^2 - k^2$ and $\varepsilon_i = 2nk$ for $Ge_{20}Te_{80-x}Bi_x$ thin films. The optical conductivity calculated from the equation $\sigma = \alpha nc/4\pi$, where c is the velocity of light. Optical conductivity has been found to increase with increasing Bi content. This increase may be a consequence of increased density of localized states in the gap itself due to the appearance of new defect states and Bi containing structural elements [48]. The dielectric constant, dielectric loss and optical conductivity directly depend on n, k and α and hence follow similar trends. The values of ε_r, ε_i, and σ are stated in table 3.3 at 1100 nm.

3.4.2.2 Optical band gap determination

Optical band gap (E_g) has been determined according to the generally accepted 'non direct transition' model for amorphous semiconductors proposed by Tauc (equation 3.18). The graph between $(\alpha h\nu)^{1/2}$ and $h\nu$ for $Ge_{20}Te_{80-x}Bi_x$ films is shown in the figure 3.15. The non linear nature of the graph provides evidence that the transition in the

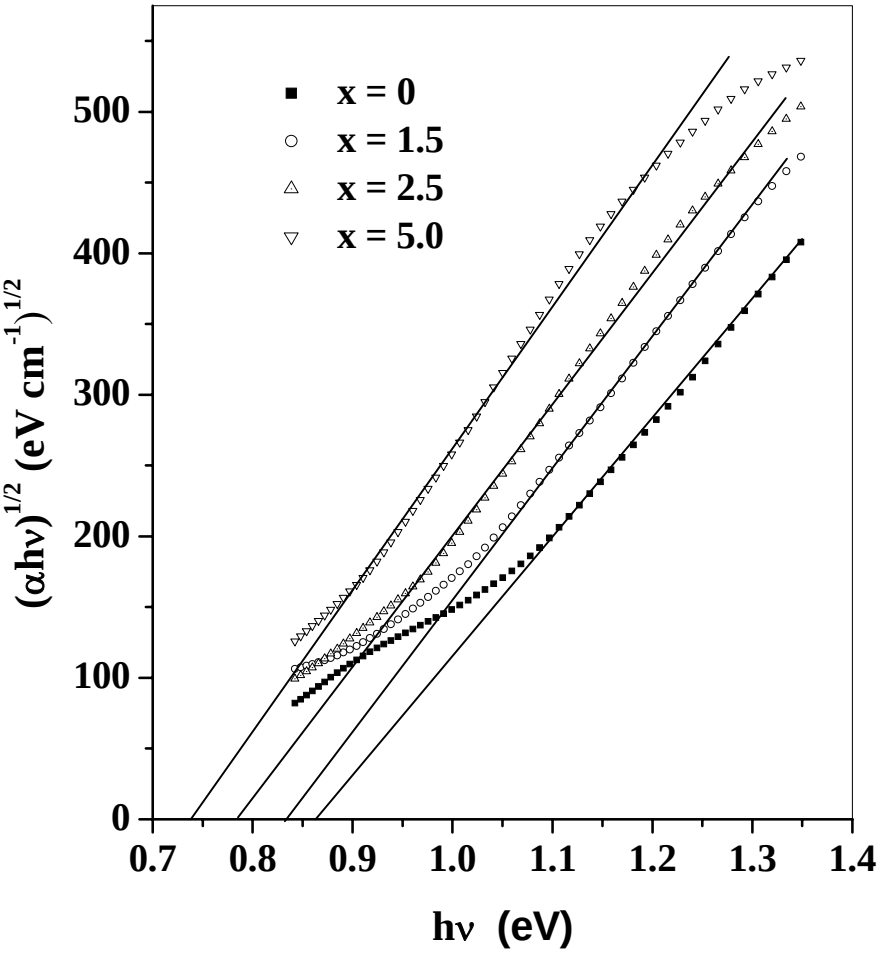

Figure 3.15 Plot of $(\alpha h\nu)^{1/2}$ and $h\nu$ for $Ge_{20}Te_{80-X}Bi_x$ (x = 0, 1.5, 2.5, 5.0) thin films.

Table 3.4

Excess Te-Te bonds, cohesive energy (CE), dispersion energy (E_d), oscillator energy (E_0),optical band gap (E_g) and $B^{1/2}$ for $Ge_{20}Te_{80-x}Bi_x$ thin films.

x	Excess Te-Te Bonds	CE (eV)	$E_d\,(eV)$	$E_0\,(eV)$	$E_g\,(eV)$	$B^{1/2}$
0	80.0	2.26	7.48	1.80	0.86	400
1.5	72.5	2.21	8.22	1.73	0.83	321.54
2.5	67.5	2.18	9.46	1.70	0.78	195.7
5.0	55.0	2.10	12.5	1.50	0.73	83.68

forbidden gap is of indirect type. It is also evident from figure that optical band gap decreases with the addition of Bi content. This decrease in optical band gap may again be correlated with the electronegativity difference of the elements involved. The electronegativities of Ge, Te and Bi are 2.01, 2.1 and 2.0 respectively. Since Bi is more electropositive than Te, the substitution of Bi for Te may raise the energy of some lone pair states and hence broaden the valence band. This leads to band tailing and hence shrinking of the band gap. This is also verified by considering the *B* factor in equation (3.18) which is inversely related to the product of static refractive index, n_0 and localized state tail width, ΔE_{tail} [49-51]. It is therefore, a clear indicator of the degree of randomness of the atomic structure of amorphous semiconductors. From the value of Tauc slope, $B^{1/2}$ (table 3.4) it is clear that ΔE_{tail} increase with increasing Bi content since $\Delta E_{tail} \propto [n_0 B]^{-1}$. It may be mentioned here that the decrease found in the values of parameter *B* is much more pronounced than the increase observed in the values of n_0. The value of band gap decreases from 0.86 to 0.73 eV as the Bi content is increased from 0 to 5 at. % in the Ge-Te glassy alloy (table 3.4). The decrease in optical band gap may also be explained on the basis of average bond energy or cohesive energy of the system. The cohesive energy is evaluated using the relation [37] (equation 3.20). In the above mentioned system, Bi enters into the Ge-Te system and saturates Bi-Te bonds, thus decreasing the concentration of Ge-Te bonds. Since the bond energy of Bi-Te bond (125.6 kJ / mol) is lower than that of the Ge-Te bond (156.7 kJ / mol), the average bond energy and hence CE of the system decreases. The excess Te-Te bonds and CE of the system is calculated and tabulated in table 3.4.

4. Conclusion

The transmission spectra of vacuum evaporated $Se_{85-x}Te_{15}Bi_x$ thin films taken at normal incidence have been analyzed in the spectral range 400-1500 nm and the various optical parameters are calculated. The refractive index and film thickness are calculated by using envelope method proposed by Swanepoel. The results indicate that n increases with the increasing Bi content which is related to the increased polarizability of the larger Bi atomic radius 1.46 Å compared with the Se atomic radius 1.16 Å. The dispersion parameters E_d, E_0 and n_0 are discussed in terms of WDD model. It has been observed that E_d and n_0 increases while E_0 decreases with increase in Bi content. The optical absorption in the given system seems to of non direct type and the optical band gap determined in the strong absorption region by Tauc's extrapolation is found to decrease from 1.46 to 1.24 eV with the addition of Bi content. The decrease in average bond energy and hence optical band gap is interpreted in terms of cohesive energy and electronegativity difference of the atoms involved. The dielectric constants and optical conductivity are determined for the system and are found to follow the similar trend as that of refractive index.

The transmission and reflection spectra of vacuum evaporated $Ge_{20}Te_{80-x}Bi_x$ thin films taken at normal incidence have been analysed in the spectral range 900-2400 nm and the various optical parameters are calculated. The results indicate that n increases with the increasing Bi content which is further related to the increased polarizability of the larger Bi atom compared to Te. The dispersion parameters E_d, E_0 and n_0 are discussed in terms of WDD model. It has been observed that E_d and n_0 increases while E_0 decreases with increase in Bi content. The optical absorption in the given system seems to be of non

direct type and the optical band gap determined in the strong absorption region by Tauc's extrapolation is found to decrease from 0.86 to 0.74 eV with the addition of Bi content. The decrease in average bond energy and hence optical band gap is interpreted in terms of cohesive energy and electronegativity difference of the atoms involved.

The effect of Bi incorporation on the optical properties of Se-Te and Ge-Te thin films has been analyzed thoroughly. The optical parameters of both of the series are found to follow the same trend with the increasing Bi content. It has been observed that the difference in the variation of refractive index of both of the series is small however there is appreciable change in the optical band gap for both the series. In case of $Se_{85-x}Te_{15}Bi_x$ glassy alloys, the optical band gap varies from 1.46 to 1.24 *eV*, whereas in case of $Ge_{20}Te_{80-x}Bi_x$ glassy alloys the optical band gap is found to decrease from 0.86 to 0.73.

References

1. Zakery A and Elliott S R 2003 J. Non-Cryst. Solids 330 1.

2. Lankhorst M H R 2005 Nature Mater. 4 347.

3. Popesco M A 2000 Non Crystalline Chalcogenides, Kluwer, Dordrecht .

4. Elshafie A and Abdel A 1999 Physica B 269 69-78.

5. Abe K, Takebe H and Maronaga K 1997 J. Non-Cryst. Solids 212 143.

6. Wei K, Machewirth D P, Wenzel J, Sigel G H 1995 J. Non-Cryst. Solids 182 *257.*

7. Majeed Khan M A, Zulfequar M and Hussain M 2001 J. Phys Chem Solids 62 1093.

8. Sharma Ishu, Tripathi S. K and Barman P B 2007 J. of Phys D: Appl. Physics 40 4460-4465.

9. Shaaban E R, Kaid M A, El Sayed Moustafa A. Adel 2008 J. Phys. D: Appl. Phys 41 125301.

10. Mishra S C K, Sharma T P, Sharma S K, Kumar R and Jain G 1990 Indian J. Technol. 28 205.

11. Khan S A, Zulfequar M, Hussain M 2002 Solid State Commun. 123 463-468.

12. Yang H Wang W and Min S 1986 J. Non Cryst. Solids 80 503.

13. Tohge N, Yamamoto Y, Minami T, Tanaka M 1979 J. Appl. Phys. Lett. 34 640.

14. Tohge N, Minami T and Tanaka M 1983 J. Non Cryst. Solids 59-60 1015.

15. Nagels P, Rotti M and Vikhrov W 1981 J. Phys (Paris) 42 907.

16. Nagels P, Tichey L, Tiska A and Ticha H 1983 J. Non Cryst. Solids 59-60 999.

17. Hudgens S and Johnson B 2004 MRS Bull. 829.

18. Maimon J D, Hunt K K, Burcin L, Rodgers J 2003 IEEE Trans. Nucl. Sci. 50 1878.

19. Katsuyama T, Matsumura H 1989 Infrared Optical Fibers (Adam Hilgers, London) 212.

20. Idem. 1986 Appl. Phys. Lett. 49 22.

21. Takamori T, Roy R and Mccarthy G. J 1970 Mater. Res. Bull. 5 529.

22. Lizima S, Suzi M, Kikuchi M, Tanaka K 1970 Solid State Commun. 8 153.

23 Savaga J A 1971 J. Mater. Sci. 6 964.

24. Idem. 1972 J. Non Cryst. Solids 11 121.

25. Bordas S, Vazquez J. Casas, Clavaguera N and Clavaguera Mora M T 1973 Thermochim Acta 28 387.

26. Majeed Khan M A, Zulfequar M and Hussain M 2001 J. Phys Chem Solids 62 1093.

27. Sharma Ishu, Tripathi S K and Barman P B 2007 J. of Phys D: Appl. Phys. 40 4460-4465.

28. Shaaban E R, Kaid M A, Sayed El Moustafa and A. Adel 2008 J. Phys. D: Appl. Phys 41 125301.

29. Manificier J C, Gasiot J and Fillard J P 1976 J. Phys. E: Sci. Instrum 9 1002.

30. Swanepoel R 1983 J. Phys. E : Sci. Instrum. 16 1214.

31. Ambrico M, Smaldone D, Spezzacatenna C, Stagno V, Perna G and Capozzi V 1998 Semicond. Sci. Technol. 13 1446.

32. Tauc J 1970 The optical properties of solids (Amsterdam: North-Holland).

33. Abdel-Aziz M M, El-Metwally E G, Fadel M, Labib H H and Afifi M A

2001 Thin solid films 386 99.

34.. Morigaki K 1999 Physics of Amorphous Semiconductors (London:Imperial College Press).

35. Shaaban E R, Abdel-Rahman M, Sayed Yousef El and Dessouky M T 2007 *Thin Solid Films* 515 3810.

36. Wemple S H and DiDomenico M 1971 Phys Rev B 3 1338.

37. Fayek S A, Balboul M. R, Marzouk K H 2007 Thin Solid Films 515 7281-7285.

38. Pauling L 1976 Die Nature der Chemischen Bindung VCH Weinheim 80-89.

39. Biecerano J, Ovshinesky S R 1985 J. Non Cryst. Solids 74 75.

40. Kastner M, Adler D, Fritzsche H 1976 Phys Rev Lett 37 1504.

41. Pattanaik A K and Srinivasan A 2003 J. Optoelectron Adv. Mater. 5 1161.

42. Wemple S H and DiDomenico M 1971 Phys. Rev. B 3 1338.

43. El-Raheem Abd M M 2007 J. Phys.: Condens. Matter 19 216209.

44. Elliott S R 2000 The Physics and Chemistry of Solids (Chichester: Wiley).

45. Tanaka K 1980 Thin Solid Films 66 271.

46. Gonzalez-Leal J M, Ledesma A, Bernal-Oliva A.M, Prieto-Alcon R, Marquez E, Angel J A and Carabe J 1999 Mater. Lett. 39 232.

47. Kosa T I, Wagner T, Ewen P J S and Owen A E 1995 Phil. Mag. B 71 311.

48. Mott N F, Davis E A 1970 Phil. Mag. 22 903.

49. Mott N F and Davis E A 1979 Electronic Processes in Non-Crystalline Materials 2nd edn (Oxford: Clarendon).

50. Zanatta A R and Chambouleyron I 1996 Phys. Rev. B 53 3833.

51. Tich´y L, Tich´a H, Nagels P and Callaerts R 1998 Mater. Lett. 36 294.

.

CHAPTER 4

Effect of Bi incorporation on electrical properties of Se-Te and Ge-Te glassy alloys

4.1 Introduction

Chalcogenides with their twofold coordination and lone pair orbital offers dual channels of structural and electronic flexibility for removal of dangling bonds in the network. As a consequence, a typical chalcogenide has a relatively sharp optical absorption edge, a single electrical activation energy and efficient photoexcited conductivity and luminescence. All these properties are the characteristics of a well defined, clean forbidden gap. Nevertheless, field effect and doping experiments indicate that Fermi level of these chalcogenide glasses is nearly pinned. Common feature of these glasses is the presence of localized states in the mobility gap due to the absence of long range order as well as inherent effects. The study of photoconductivity provides an understanding of the photo generations and transport of free carriers. Moreover it also acts as a valuable tool in understanding the recombination kinetics, which in turn gives information about the localized states in the amorphous materials [1].

The conductivity in chalcogenide glasses is suggested to be of p-type [2] based on the asymmetry of conduction band (formed of antibonding orbitals) and valence band (constituted by non bonding or lone pair electrons). It was postulated that disorder should have a larger effect on antibonding states than on non bonding states resulting in a deeper tail for the conduction band states. This effect in turn was supposed to result in stronger localization of electrons compared to that of holes, leading to p-type conductivity. The metallic impurities like Pb and Bi have produced a remarkable change in the electrical properties of chalcogenide glasses. The conductivity of chalcogenide glasses switches from p to n type due to Bi addition [3-6]. High field electrical conduction in chalcogenide glasses is quite complex because of the possibilities of several mechanisms (*e.g.* Space Charge Limited Conduction, Hoping Conduction, Small Polaron Conduction, Poole

Frenkel effect *etc*.) involved. These mechanisms are usually governed by a number of factors *viz*. the work function of the electrodes and that of the sandwich layer, applied field and structural defects. These defects are acting as potential trapping centres for current carriers. Chalcogenide materials have a large number of defects due to dangling bonds that give rise to a large number of localized defect states. These localized states act as carrier trapping centres and after trapping the injected charge from electrodes, they become charged and thus are expected to build-up a space charge. This build- up of space charge by the inherent native defects plays the key role in the determination of Space charge limited conduction (SCLC) process. For SCLC, the ln *(I/V*) vs. *V* curves (where *I* is the current and *V* is the voltage) should be a straight line and slope *S* of these curves should be inversely proportional to the temperature. Schottky emission is the increase in the discharge of electrons from the surface of a heated material by application of an electric field that reduces the value of the energy required for electron emission. A very weak electric field may be applied that simply sweeps the already emitted electrons away from the surface of the material. When the field is increased, a point is reached for quite moderate fields at which the value of the work function itself is lowered. As the applied field (voltage) is further increased, the work function continues to decrease so that the electron emission current continues to increase. At very high values of the applied field, the electron emission undergoes an excessive increase because of the onset of high-field emission or simply, field emission. For Schottky emission the plot between ln(*J*) and *T* should be straight line, where *J* is the current density.

The Poole-Frenkel effect is the lowering of Columbic potential barrier when it interacts with an electric field, *i.e.* when the electric field interacts with the Columbic potential barrier of a donor sender or trap, the height of the barriers is lowered. The structural

defects in the material are responsible for the production of additional energy states (also called traps) close to the band edge which restrict the current flow because of a capture and emission process, thereby becoming the dominant current mechanism.

In many non crystalline materials, dc conduction as a function of temperature can be expressed by the relation $\sigma = \sigma_0 \exp(-\Delta E/T)$ with constant activation energy ΔE over the whole temperature range of the measurements. The activation energy is usually referred to half of the energy gap. The activation energy is usually situated in the range of 0.5 – 1.0 eV, although values are as low as 0.2 eV and as high as 1.5 eV have also been observed. The pre exponential factor is often situated in the range 10^3 to 10^4 $(\Omega^{-1}cm^{-1})$ but it can be as low as 10^{-5} $\Omega^{-1}cm^{-1}$ and as high as 10^8 $\Omega^{-1}cm^{-1}$. Generally the annealing of the chalcogenides leads to decrease of the electrical conductivity and to a small increase of activation energy [37].

In present section authors have decided to study the *I-V* characteristics, the mechanism of conduction and photoconductive properties of $Se_{85-x}Te_{15}Bi_x$ (x = 0, 1, 2, 3, 4, 5) and $Ge_{20}Te_{80-x}Bi_x$ (x = 0, 1.5, 2.5, 5.0) system in detail. These properties are very important from the basic physics as well as application point of view. Temperature and intensity dependent steady state photoconductivity measurements have been carried out for all compositions. Rise and decay of photocurrent has also been measured at room temperature at 1035 Lux intensity for all compositions.

4.2 Experimental Details

The growth of bulk samples and their respective films is described earlier (section 2.1 and 2.2). Predeposited thick indium electrodes on well-degassed Corning 7059 glass substrates have been used for the electrical contacts. A planar geometry of the film (length ~ 1.78 cm; electrode gap ~ 8×10^{-2} cm, shown in figure 2.1) is used for the

electrical measurements. The thickness of the films was kept constant (~500 nm). The films were annealed below their glass transition temperature in order to attain a metastable thermodynamic equilibrium and then kept in dark for about 24 h before mounting them in the sample holder. For the *I-V* measurements at room temperature (303 K) the samples were mounted in a specially designed metallic sample holder in which a vacuum ~10^{-3} mbar is maintained throughout the measurements. A dc voltage (0-300V) was applied across the sample and the resulting current was measured by a digital picometer (Keithley, model 6487). The temperature dependent dark and photoconductivity of the amorphous films were studied by mounting the film in a specially designed metallic sample holder where heat filtered white light (200 W tungsten lamp) can be shone through a transparent quartz window. The temperature was measured by mounting a copper- constant thermocouple near to the sample. The light intensity is measured using a digital Luxmeter (Testron, model TES-1332). The photocurrent is obtained after subtracting the dark current from the current measured in the presence of light.

4.3 Results and Discussion

4.3.1 Electrical properties of $Se_{85-x}Te_{15}Bi_x$ (x = 0, 1, 2, 3, 4, 5) system

4.3.1.1 I-V characteristics; verification of Poole Frenkel law

I-V characteristics for $Se_{85-x}Te_{15}Bi_x$ (x = 0, 1, 2, 3, 4, 5) thin films are recorded in the voltage range 0-300 V at different temperatures (from 303-333K) and the curves are shown in figure 4.1 typically for 303 K. This figure shows the linear behaviour of current at low voltage range (0-90 V) and deviate from linearity i.e. tend towards non-Ohmic behaviour in the higher voltage range. Observed *I-V* characteristics reveals the minimum current (maximum resistance) for x = 1, and maximum current (minimum resistance) for

x = 5. Three linear regions are observed in these *I-V* characteristics in three voltage ranges *i.e.* (0-90 V), (110-200 V) and (220-300 V). The slope of these regions gives us value of resistance for that particular voltage range, as given in table 4.1. It is clear that at higher voltage range the value of resistance decreases. As the voltage is increased across the sample, thermal effects may be induced resulting to increase in carrier mobility and thus decrease in the resistance. This allows more and more current to flow through the samples. The mechanism of conduction in amorphous solids can be explained on the basis of model put forward by Jonscher [8], which states that the amorphous solids conduct electricity by means of electron motion either in localized levels (hoping) or in free bands. The effective mobility in the latter is higher than in the former. The localized levels are donor like depending on their ability to donate or accept electrons and their characteristics determines their role in the conduction process. The level of conductivity depends on the density and mobility of charge carrier in the vicinity of Fermi level. If the latter falls near the valance or conduction band, conductivity prevails; otherwise conduction is by carrier hoping. In our present investigation, the field dependence studies for a film of thickness 500 nm reveals the ohmic nature of current for $V < 100V$ and non ohmic nature of current for $V > 100V$. The current exhibits an applied voltage dependence of the form $I \alpha V^{1/2}$ for higher voltage range (V > 100V) for all the samples as shown in figure 4.2.

The relation between the current and square root of the applied voltage as given by Jonscher and Hill [18] is

$$I = I_{Ph} \exp(\beta V^{1/2} / kT) \qquad (4.1)$$

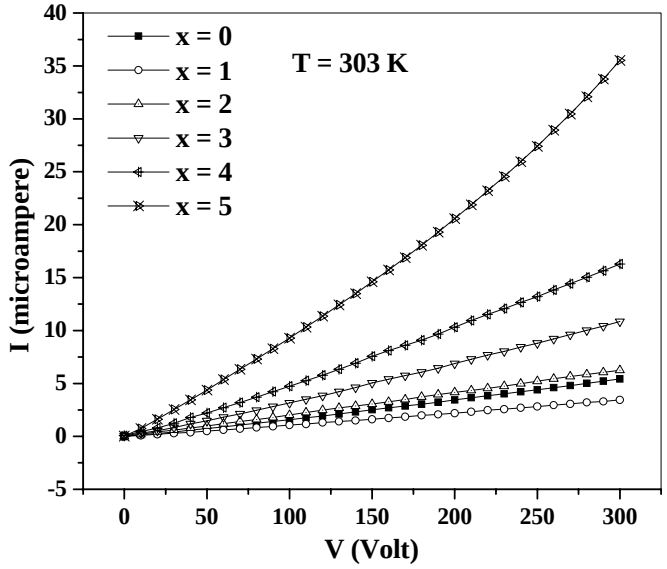

Figure 4.1 Plot of *I-V* characteristics for $Se_{85-x}Te_{15}Bi_x$ thin films.

Table 4.1

Resistance for 500 nm thick $Se_{85-x}Te_{15}Bi_x$ thin film for three different voltage ranges

Composition	$R_1(M\Omega)$ for 0-90 V	$R_2(M\Omega)$ for110-200 V	$R_3(M\Omega)$ for 220-300 V
$Se_{85}Te_{15}$	114.23	91.44	73.14
$Se_{84}Te_{15}Bi_1$	128.21	96.15	75.80
$Se_{83}Te_{15}Bi_2$	102.09	88.29	70.42
$Se_{82}Te_{15}Bi_3$	36.09	26.40	22.42
$Se_{81}Te_{15}Bi_4$	20.16	19.53	15.24
$Se_{80}Te_{15}Bi_5$	10.87	7.82	6.27

where

$$\beta = (e^3 / 4\pi\varepsilon_0\varepsilon_r d)^{1/2} \tag{4.2}$$

In equation (4.2) ε_0 is the permittivity of free space, ε_r is the relative permittivity of sample, d is the interspacing between field and empty sites (jump distance) and I_{PF} (at $V = 0$) is given by

$$I_{PF} = I_0 \exp(-\phi / kT), \tag{4.3}$$

where ϕ is the trap depth and

$$I_0 = Anedv \tag{4.4}$$

In equation (4.4) A is the electrode area, n is the carrier concentration, e is the electronic charge and v is the phonon frequency ($\approx 10^{13} / s$) taken as constant. The linearity of ln (I) vs. $V^{1/2}$ graph (figure 4.2) in 100-300V range suggests that the conduction in the studied materials obey the Poole-Frenkel conduction mechanism [19] in the given voltage range. The Poole-Frenkel effect is the lowering of Columbic potential barrier when it interacts with an electric field, *i.e.* when the electric field interacts with the Columbic potential barrier of a donor sender or trap; the height of the barriers is lowered. The structural defects in the material are responsible for the production of additional energy states (also called traps) close to the band edge which restrict the current flow because of a capture and emission process, thereby becoming the dominant current mechanism.

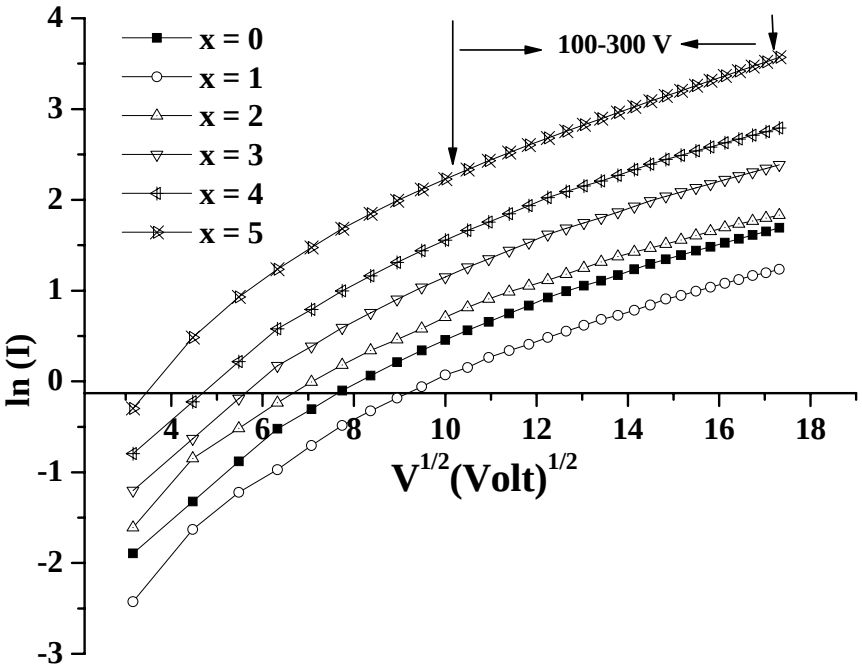

Figure 4.2 Plot of *ln (I)* versus $V^{1/2}$ for $Se_{85-x}Te_{15}Bi_x$ thin films.

4.3.1.2 Temperature dependent dark and photo conductivity

Figure 4.3 shows the temperature dependence of dark conductivity (σ_d) for $Se_{85-x}Te_{15}Bi_x$ thin films. The plots of ln (σ_d) versus 1000/T are found to straight lines indicating that the conduction is through an activated process having single activation energy in the temperature range 303-333 K. In most of the chalcogenide glasses, σ_d can therefore be expressed by Arrhenius relation [11]

$$\sigma_d = \sigma_0 \exp\left(\frac{-\Delta E_d}{kT}\right) \tag{4.5}$$

Where σ_0 is the material related pre exponential factor, ΔE_d is the activation energy for dc conduction, *k* is the Boltzman constant and *T* is the temperature. The value of ΔE_d is estimated from the slope of ln (σ_d) versus 1000/T curves. The calculated values of ΔE_d, σ_d and σ_0 at room temperature are inserted in table 4.2. The composition dependent dark conductivity is studied and it is observed that σ_d decreases first as Bi is introduced in the host $Se_{85-x}Te_{15}$ glassy alloy. However, further increase in the Bi (≥ 2 at. %) content enhances the conductivity. Activation energy ΔE_d is found to follow the opposite trend *i.e.* it increases first as Bi is introduced and than decreases with further increases of Bi content. As Bi (=1 at %) is introduced in the host $Se_{85-x}Te_{15}$ glassy alloy, its atoms may enter into Se chain and rearrange the network of host Se. It makes bonds with host Se to satisfy their bonding states and therefore reducing the number of defects states. The reduction of defect states results in increase in activation energy and hence decreases the conductivity. With the further increase of Bi (≥ 2 at. %) content conductivity increase and activation energy decreases. This behaviour may be explained on the basis of Mott and Davis model. According to this model there can be three

processes leading to conduction in amorphous semiconductors. At very low temperature conduction can occur by thermally assisted tunneling between states at the Fermi level. At higher temperature charge carrier are excited into the localized states of the band tails; carriers in their localized states can take part in the electric charge transport only by hoping. At still higher temperature, carriers are excited across the mobility edges into the extended states. In our case the values of σ_0 are very small which indicates that the conduction should be through localized states [11]. Similar behaviour has also been observed in some other systems [12, 13], where the range obtained for σ_0 is quite small and conduction is supposed to be through localized states. The variation of dc parameters with Bi for the investigated composition may also be explained by assuming that Bi atoms act as impurity centers in the mobility gap and induces structural changes in the network which may disturb the balance of charged defects and consequently change the electric conduction. New trap states are created in the mobility gap due to the Bi addition and the concentration of D^+ defects get reduced as compared with D^- states. It is observed that for the composition x = 5 conductivity increases abruptly, but without thermoelectric power measurement it is difficult to assess this abrupt enhancement. This increase in conductivity may be attributed to current due to electrons only. The increase in σ_d and consequent decrease in ΔE_d with Bi may also be explained on the basis of the binding energy of the system which is found to decrease with the increase in Bi concentration [14]. Moreover, the behaviour of σ_d can also be related to the thermal studies of the sample under investigation which shows that glass transition temperature increases with increase in Bi (≥ 2 at. %) concentration [15]. It further implies that rigidity of the system increases with the Bi concentration and hence σ_d also increases.

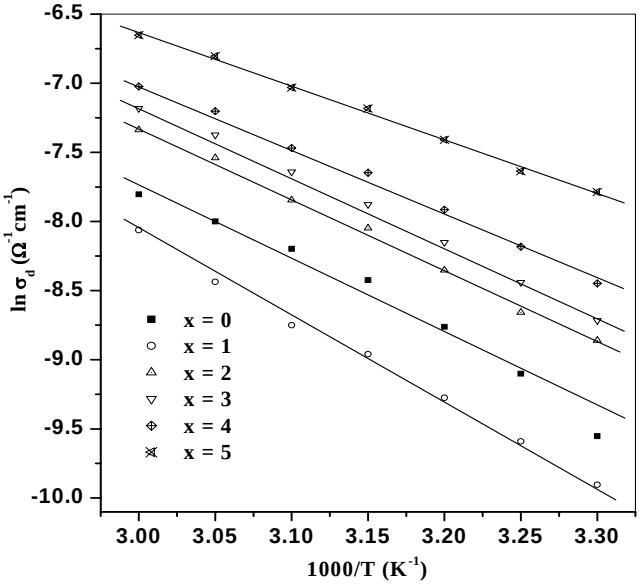

Figure 4.3 Plot of ln (σ_d) versus 1000/T for $Se_{85-x}Te_{15}Bi_x$ thin films.

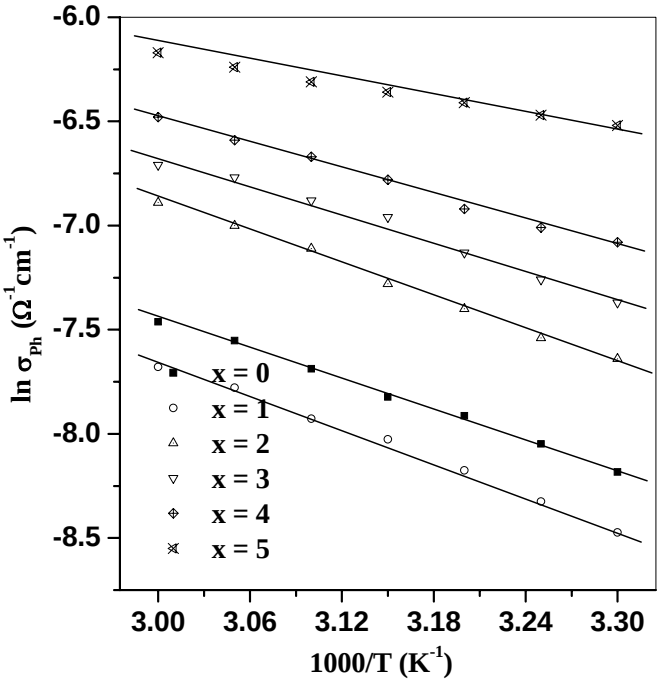

Figure 4.4 Plot of ln (σ_{Ph}) versus 1000/T for $Se_{85-x}Te_{15}Bi_x$ thin films.

Variation of steady state photoconductivity (σ_{Ph}) of $Se_{85-x}Te_{15}Bi_x$ thin films with temperature (i.e. σ_{Ph} versus 1000/T) at a particular intensity 1085 lux is shown in figure 4.4. The value of ΔE_{Ph} is calculated from the slope of figure 4.4 and are tabulated in table 4.2 along with the values of σ_{Ph} at 303 K. It is observed that the value of σ_{Ph} is much higher than σ_d for a particular Bi concentration. This is presumably due to the increased density of charged carriers compared with their value at thermal equilibrium when the material is exposed to electromagnetic radiation. The value of ΔE_{Ph} is found to be much smaller than ΔE_d and it shows the same trend as that of ΔE_d, for the entire samples. Similar results have also been reported in various other Chalcogenide glasses [16, 17].

4.3.1.3 Intensity dependent photoconductivity

Intensity (*F*) dependence of steady state photoconductivity (σ_{Ph}) has been studied at room temperature (303 K) to investigate the nature of recombination process in $Se_{85-x}Te_{15}Bi_x$ thin films. Figure 4.5 shows the plots of ln (σ_{Ph}) versus ln (*F*) and are found to be straight for all the composition. This indicate that the σ_{Ph} follows a power law with *F* *i.e.* $\sigma_{Ph} \alpha F^{\gamma}$, where γ is the exponent that characterizes the recombination mechanism. For γ = 0.5, the recombination is predominantly bimolecular in nature, whereas for γ = 1.0, it is supposed to be mono-molecular. For the present samples under investigation, γ is calculated from the slope of ln (σ_{Ph}) versus ln (*F*) and is found to be closed to 0.5 for all the compositions. This further confirms a bi-molecular recombination mechanism in the studied films. The bi-molecular recombination mechanism may be discussed on the basis of Street and Mott model of dangling bonds. They suggested that chalcogenide

glasses contain a high number of frozen-in structural defects at the missing chalcogen atom, leaving broken or dangling bonds on the neighbouring atoms which could be the source of localized defects states. The dangling bond states are either unoccupied or occupied by pairs of electrons so that D^+ and D^- dangling bonds are formed i.e. $2D^0 = D^+ + D^-$. The energy level of neutral unpaired dangling bond D^0 lies intermediate between that of D^+ and D^-. The D^+ and D^- centres can acts as discrete traps for electrons and holes generated by light excitation. This capture of photo excited charge carriers leads to an excess concentration of D^0 centres. The trapped carriers can be released to the valance or conduction band and hence enhancing conductivity. In the photoconductivity measurements, photosensitivity (σ_{Ph}/σ_d) and density of defect states (n_σ) are two important parameters to describe the usefulness of a particular material from optoelectronic device point of view. The value of (n_σ) for different samples is calculated using the equation [18, 19]

$$n_\sigma = 2\left(\frac{2\pi m k_B T}{h^2}\right)\exp\left(\frac{-\Delta E_\sigma}{k_B T}\right) \qquad (4.6)$$

where m is the mass of charge carrier and k_B is the Boltzman constant. The calculated values of σ_{Ph}/σ_d and n_σ for $Se_{85-x}Te_{15}Bi_x$ thin films at absolute temperature (303 K) and at intensity 20-1085 lux are inserted in table 4.2. It is observed that at a particular intensity, photosensitivity increases as Bi is introduced to host $Se_{85}Te_{15}$ glassy alloy and then decreases with the further addition of Bi (≥ 2 at. %), whereas exactly opposite trend has been observed in case of n_σ. σ_{Ph}/σ_d depends upon the lifetime time of excess charge carriers which further depends upon the density of localized states in a particular material. The higher the density of states, the lower will be the lifetime, as

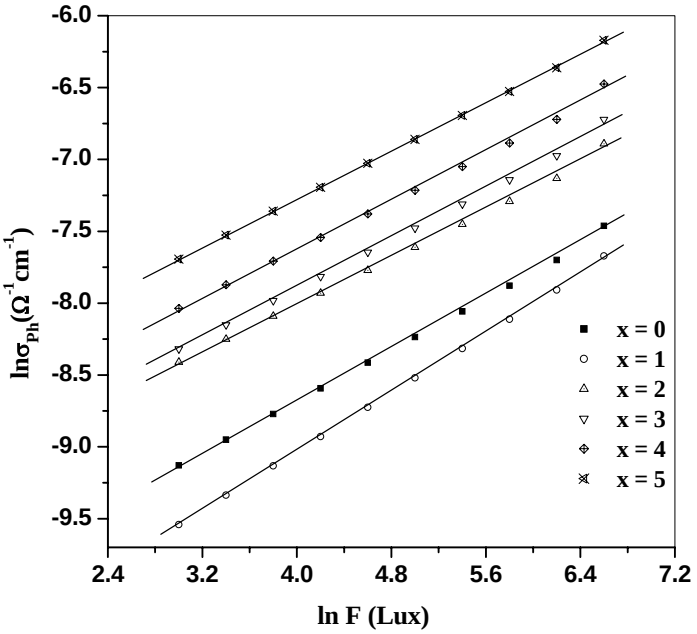

Figure 4.5 Plot of ln (σ_{Ph}) versus *ln (F)* for $Se_{85-x}Te_{15}Bi_x$ thin films.

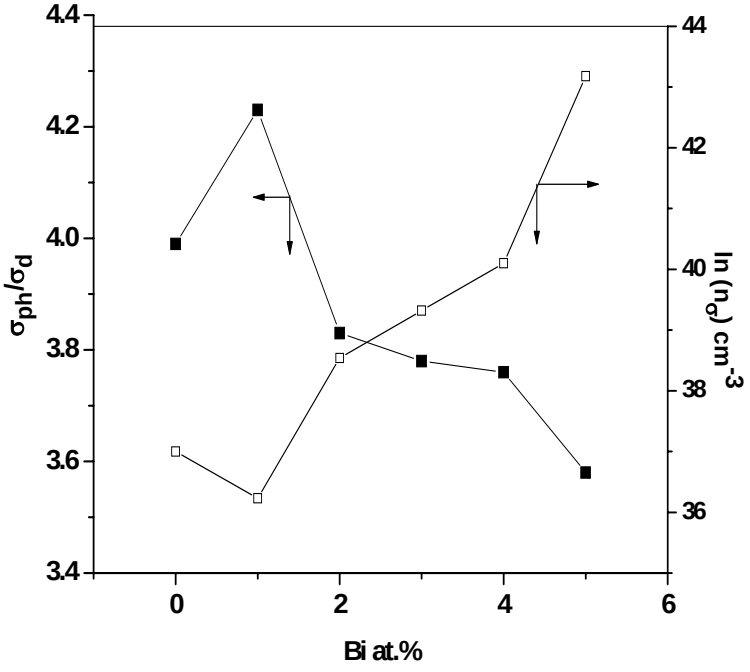

Figure 4.6 Plot of σ_{ph}/σ_d and n_σ versus Bi concentration for $Se_{85-x}Te_{15}Bi_x$ thin films.

Table 4.2

The dc dark conductivity (σ_d), the pre-exponential factor (σ_0), the activation energy for dc conduction (ΔE_d), photoconductivity (σ_{Ph}), the activation energy of photoconduction (ΔE_{Ph}), power exponent (γ), photosensitivity (σ_{Ph}/σ_d) and charge carrier density (n_σ) for $Se_{85-x}Te_{15}Bi_x$ thin films.

Composition	$\sigma_0(dark)$ $(\Omega^{-1}cm^{-1})$	σ_d $(\Omega^{-1}cm^{-1})$	ΔE_d (eV)	σ_{Ph} *(photo)* $(\Omega^{-1}cm^{-1})$	ΔE_{Ph} (eV)	σ_{Ph}/σ_d	γ	n_σ (cm^{-3})
$Se_{85}Te_{15}$	0.00328	7.12×10^{-5}	0.49	2.83×10^{-4}	0.21	3.99	0.51	1.17×10^{16}
$Se_{84}Te_{15}Bi_1$	0.00255	4.97×10^{-5}	0.51	2.10×10^{-4}	0.23	4.23	0.50	5.4×10^{15}
$Se_{83}Te_{15}Bi_2$	0.00541	1.30×10^{-4}	0.45	4.98×10^{-4}	0.22	3.83	0.50	5.49×10^{16}
$Se_{82}Te_{15}Bi_3$	0.00563	1.65×10^{-4}	0.43	6.25×10^{-4}	0.20	3.78	0.51	1.19×10^{17}
$Se_{81}Te_{15}Bi_4$	0.00848	2.23×10^{-4}	0.41	8.35×10^{-4}	0.18	3.76	0.51	2.58×10^{17}
$Se_{80}Te_{15}Bi_5$	0.021	4.14×10^{-4}	0.33	1.47×10^{-3}	0.10	3.58	0.52	5.67×10^{18}

these defect states may act as recombination centres in the presence of light. This might be due to the formation of intimate valence alternation pairs (IVAPs) under illumination. The defects are converted to random pairs of charged defects, known as light induced metastable defects (LIMDs) [20-22]. These LIMDs act as electron/hole trapping centres and decrease the photocurrent. Therefore σ_{Ph}/σ_d will be maximum when the density of states will be minimum. The results are confirmed in figure 4.6 which shows a minimum value of n_σ and maximum value of σ_{Ph}/σ_d at x = 1.

4.3.1.4 Transient photoconductivity

In order to understand the recombination and trapping mechanisms, transient photoconductive measurements are conducted by exposing all the samples to light (1035 lx intensity) at 303 K. Figure 4.7 shows the rise and decay of photocurrent for all compositions. It is evident from figure that the photocurrent rises in a monotonic manner up to the steady state value. After cessation of steady illumination, trapped electrons and holes combine and the photocurrent decay is quite fast initially and reaches its steady state value known as persistent photocurrent. This persistent photocurrent is due to some kind of photoinduced effects and takes many hours to reach to zero. To understand the trapping effects, the persistent photocurrent is subtracted from the measured photocurrent and then the corrected photocurrent against time (t) is plotted for all compositions and shown in figure 4.8. In the case of a single trap level, these curves must be straight lines. However, in the present case these curves do not maintain the same slope and the slope goes on decreasing continuously as the time of decay increases. This indicates that the traps exist at all the energies in the band gap which have different time constants and hence give the non exponential decay of photoconductivity. To analyse the decay rates in

the case of non-exponential decay, the differential lifetime (τ_d) has been calculated using the relation given by Fuhs and Stuke [23]:

$$\tau_d = -\left[\frac{1}{I_{ph}}\left(\frac{dI_{ph}}{dt}\right)\right]^{-1} \tag{4.9}$$

In the case of exponential decay, the differential lifetime will be equal to the carrier lifetime. However, in the case of a non-exponential decay, τ_d will increase with time and only the value at $t = 0$ will correspond to the carrier lifetime. From the slope of I_{ph} versus time curves (figure 4.8), the values of τ_d have been calculated using equation (4.9) at different times of the decay curves. Figure 4.9 shows the plots of variation of τ_d (typically for x = 3 at %) with time at 300K and 1035 lx intensity. It is clear from the figure that τ_d increases with the increase in time. This confirms the non-exponential decay in the present case (as for an exponential decay τ_d should be constant with time). Other composition also follows the similar trend of variation of τ_d with time. In order to compare the value of τ_d for various samples under investigation, the value of τ_d at $t = 50$ s is calculated for the samples with the variation of Bi additive at room temperature (shown in the inset of figure 4.9). The values of τ_d is found to increase with increasing Bi content, indicating the slower rate of decay of $I_{ph.}$ Addition of Bi gives rise to defect centres. These defects could induce more localized states which might act as trapping centres. Because of the involvement of electron and hole traps in the recombination process, additional processes of trap filling during the rise and trap emptying during the decay get involved. These traps 'store' the charge carrier and hence delay the recombination rate corresponding to the increase in the differential lifetime with the increase in the Bi content [21].

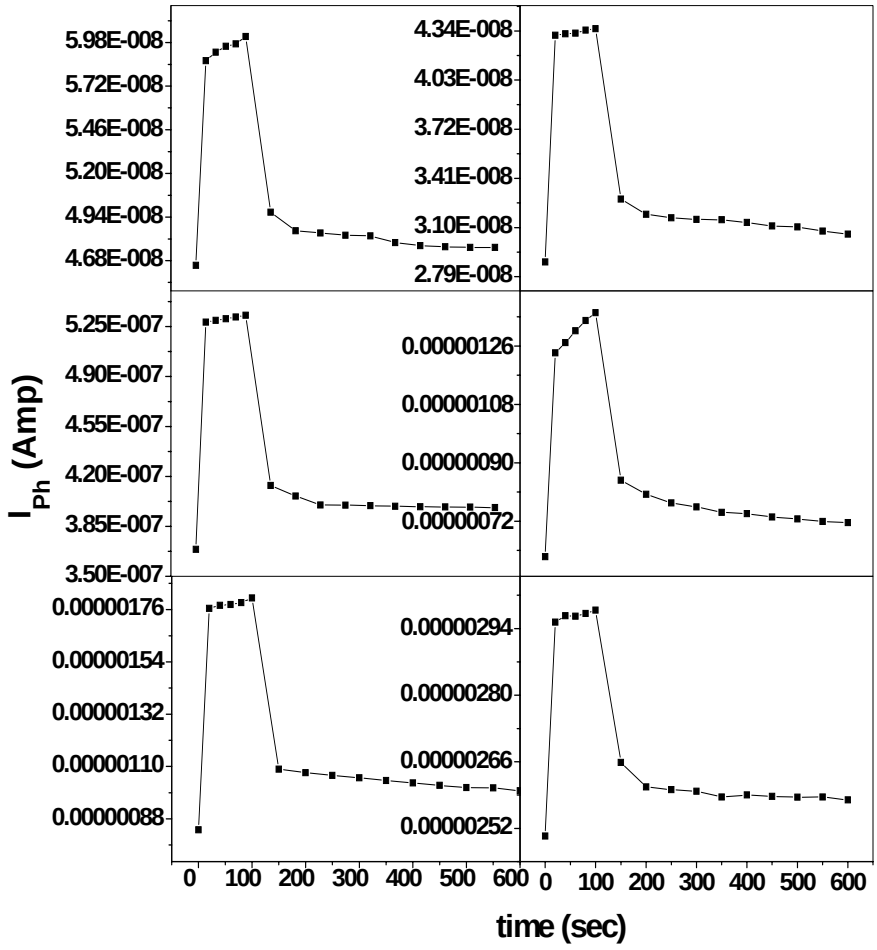

Figure 4.7 Plot of photocurrent (I_{ph}) rise and decay curves for $Se_{85-x}Te_{15}Bi_x$ thin films.

According to the trap controlled recombination model, the photocurrent decay depends on the initial density of photogeneration pulse when the total filling of gap states is not achieved. Therefore, an initial portion of the decay is governed by the capture process and the recombination is delayed. Over this portion $I_{ph} = I_0 t^{-(1-\alpha)}$, where I_0 is the photocurrent at the moment when the light is switched off and α is the dispersion parameter. The value of α is calculated from the slope of ln (I_{ph}) and ln (t) and are tabulated in table 4.3. The localized state distribution parameter E_0 is estimated using the values of the dispersion parameter α calculated from the relation $\alpha = kT/E_0$, where k is Boltzmann's constant and T is the ambient temperature. E_0 may also be calculated by using $E_0 = kT_0$ which is the characteristic energy of the density of state distribution and T_0 is the characteristic temperature. According to Vaninov et. al. [24], T_0 reflects the temperature at which the impurities or the fluctuations of the potentials are frozen at the cooling process of chalcogenide glasses. Moreover, T_0 determined for different impurities also reflects the temperature for which the diffusion coefficient of the impurities becomes negligibly small [25]. For the investigated films the value of α is 0.28 for the base alloy but increases with further substitution of Bi. A similar trend has also been shown by Kushwaha et al [26] and Iovu et al [27].

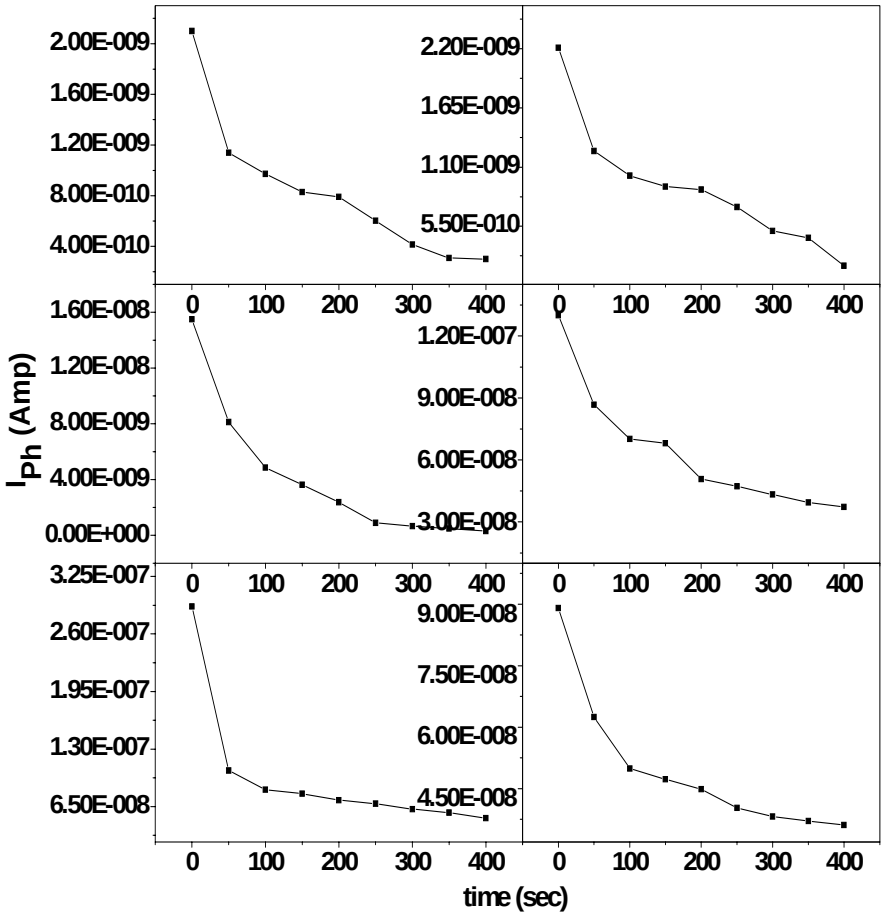

Figure 4.8 Plot of photocurrent (I_{ph}) decay curves for $Se_{85-x}Te_{15}Bi_x$ thin films.

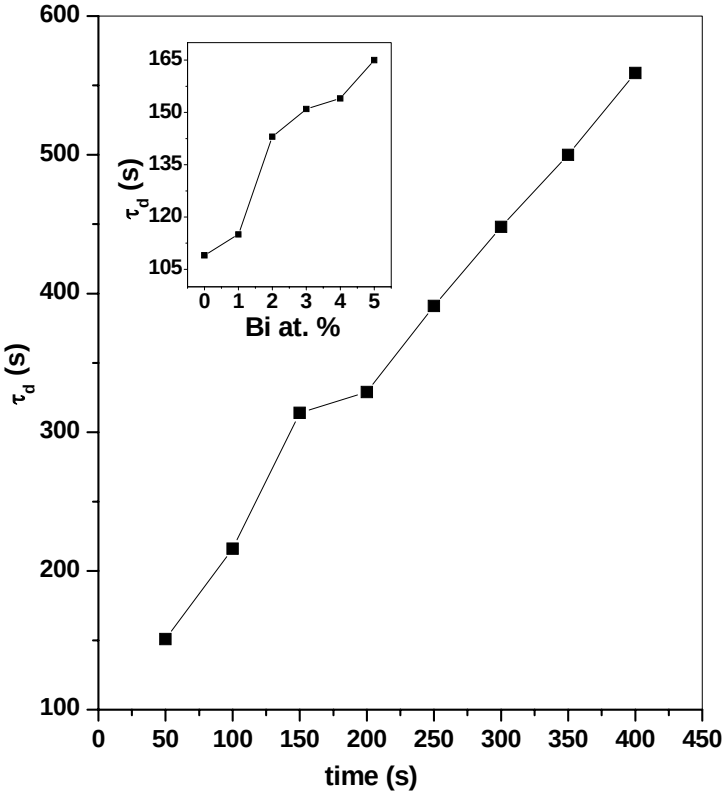

Figure 4.9 Plot of τ_d (sec) versus time (sec) curves for $Se_{85-x}Te_{15}Bi_x$ thin films.

Table 4.3

The Differential life time (τ_d) and Dispersion parameters (α, E_0 and T_0) for $Se_{85-x}Te_{15}Bi_x$ thin films.

Composition	τ_d (sec) (at t = 50 s)	A	E_0 (eV)	T_0 (K)
$Se_{85}Te_{15}$	109	0.39	0.067	776.8
$Se_{84}Te_{15}Bi_1$	115	0.28	0.093	1081
$Se_{83}Te_{15}Bi_2$	143	0.49	0.053	616
$Se_{82}Te_{15}Bi_3$	151	0.58	0.045	523
$Se_{81}Te_{15}Bi_4$	154	0.72	0.036	418
$Se_{80}Te_{15}Bi_5$	165	0.80	0.033	383

4.3.2 Electrical properties of $Ge_{20}Te_{80-X}Bi_x$ (x = 0, 1.5, 2.5, 5.0) system

4.3.2.1 Study of conduction mechanism

Figure 4.10 shows the typical *I-V* characteristics for $Ge_{20}Te_{80-X}Bi_x$ (x = 0, 1.5, 2.5, 5.0) thin films recorded at 300 K. It is evident from figure that for x = 0 and 1.5, an ohmic behaviour of current with voltage is observed in the range 0-100 V. However, for x = 2.5 and 5.0 the current deviate from linearity i.e. tend towards the non-Ohmic behaviour in the higher voltage range (V > 40V). Observed *I-V* characteristics reveals the minimum current flow (maximum resistance) for x = 0, and maximum current flow (minimum resistance) for x = 5.0. For x = 2.5 and 5.0 three linear regions are observed in the voltage ranges (10-30 V), (40-70 V) and (80-100 V). The slope of these regions gives us the value of resistance for that particular voltage range, as stated in table 4.4. Compared to low voltage range, the resistance decreases for higher voltage for x = 2.5 and 5.0. As the voltage is increased across these samples, thermal effects might be induced resulting to decrease in the resistance and allowing more current to flow through the sample.

Table 4.4

Resistance for 500 nm thick $Ge_{20}Te_{80-X}Bi_x$ thin film for three different voltage ranges.

Range	x = 0	x = 1.5	x = 2.5	x = 5.0
Resistance in (0-100 V) range (M Ω)	0.97	0.072	---	---
Resistance in (10-30 V) range (M Ω)	---	---	0.090	0.040
Resistance in (40-70 V) range (M Ω)			0.021	0.009
Resistance in (80-100 V) range (M Ω)	---	---	0.006	0.004

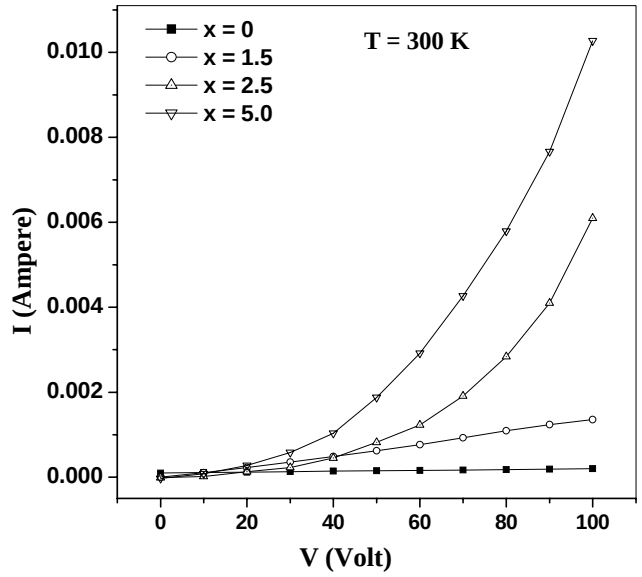

Figure 4.10 Plot of *I-V* characteristics for $Ge_{20}Te_{80-X}Bi_x$ thin films.

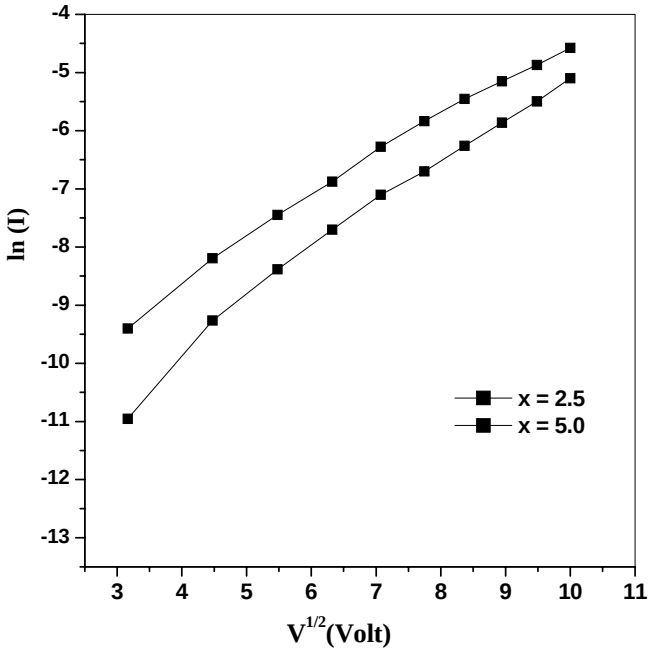

Figure 4.11 Plot of *ln (I)* versus $V^{1/2}$ for $Ge_{20}Te_{80-X}Bi_x$ (x = 2.5, 5.0) thin films

In our present investigation, the field dependence studies for a film of typical thickness 500 nm reveals the non ohmic nature *i.e.* the current exhibits an applied voltage dependence of the form $I \alpha V^{1/2}$ for x = 2.5 and 5.0 for the voltage range V > 40V (figure 4.11). This again indicates that the conduction in such materials (*i.e*; x = 2.5 and x = 5.0) obey the Poole-Frenkel conduction mechanism [10].

4.3.2.2 Temperature dependent dark and photo conductivity

Figure 4.12 shows the temperature dependence of dark conductivity (σ_d) for $Ge_{20}Te_{80-X}Bi_x$ thin films typically at 80 V. The plots of ln (σ_d) versus 1000/T are found to straight lines indicating that the conduction is through an activated process having single activation energy in the temperature range 300-360 K. The (σ_d) for $Ge_{20}Te_{80-X}Bi_x$ thin films is calculated using equation 4.5. The value of dark activation energy ΔE_d is estimated from the slope of ln (σ_d) versus 1000/T curves. The calculated values of ΔE_d, σ_d and pre exponential factor σ_0 at room temperature are inserted in table 4.5. The composition dependent dark conductivity and activation energy is studied and it is observed that with the increase of Bi content conductivity increase with the decrease in activation energy. This behaviour may be explained on the basis of Mott and Davis model. In the present case the values of σ_0 is of the order of 10^3, indicating that conduction is through extended states [11]. The variation of dc parameters with Bi for the investigated composition may also be explained by assuming that Bi atoms act as impurity centres in the mobility gap and induces structural changes in the network which may disturb the balance of charged defects and consequently change the electric conduction.

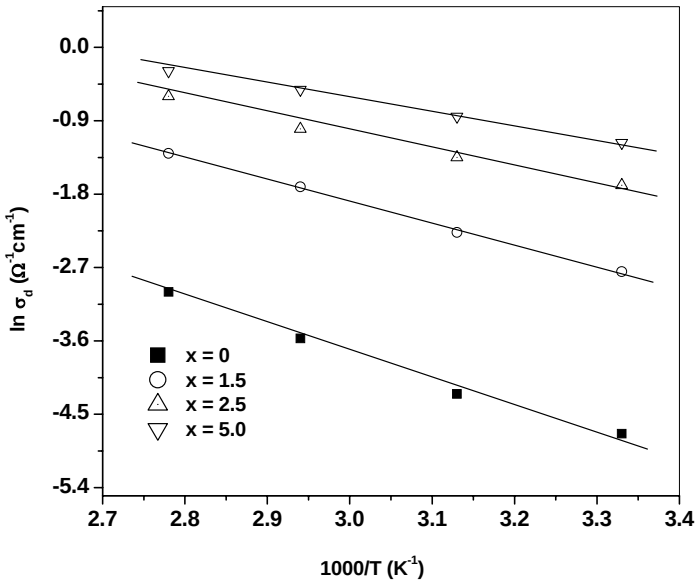

Figure 4.12 Plot of ln (σ_d) versus 1000/T for $Ge_{20}Te_{80-X}Bi_x$ thin films.

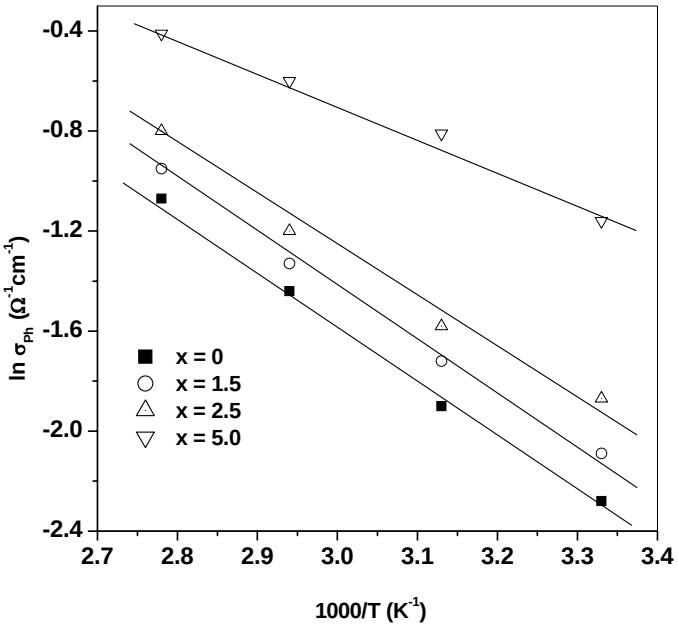

Figure 4.13 Plot of ln (σ_{Ph}) versus 1000/T for $Ge_{20}Te_{80-X}Bi_x$ thin films.

New trap states are created in the mobility gap due to the Bi addition and the concentration of positive defects (D^+) defects get reduced as compared with that of negative (D^-) states. The increase in σ_d and consequent decrease in ΔE_d with Bi may also be explained on the basis of the binding energy of the system which is found to decrease with the increase in Bi concentration. In the above mentioned system, Bi enters into the Ge-Te system and saturates Bi-Te bonds thus decreasing the concentration of Ge-Te bonds. Since the bond energy of Bi-Te bond (125.6 kJ / mol) is lower than that of the Ge-Te bond (156.7 kJ / mol), the average bond energy of the system decreases. Moreover the behaviour of σ_d can also be related to the thermal studies of the samples under investigation which shows that glass transition temperature increases with increase in Bi concentration. It further implies that rigidity of the system increases with the Bi concentration and hence σ_d also increases.

Figure 4.13 shows the variation of steady state photoconductivity (σ_{Ph}) of $Ge_{20}Te_{80-X}Bi_x$ thin films with temperature (*i.e.* σ_{Ph} versus 1000/T) at a particular intensity 1085 lux. The value of ΔE_{Ph} is calculated from the slope of figure 4.13 and are tabulated in table 4.5, along with the values of σ_{Ph} at 300 K. It is observed that the value of σ_{Ph} is much higher than σ_d for a particular Bi concentration. This is presumably due to the increased density of charged carriers compared with their value at thermal equilibrium, when the material is exposed to electromagnetic radiation. The value of ΔE_{Ph} is found to be much smaller than ΔE_d and it shows the same trend as that of ΔE_d, for the entire samples.

4.3.2.3 Intensity dependent photoconductivity

Intensity (*F*) dependence of steady state photoconductivity (σ_{Ph}) has been studied at room temperature (300 K) typically at 80 V to investigate the nature of recombination

process in $Ge_{20}Te_{80-X}Bi_x$ thin films. Figure 4.14 shows the plots of ln (σ_{Ph}) versus ln (F) and are found to be straight for all the compositions, indicating that σ_{Ph} also follows a power law with F *i.e.* $\sigma_{Ph} \alpha F^{\gamma}$. For the present samples under investigation the value of γ is calculated from the slope of ln (σ_{Ph}) versus ln (F) and is found to be closed to 0.5 for all the compositions. This further confirms a bi-molecular recombination mechanism in the studied films.

In the photoconductivity measurements, photosensitivity (σ_{Ph}/σ_d) and density of defect states (n_σ) are two important parameters to describe the usefulness of a particular material from optoelectronic device point of view. The value of (n_σ) for different samples is calculated using the equation 4.8. The calculated values of σ_{Ph}/σ_d and n_σ for $Ge_{20}Te_{80-X}Bi_x$ thin films at absolute temperature (300 K) and at intensity 20-1085 lux at fixed voltage of 80 V are inserted in table 4.5. It is observed that at a particular intensity, photosensitivity decreases with the addition of Bi, whereas exactly opposite trend has been observed in case of n_σ. σ_{Ph}/σ_d depends upon the lifetime time of excess charge carriers which further depends upon the density of localized states in a particular material. The higher the density of states, the lower will be the lifetime as these defect states may act as recombination centres in the presence of light. This is attributed to the formation of intimate valence alternation pairs (IVAPs) under illumination. The defects are converted to random pairs of charged defects known as light induced metastable defects (LIMDs) [30, 31]. These LIMDs act as electron/hole trapping centres and thus decrease the photocurrent. Therefore σ_{Ph}/σ_d will be maximum when the density of states will be minimum. The results are confirmed in table 4.5 which shows a minimum value of n_σ and maximum value of σ_{Ph}/σ_d at x = 0.

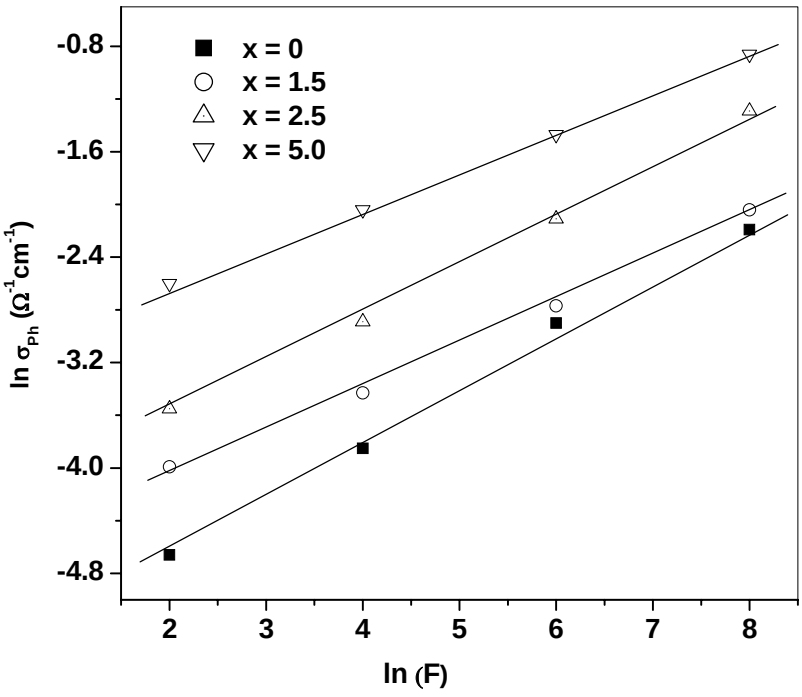

Figure 4.14 Plot of ln (σ_{Ph}) versus *ln (F)* for $Ge_{20}Te_{80-X}Bi_x$ thin films

Table 4.5

The dc dark conductivity (σ_d), the pre-exponential factor (σ_0), the activation energy for dc conduction (ΔE_d), photoconductivity (σ_{Ph}), the activation energy of photoconduction (ΔE_{Ph}), power exponent (γ), photosensitivity (σ_{Ph}/σ_d), and charge carrier density (n_σ) for $Ge_{20}Te_{80-X}Bi_x$ thin films.

Composition	$\sigma_0(dark)$ $(\Omega^{-1}cm^{-1})$	σ_d $(\Omega^{-1}cm^{-1})$	ΔE_d (eV)	σ_{Ph} *(photo)* $(\Omega^{-1}cm^{-1})$	ΔE_{Ph} (eV)	σ_{Ph}/σ_d	γ	n_σ (cm^{-3})
$Ge_{20}Te_{80}$	343.78	0.0088	0.28	0.10	0.20	11.36	0.42	3.91×10^{19}
$Ge_{20}Te_{78.5}Bi_{1.5}$	450.34	0.0652	0.23	0.12	0.16	1.84	0.35	2.71×10^{20}
$Ge_{20}Te_{77.5}Bi_{2.5}$	121	0.17	0.18	0.19	0.13	1.12	0.38	1.87×10^{21}
$Ge_{20}Te_{75}Bi_{5.0}$	67.31	0.310	0.14	0.31	0.11	1.00	0.30	8.77×10^{21}

4.3.2.4 Transient photoconductivity

Transient photoconductive measurements are conducted by exposing all the samples to light (1035 lx intensity) at 300 K. Figure 4.15 shows the rise and decay of photocurrent (I_{ph}) for all compositions. It is evident from the figure that the photocurrent rises in a monotonic manner up to the steady state value. After cessation of steady illumination, trapped electrons and holes combine and the photocurrent decay is quite fast initially and then it reaches to a steady state value known as persistent photocurrent. To understand the trapping effects, the persistent photocurrent is subtracted from the measured photocurrent and then the corrected photocurrent against time (t) is plotted for all compositions and shown in figure 4.16. From the figure it is evident that the slope goes on decreasing with the increase in time of decay. This indicates that the traps exist at all the energies in the band gap which have different time constants and hence give the non exponential decay of photoconductivity. To analyse the decay rates in the case of non-exponential decay, the differential lifetime (τ_d) has been calculated using the equation 4.9. Using the slope of I_{ph} versus time curves (figure 4.16), the values of τ_d have been calculated using equation 4.9 at different times of the decay curves. Figure 4.17 shows the plots of variation of τ_d (typically for x = 5 at %) with time at 300 K and 1035 lx intensity. It is clear from the figure that τ_d increases with the increase in time. This confirms the non-exponential decay in the present case (as for an exponential decay τ_d should be constant with time). Other composition also follows the similar trend of variation of τ_d with time. In order to compare the value of τ_d for various samples under investigation, the value of τ_d typically at t = 50 s is calculated for the samples with the

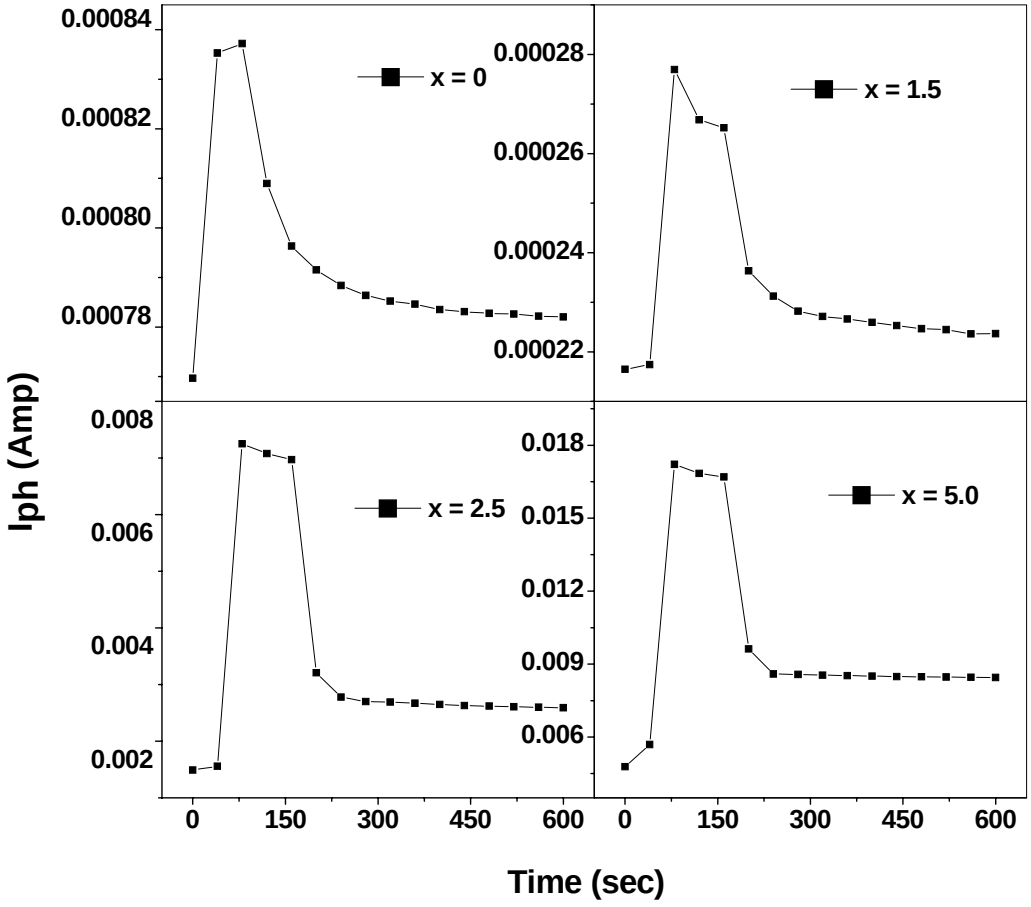

Figure 4.15 Plot of photocurrent (I_{ph}) rise and decay curves for $Ge_{20}Te_{80-X}Bi_x$ thin films.

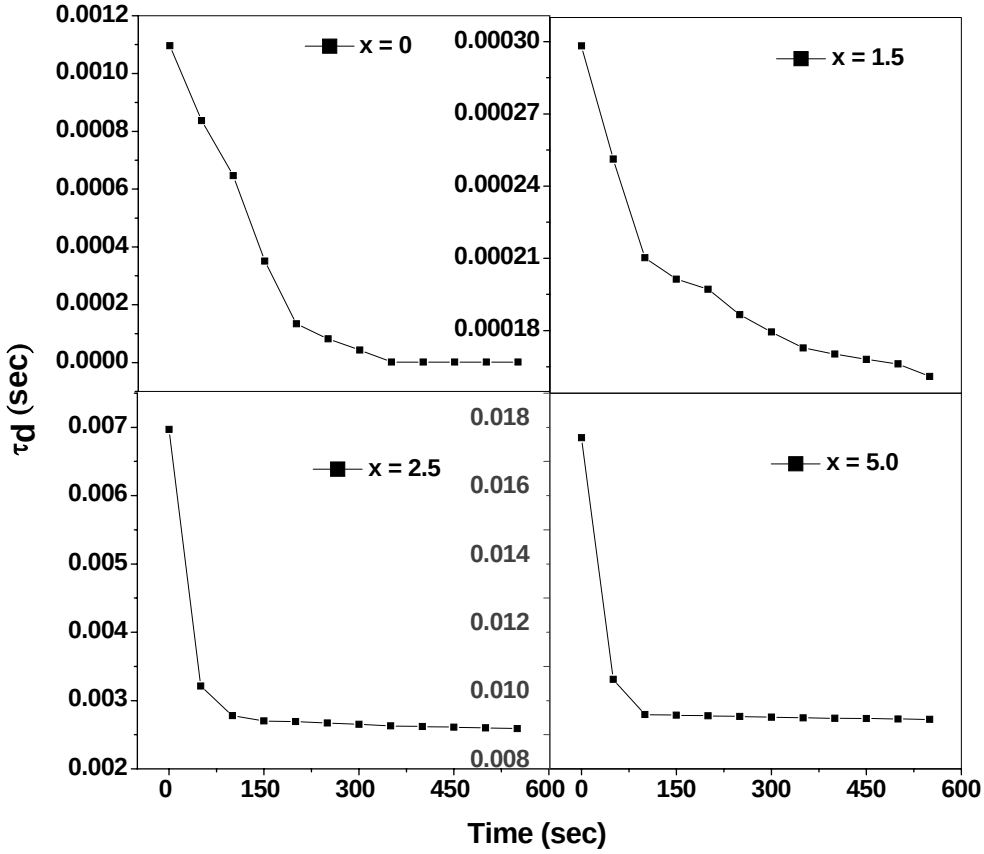

Figure 4.16 Plot of photocurrent (I_{ph}) decay curves for $Ge_{20}Te_{80-X}Bi_x$ thin films.

variation of Bi additive at room temperature (shown in the inset of figure 4.17). The values of τ_d is found to increase with increasing Bi content. The values of τ_d increases with the increase in Bi additive. The higher value of τ_d after Bi incorporation indicates the slower rate of decay of I_{ph}. Simple kinetics involving trapping and recombination centres influence the photoconductivity of solids. Two relevant recombination steps are; (i) tunnelling of band tail electrons to neutral dangling bonds D^0, producing D^- states and (ii) the diffusion of holes in the tail states to recombine with D^- states formed in step (i). According to the trap controlled recombination model, the photocurrent decay depends on the initial density of photogeneration pulse when the total filling of gap states is not achieved. Therefore, an initial portion of the decay is governed by the capture process and the recombination is delayed. Over this portion also $I_{ph} = I_0 t^{-(1-\alpha)}$ is followed. The value of α, E_0 and T_0 are determined for the glassy alloys and tabulated in table 4.6.

Table 4.6

The Differential life time (τ_d) and Dispersion parameters (α, E_0 and T_0) for $Ge_{20}Te_{80-x}Bi_x$ thin films

Composition	τ_d (sec) (at t = 50 s)	A	E_0 (eV)	T_0 (K)
$Ge_{20}Te_{80}$	186	0.53	0.049	568
$Ge_{20}Te_{78.5}Bi_{1.5}$	218	0.67	0.046	736
$Ge_{20}Te_{77.5}Bi_{2.5}$	245	0.73	0.039	616
$Ge_{20}Te_{75}Bi_{5.0}$	296	0.86	0.029	523

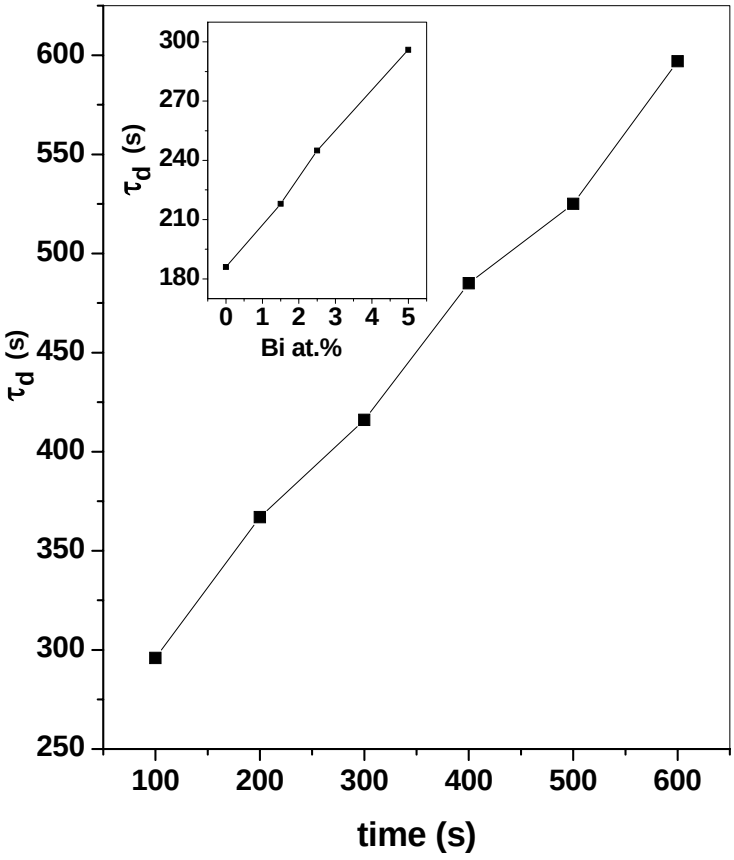

Figure 4.17 Plot of τ_d (sec) versus time (sec) curves for $Ge_{20}Te_{80-X}Bi_x$ thin films. (Inset) Plot of τ_d (sec) versus Bi at. % curves for $Ge_{20}Te_{80-X}Bi_x$ thin films.

4.4 Conclusion

The *I-V* characteristics of $Se_{85-x}Te_{15}Bi_x$ (where x = 0, 1, 2, 3, 4, 5) and $Ge_{20}Te_{80-X}Bi_x$ (x = 0, 1.5, 2.5, 5.0) thin films have been discussed and the conduction is explained qualitatively in terms of Poole Frenkel conduction mechanism in a specific voltage range. The mechanism is further confirmed by the dependence of *I* on square root of *V*. However for $Ge_{20}Te_{80-X}Bi_x$ (x = 0, 1.5) thin films the *I-V* characteristics are of Ohmic nature. The study of dark and photoconductivity of the thin films of both of the glassy alloys as a function of temperature (303-333 K) reveals that the conduction is through an activated process with single activation energy. Activation energy for photoconduction is found to be much smaller than its value for dark conduction. Dark as well as photo conductivity (at 1085 lux) is found to decrease as Bi is introduced to the host $Se_{85}Te_{15}$ glassy alloy whereas, its further addition (> 1 Bi at. %) causes the conductivity to increase. However in case of $Ge_{20}Te_{80-X}Bi_x$ thin films conductivity is found to increase with increase in Bi content. Intensity dependent photoconductivity has also been studied and it shows the existence of bimolecular recombination in both of the glassy systems. The values of σ_{Ph}/σ_d and n_σ are calculated for $Se_{85-x}Te_{15}Bi_x$ thin films at absolute temperature (303 K) within the intensity range 20-1085 lux. It is observed that at a particular intensity, photosensitivity increases as Bi is introduced to host $Se_{85}Te_{15}$ glassy alloy and then decreases with the further addition of Bi (≥ 2 at. %) but exactly opposite trend has been observed in case of n_σ. In case of $Ge_{20}Te_{80-X}Bi_x$ thin films photosensitivity decreases with the addition of Bi and again opposite trend has been followed by n_σ. The results were successfully explained on the basis of density of defect states. The value of mobility is also determined for the system and it is found to follow the opposite trend as that of σ_d. The transient photoconductivity measurements for

investigated thin films at room temperature and 1035 lx intensity shows that the photocurrent rises in a monotonic manner up to a steady state value, and after cessation of illumination, it follows a non-exponential decay. An increase in the differential lifetime is also observed with time (for all compositions) as well as with the increase in the Bi concentration.

References

1. Dahshan A., Ameer H H, Moharam A H and Othman A A 2006 Thin Solid Films 513 369.
2. Baranovski S D 1984 Soviet Phys: Semiconductors 18 633.
3. Macfarane D R, Maecki M, Paulain M 1984 J. Non-Cryst. Solids 64 351.
4. Matusita K, Komatsu T, Yokata R 1984 J. Mater. Sci. 19 291.
5. Shiryaev V S, Adam J -L, Zhang X H 2004 J. Phys. Chem. Solids 65 1737.
6. Mahadevan S, Giridhar A, Singh A K 1986 J. Non-Cryst. Solids 88 11.
7. Jonschere A K 1971 Electronic Conduction in Amorphous Semiconductors, Journal of Vacuum Science and Technology 8 135-144.
8. Popescu M 2000 Non Crystalline Chalcogenides (Dordrecht: Kluwer Academic).
9. Jonschere A K, Hill R M, Hass G M H, Hofman R W (Eds.) 1975 Physics of Thin Films (New York: Academic Press).
10. Abdel Latif R M 1998 Physica B 254 273.
11. Mott N F and Davis E 1971 Electronics Process in Non-Crystalline Materials (Oxford: Clarendon).
12. Sharma V 2006 J. Opto-Electron. Adv. Mater. 8 1823.
13. Kumar D and Kumar S, Turk J Phys. 29 91 (2005).
14. Sharma Ambika and Barman P B 2008 Journal of Thermal Analysis and Calorimetry doi: 10.1007/s10973-008-9312-8.
15. Sharma I, Tripathi S K, Monga A and Barman P B 2008 Journal of Non-Crystalline Solids 354 3215.
16. Sharma Ishu, Kumar Akshay, Tripathi S K and Barman P B, 2008 J. Phys. D: Appl. Phys. 41**,** 175504.

17. El-Korashy A, El-Zahed H, Zayed H A and Kenawy M A 1995 Solid State Commun. **95** 335.

18. Sharma V, *Thakur* A, Goyal N, Saini G S S and Tripathi S K 2005 Semicond. Sci. Technol. **20** 103.

19. Shimakawa K 1985 J. Non-Cryst. Solids 77 1253.

20. Shimakawa K, Inami S, Kato T, Elliot S R 1992 Phys Rev. B 46 10062.

21. Shimakawa K, Kolobov A V, Elliot S R 1995 Adv. Phys. 44 475.

22. Fuhs W, Stuke J 1968 Phys. Status Solidi 27 171.

23. Sharma Ishu, Kumar Akshay, Tripathi S K and Barman P B 2008 J. Phys. D: Appl. Phys. 41175504.

24. Vaninov V, Orenstein J and Kastner M A 1982 Phil. Mag. B 45 399.

25. Kastner M A 1978 Phil. Mag. B 37 127.

26. Kushwaha N, Kushwaha V S, Shukla R K and Kumar A 2005 J. Non-Cryst. Solids 351 3414.

27. Iovu M A, Iovu M S and Colomeico E P 2003 J. Optoelectron. Adv. Mater. 5 1209.

CHAPTER 5

Effect of Bi incorporation on thermal properties of Se-Te and Ge-Te glassy alloys

5.1 Introduction

All the amorphous solids are thermodynamically unstable and tend to relax towards a stable or metastable phase. The time scale on which these changes occur varies enormously is usually a sensitive function of temperature. A class of non-crystalline solids prepared from the liquid state is called glass. These are characterized by being structurally continuous with liquid state and are prepared by quenching the molten liquid to a temperature far below their equilibrium melting point without crystallizing and can remain in their metastable states indefinitely. When the temperature decreases from the liquid phase, some materials do not crystallize below their melting point, but they become a super cooled liquid. As the temperature keeps decreasing, glass transition occurs at a certain temperature, 'T_g', below which they become glass. These behaviours are explained by volume versus temperature curve as shown in figure 5.1. T_g is defined by the temperature at which the extrapolations of the liquid and glassy lines are intersected. This shows that when the cooling rate is fast, T_g becomes higher or vice versa. The slower the rate of cooling, larger is the region for which liquid is super-cooled and hence lower is the glass transition temperature. The glass transition of a particular material partly depends on its thermal history. The value of T_g is influenced by the prevailing experimental conditions to a large extent, *e.g.* the cooling rate of the melt. Glass formation becomes more probable, when the cooling rate is greater, the sample volume is smaller and the crystallization rate is slower. However, fast quenching to avoid crystallization introduces a volume change which results in a large density fluctuation

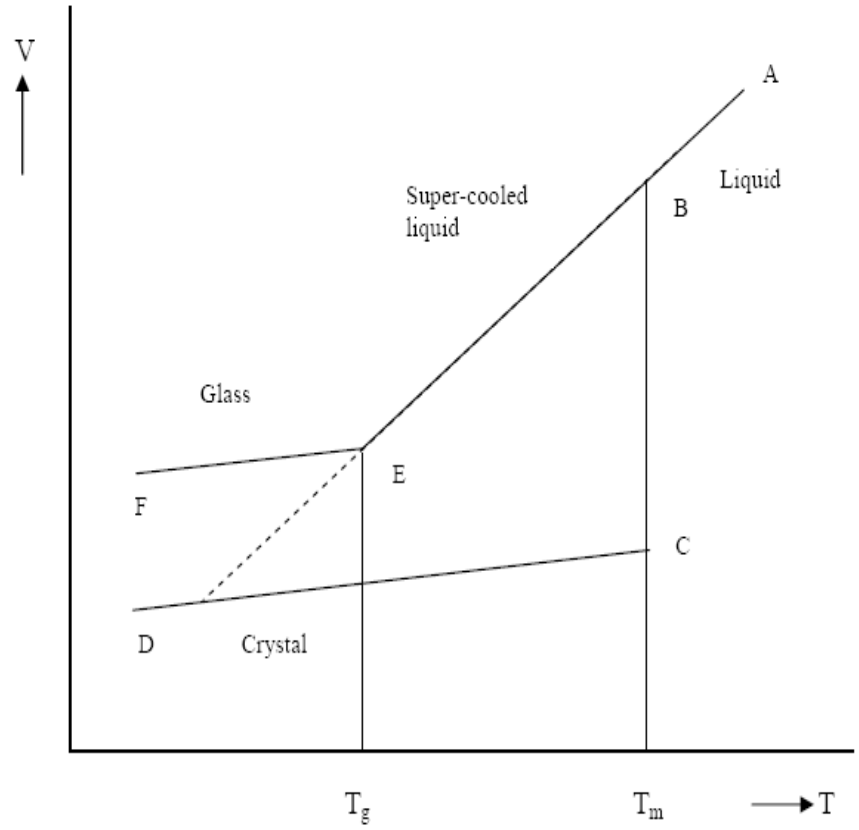

Figure 5.1 Schematic illustration of volume versus temperature curve: transition from the crystalline state to glassy state.

and vice-versa. $T_g = 2T_m /3$, where T_m is the melting temperature [1]. Cooling a liquid with a rate high enough to avoid the crystallisation will lead it to the supercooled regime in which the viscosity will increase drastically as the temperature will decrease. For a given temperature (T_g) or more precisely for a given domain of temperatures (called the glass transition), firstly the supercooled liquid is frozen in and the viscosity reaches values as large as 10^{12} poises. However for $T < T_g$, a glassy structure is obtained. As exemplified on figure 5.2, this glassy structure is characterised by an excess of free volume which is equivalent to an excess of enthalpy or an excess of configurational entropy when comparison is made with the corresponding thermodynamic equilibrium state. Then the disorder engaged into the glassy structure can be defined at different scales (short, medium or long range). As a consequence, a glass kept at $T < T_g$ will loose its excess of enthalpy by molecular relaxation to reach more favourable thermodynamic states. Thus, a glass kept during an infinite time at $T < T_g$ must reach the thermodynamic equilibrium. This goal is obtained with the supercooled liquid state (extrapolated in the temperature domain $T < T_g$) and not with the crystalline one (sees figure 5.2). In other words, a glass cannot crystallise by physical ageing. To crystallise the material, it is necessary to heat the glass above its glass transition in order to reach a viscosity value low enough to authorise molecular rearrangements or atomic diffusions. Many models are now available to analyse the relaxation kinetic [2-5] and it is now established that a good model must be taken into account with following characteristics. (*i*) Molecular relaxations in the glass and for temperatures close to T_g are of cooperative natures. (*ii*) Relaxation kinetics cannot only be described by a linear or an exponential time relaxation function but also distribution of relaxation time function must be taken into account. The

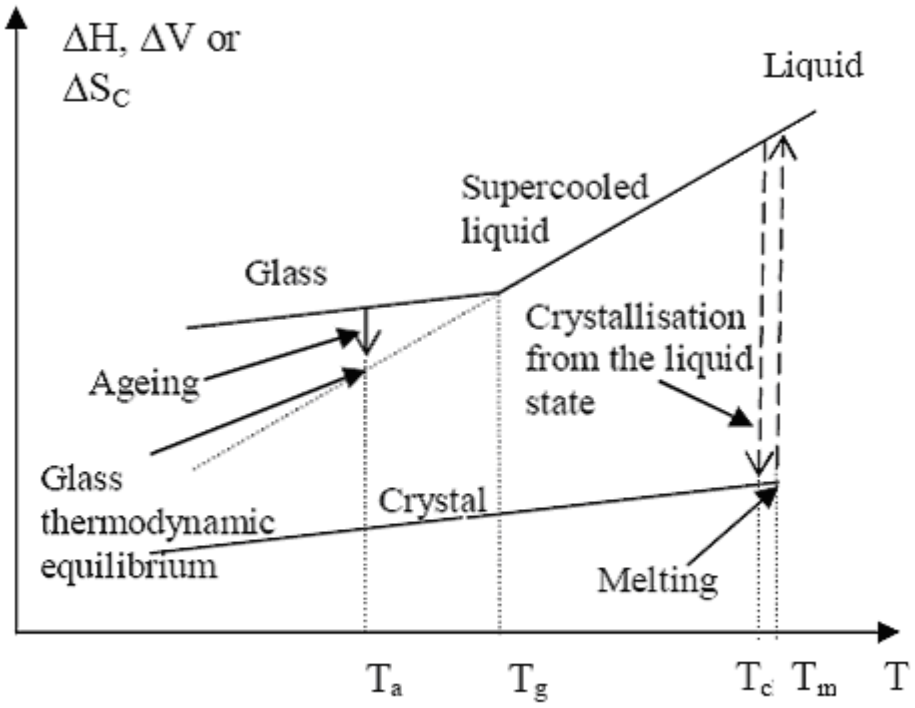

Figure. 5.2. Enthalpic diagram showing the glass transition and the crystallisation from the liquid state T_c and the melting T_m.

phenomenon is reversible by a thermal cycle consisting of heating the glass above T_g and then cooling back to the annealing temperature, of course if no crystallisation occurs in the supercooled state. To analyse a glass, one of the easiest methods consists of performing calorimetric measurements. In this method, tens of milligrams of a glass sample of interest contained in an Al pan is heated at a pre-determined scan rate (dT / dt) typically at 10 ºC / min, and the heat flow to a sample (dH_t / dt) compared to that of an empty reference Al pan.

Figure 5.3 shows a typical differential scanning calorimetric (DSC) curve that could be obtained for any chalcogenide glass. At low temperature, the glass transition is observed only by an endothermic ΔC_p step, if the sample is non-aged and by an endothermic peak if the sample is aged. At higher temperature, an exothermic peak of crystallisation (also called cold crystallisation) or devitrification is obtained. Finally, the melting of the crystalline part occurs at higher temperature as an endothermic peak. Thus to characterise a glass, such measurements give us many facilities. We have: (*i*) the glass transition temperature T_g (*ii*) the value of ΔC_p at T_g (*iii*) the domain of temperature on which the glass transition occurs $\Delta T_g = T_{gmax} - T_{gmin}$ (*iv*) the area of the endothermic relaxation peak δH (*v*) the value of the crystallisation temperature (T_c or T_m) (*vi*) the enthalpy of crystallisation ΔH_c and finally (*vii*) the distance T_c - T_g. Each of these quantities can give us precious information's for the considered glass. For instance, for only the glass transition:

1) Greatest the T_g, greatest must be the rigidity of the medium [6, 7].

2) Greatest ΔT_g, greatest must be the width of the time relaxation distribution [8].

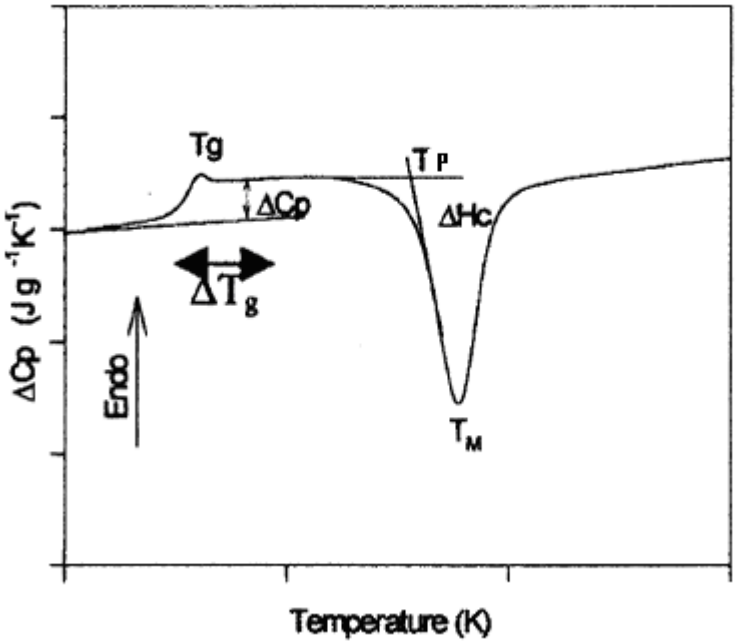

Figure 5.3 Typical DSC trace obtained with a chalcogenide glass.

3) Greatest ΔC_p, greatest must be the fragility (from the Angell strong fragile liquid glass former concept [9]).

Most of these quantities are not material constants, but depend also on the measurement methods, on the constraints undergone and on the thermal history of the samples. For instance, the values of cooling rate, heating rate, sample age and value of the annealing temperature influence and modify the values of T_g, ΔT_g, δH, T_c, ΔH_c [10-14]. In other words, to compare the data of different origins, many precautions must be taken but these dependencies can also give us many new opportunities to characterise a glassy structure. In this field, among all the different materials to be studied; chalcogenide elements and alloys exhibit the great advantage to give a large variety of systems of tailor made structures. In the following, this opportunity will be analysed for different vitreous chalcogenide based alloys. In particular, the glass transition temperature and the relaxation kinetics will be investigated.

The impurities like Bi have produced a remarkable change in the thermal properties of chalcogenide glasses. The addition of Bi as a third element with simultaneous replacement of Se increases the glass transition temperature of the Se-Te-Bi system [15-17] indicating the hardening of host Se-Te alloy. The glass forming ability of a sample is defined as the capacity to obtain amorphous phase when the sample is rapidly quenched. If the cooling rate is sufficiently high the crystallization is inhibited. In this case, the sample in liquid state at the melting temperature is rapidly quenched down to glass transition temperature where the liquid is transformed to amorphous phase. The

composition dependence of glass forming ability is analyzed in the present system and it has been found to increase as Bi is introduced to host Se-Te alloy. However, further increase of Bi reduces the glass forming ability. In the present work, DSC studies on bulk glasses have been carried out to determine glass transition temperature (T_g), peak crystallization temperature (T_p) and melting temperature (T_m) as a function of heating rate as well as Bi concentration in the $Se_{85-x}Te_{15}Bi_x$ chalcogenide system. However in case of $Ge_{20}Te_{80-x}Bi_x$ system thermal behaviour is recorded using Shimadzu DTG-60. It is supposed that amorphous $GeTe_2$ structure with fourfold coordination of Ge and two fold coordination of Te is most stable in the alloys containing less than 33 at.% of Ge. The existence of strong covalent bonding in *a*-Ge-Te has been proven by photoemission measurements [18]. Moreover, the covalency in amorphous phase was shown to be stronger than in crystalline phase. From the experimental structure factors and pair correlation functions of Ge-Te alloys as investigated by I. Kaban *et.al.* [19], one may guess that amorphous Ge-Te alloys are a random mixture of Ge and Te atoms and Ge-Te bonds are formed statistically when Ge is added. On the other hand, it can be supposed that Te- rich Ge-Te amorphous alloys are chemically ordered on the microlebel and some structural units with strong Ge-Te bonds are distributed among Te atoms. It was established that $Ge_{20}Te_{80}$ composition alloy shows single- stage amorphous - to - crystalline transformation due to simultaneous formation of Ge-Te and Te crystallites, whereas the alloy containing 15 at.% Ge exhibits two - stage transformation due to segregation of Te and subsequent formation of GeTe crystallites. Obviously this difference in the crystallization of the Ge-Te alloys is explained by differences in their

atomic structure. We suppose that all Ge atoms in $Ge_{20}Te_{80}$ composition alloy are bonded with Te atoms with stiochiometry $GeTe_4$. On the other hand the alloy between $Ge_{20}Te_{80}$ and pure Te contain $GeTe_4$ tetrahedra as structural units and Te atoms are distributed among them. For $Ge_{20}Te_{80}$ glassy alloy, elastic recovery of deformation is maximum [20]. $Ge_{20}Te_{80}$ composition glassy network lies at the threshold of the mode change i.e. floppy to intermediate region having an average coordination number $m = 2.4$. According to constraint model and development theories [21, 22], by equating the number of operative constraints to the number of degrees of freedom, m of the most stable glass is shown to be $m = 2.4$. So the addition of third element in Ge–Te tetrahedral glassy network makes the glass an interesting material and new properties are expected. The addition of Bismuth (Bi) into $Ge_{20}Te_{80}$ system in an effective way controls its electrical, optical and physical properties as this will lead the system towards the intermediate region. In the present paper the cohesive energy has been calculated using chemical bond approach and is correlated with energy gap. Other physical parameters *viz*. coordination number, constraints, density, molar volume etc. has also been investigated. The variation of these parameters has been shown in terms of composition or equivalently with the average coordination number *m*.

5.2 Theoretical Background

5.2.1 Deducing volume fraction transformed

The theoretical basis for interpreting DSC results is provided by the formal theory of transformation kinetics [23-26]. This theory supposes that the crystal growth rate in general is anisotropic. In the case of a quenched glass where a large number of nuclei

already exists and no new nuclei are formed during the thermal treatment (site saturation) [27], the volume of a transformed region is given by

$$v = g\prod_i \int_0^t u_i\left(t'\right)dt' \tag{5.1}$$

where the expression $g\prod_i \int_0^t u_i\left(t'\right)dt'$ condenses the product of the integrals corresponding to the values of the above quoted subscript *i* and *g* is a geometric factor which depends upon the dimensionality and shape of the crystal growth. Defining an extended volume of transformed material and assuming spatially random transformed regions [28], the elemental extended volume fraction dx_e is expressed as

$$dx_e = vdN' = g\left(\prod_i \int_0^t u_i\left(t'\right)dt'\right)dN' \tag{5.2}$$

where dN' being the number of nuclei existing in a volume element of material. When the crystal growth rate is isotropic, $u_i = u$; an assumption which is in agreement with the experimental evidence. In many transformations the reaction product grow approximately as spherical nodules [20] and equation (5.2) can be written as [25, 29]

$$dx_e = g\left(\int_0^t u\left(t'\right)dt'\right)^f dN' \tag{5.3}$$

where *f* is the exponent related to the dimensionality of crystal growth. In the considered case of site saturation [27], the kinetic exponent $n = f$. Assuming an Arrhenian temperature dependent for *u* [25], at constant heating rate $\beta = (dT/dt)$ [30], equation (5.3) becomes

$$x_e = gN_0 u_0^n \beta^{-n} \left(\int_{T_0}^{T} e^{-E_G / RT'} dT' \right)^n = qI^n \tag{5.4}$$

where E_G is the effective activation energy for crystal growth and N_0 is the number of pre-existing nuclei per unit volume. By using the substitution $z' = E_G / RT'$ the integral I can be represented by the sum of alternating series [31]

$$S(z') = \frac{-e^{-z'}}{z'^2} \sum_{k=0}^{\infty} \frac{(-1)^k (k+1)!}{z'^k}$$

In this type of series the error produced is less than the first term neglected and in most crystallization reaction $z' = E_G / RT' >> 1$. Usually with $z' >> 25$ [32], it is possible to use only the first term of this series without making any appreciable error and thus the above mentioned integral I can be written as

$$I = \frac{E_G}{R} e^{-z} z^{-2} = RT^2 E_G^{-1} \exp\left(-\frac{E_G}{RT} \right) \tag{5.5}$$

If it is assumed that $T_0 << T$ (T_0 is the starting temperature), z_0 can be taken as infinity. This assumption is justifiable for any thermal treatment that begins at a temperature where crystal growth is negligible, *i.e.* below the glass transition temperature T_g [32]. Substituting equation (5.5) into equation (5.4), introducing the parameter $P = (R/E_G)^n$ and defining the reaction rate constant $K_R = (gN_0)^{1/n} u_0 \exp(-E_G / RT)$ with Arrhenian temperature dependence, the extended volume fraction under non isothermal regime is expressed as

$$x_e = P(K_R T^2 \beta^{-1})^n \tag{5.6}$$

This is a general expression for all possible values of the exponent, *n* which depends upon the dimensionality of the crystal growth. The extended volume fraction gives information about the kinetic laws which governs the crystal growth. However, a general kinetic equation must also consider the geometrical problem of the impingement between regions growing from separated nuclei. In this sense we will simply state that a relationship between the actual fraction transformed, *x* and the extended x_e can be written as

$$dx = (1 - x)dx_e \tag{5.7}$$

when the termed impingement exponent, $\gamma_i = 1$ [33]. Bearing in mind equation (5.6), the general solution of equation (5.7) is given by

$$x = 1 - \exp[-P(K_R T^2 \beta^{-1})^n] \tag{5.8}$$

This equation is used to obtain the kinetic parameters.

5.2.2 Calculating Kinetic parameters

The usual analytical methods proposed in the literature [32] for analysing the transformation kinetics, assume that the reaction rate constant can be defined by Arrhenian temperature dependence. In order for this condition to hold for the present work assumes that the crystal growth rate *u* has an Arrhenian temperature dependence [25] and over the temperature range where the thermoanalytical measurements are carried out, the nucleation rate is negligible (*i.e.* the condition of site saturation) [25, 27]. From this point of view the crystallization rate is obtained by differentiating equation (5.8) with respect to time [30], yielding

$$dx/dt = nP(K_R T^2 \beta^{-1})^{n-1}(1 - x)\left(K_R E_G R^{-1} + 2K_R T\right) \tag{5.9}$$

where it is assumed that the reaction rate constant is a time function through its Arrhenian temperature dependence.

The maximum crystallization rate is obtained by making $d^2x / dt^2 = 0$ [30], thus obtaining the relationship

$$P[(K_R)\big|_p T_p^2 \beta^{-1}]^n = 1 - \left(\frac{2}{n}\right)\left(1 + \frac{E_G}{RT_p}\right)\left(2 + \frac{E_G}{RT_p}\right)^{-2} \tag{5.10}$$

where the subscript p denotes the quantity values corresponding to the maximum crystallization rate. Assuming the above mentioned hypothesis $E_G / RT' >> 1$; the logarithmic form of equation (5.10) is written as

$$\ln\left(\frac{T_p^2}{\beta}\right) = \frac{E_G}{RT_p} - \ln\left(P^{1/n} K_{R0}\right) \tag{5.11}$$

which is the equation of a straight line, whose slope gives the activation energy, E_G. The intercept of this line gives the factor $p = P^{1/1n} K_{R0}$, which is related to probability of effective collisions for the formation of activated complex. On the other hand, the quoted assumption, $E_G / RT' >> 1$, together with equations (5.8) - (5.10) for $d^2x / dt^2 = 0$, allows us to express the maximum crystallization rate by the relationship

$$\frac{dx}{dt}\Big|_p = 0.37 \beta E_G n \left(RT_p^2\right)^{-1} \tag{5.12}$$

which makes it possible to obtain a value of kinetic exponent n for each heating rate. The corresponding mean value may be taken as the most probable value of the quoted exponent.

5.2.3 Single scan technique

It has been indicated in the literature [25, 34, 35], that a single temperature scan can be used to determine kinetic parameters, E and n of the glass crystal transformation. The Johnson-Mehl-Avrami (JMA) transformation rate equation

$$\frac{dx}{dt} = nK(1-x)[-\ln(1-x)]^{(n-1)/n} = nKf(x), \tag{5.13}$$

can be integrated obtaining an equation and can be expressed in logarithmic form as

$$\ln[-\ln(1-x)] - 2n\ln T = n\ln\frac{K_0 R}{\beta E} - \frac{nE}{RT} \tag{5.14}$$

Moreover, taking logarithm in equation (5.13), results in

$$\ln\left(\frac{dx}{dt}\right) = \ln(nK_0) + \ln|f(x)| - \frac{E}{RT} \tag{5.15}$$

In equation (5.14) and (5.15) over a temperature range of 100 K, the contribution of the term *2nln(T)*, can be ignored without causing a substantial error in the calculated slope. Regarding the second equation, the function $\ln|f(x)|$ may be considered constant, provided $0.25 < x < 0.75$. Bearing in mind these assumptions, the slopes of equations (5.14) and (5.15) allow us to obtain the product nE and E respectively.

5.2.4 Details of Non-isothermal Methods Used

Three different methods of analysis (as described below) have been used to study the crystallization kinetics of the above-mentioned glassy alloys under non-isothermal condition. Using DSC thermograms of these alloys, the values of activation energy of crystallization E_c have been determined.

5.2.4.1 Moynihan's relation

The heating rate dependence of the glass transition temperature in chalcogenide glasses is interpreted by Moynihan et. al. [36] in terms of thermal relaxation phenomenon. In this kinetic interpretation, the enthalpy at a particular temperature and time *H (T, t)* of the glassy system after an instantaneous isobaric change in temperature, relaxes isothermally towards a new equilibrium value $H_e(T)$. The relaxation equation can be written in the form [37]

$$(\delta H / \delta t)_T = -(H - H_g) / \tau \tag{5.16}$$

where τ is a temperature dependent structural relaxation time and is given by the relation

$$\tau = \tau_0 \exp(-E_\tau / RT) \exp[-C(H - H_c)] \tag{5.17}$$

where τ_0 and C are constants and E_τ is the activation energy of relaxation time. Using the above equations, it can be shown [36, 38] that:

$$d \ln \beta / d(1/T_g) = -E_\tau / R \tag{5.18}$$

Equation (5.18) states that $\ln \beta$ vs I / T_g plot should be straight line and the activation energy involved in the molecular motions and rearrangements around T_g can be calculated from the slope of this plot.

5.2.4.2 Johnson-Mehl-Avrami (JMA) Method

The crystallization kinetics of amorphous alloys has been intensively studied in the past using the classical Johnson-Mehl-Avrami (JMA) theoretical model in which the crystallization fraction can be described as a function of time *t* according to the formula

$$\alpha(t) = 1 - \exp[-(Kt)^n] \tag{5.19}$$

where *n* is the Avrami index and *K* is the rate constant given by

$$K = K_0 \exp(-E_c / RT) \tag{5.20}$$

Here, E_c is the activation energy of crystallization, R is the universal gas constant and K_o is also a constant. Based on JMA model, different authors have developed very diverse methods to study the amorphous to crystalline (a-c) transformation of glassy alloys. Given below are the details of three important and useful methods, which have been used in the present study.

5.2.4.3 Kissinger's relation

This method is most commonly used in analyzing crystallization data in DSC. During the isothermal transformation, the extent of crystallization (α) of a certain material is represented by the Avrami's equation (5.19).According to Kissinger, the Eq. (5.19) can be approximated as:

$$d\alpha / dt = nK^n t^{n-1}(1-\alpha) \tag{5.21}$$

Expressing t in terms of α from Eq. (5.21), the crystallization rate $d\alpha / dt$ becomes

$$(d\alpha/dt) = AnK(1-\alpha) \tag{5.22}$$

where $A = [-\ln(1-\alpha)]^{(n-1)/n}$

In non-isothermal crystallization, it is assumed that there is a constant heating rate in the experiment. The relation between the sample temperature T and the heating rate β can be written in the form:

$$T = T_i + \beta t \tag{5.23}$$

where T_i is the initial temperature.

The derivative of K with respect to time can be obtained from equations (5.20) and (5.23) as follows:

$$\frac{dK}{dt} = \left(\frac{dK}{dT}\right)\left(\frac{dT}{dt}\right) = \left(\frac{\beta E_c}{RT^2}\right)K \tag{5.24}$$

Using the equations (5.22) and (5.24), Kissinger showed that:

$$\ln\left(\beta / T_P^2\right) = const(t) - E_c / RT_c \tag{5.25}$$

where T_P is peak crystallization temperature. Although originally derived for the crystallization process, it is suggested that this relation is valid for glass transition process [31, 32] and hence the above equation takes the following form for its use in glass transition kinetics:

$$\ln\left(\beta / T_g^2\right) = -E_g / RT_g + cons\tan t \tag{5.26}$$

5.3 Experimental Details

Glasses of $Se_{85-x}Te_{15}Bi_x$, where x = 0, 1, 2, 3, 4, 5 were prepared by the melt quenching technique. Thermal behavior of the sample is recorded using Mettler Toledo Star^e DSC system. In each study approximately 10 mg bulk material is used. DSC runs are taken at four heating rates (5, 10, 15, 20 K min^{-1}) for each of the composition so as to get (T_g), (T_p) and (T_m) for the system. For $Ge_{20}Te_{80-x}Bi_x$ glassy alloys the thermal behaviour of samples is recorded using Shimadzu DTG-60. DTA has been performed for second series because it is more versatile than DSC at higher temperature.

5.4 Results and Discussion

5.4.1 Thermal properties of Se-Te-Bi glassy alloys

5.4.1.1 Thermal studies

Differential scanning calorimetric (DSC) thermograms were recorded for $Se_{85-x}Te_{15}Bi_x$ glassy alloys at different heating rates. Figure 5.4 shows the thermograms of the as prepared $Se_{85-x}Te_{15}Bi_x$ (typically for x = 5) glassy alloy at four heating rates (5, 10, 15 and 20 K min^{-1}). It has been observed from figure 5.4 that T_g and T_p shift towards higher temperature with increasing heating rate. Similar behaviour is also observed with other values of x. The value of T_p of each alloy is found to be much higher than room temperature which is an advantage of these glassy alloys and is essential to prevent self transition of recording materials between two phases; amorphous and crystalline phase at room temperature. Figure 5.5 shows the increase of T_g with increasing Bi concentration. This behaviour of T_g with Bi content can be explained on the basis of chemically ordered network model according to which heteropolar bonds are favoured over homo-polar bonds and bonds are formed in sequence of their decreasing bond energies. When Bi is added to the system it is expected to form bonds with Se rather than with Te. As the bond energy of Bi-Se bond (170.4 kJ/mol)) is higher than the bond energy of Bi-Te (125.6 kJ/mol), the average bond energy of the system and hence the T_g increases. The value of T_g for studied composition at heating rate of 10 K min^{-1} is given in table 5.2. The apparent activation energy for glass transition E_t is calculated by using the Kissinger formula [41]

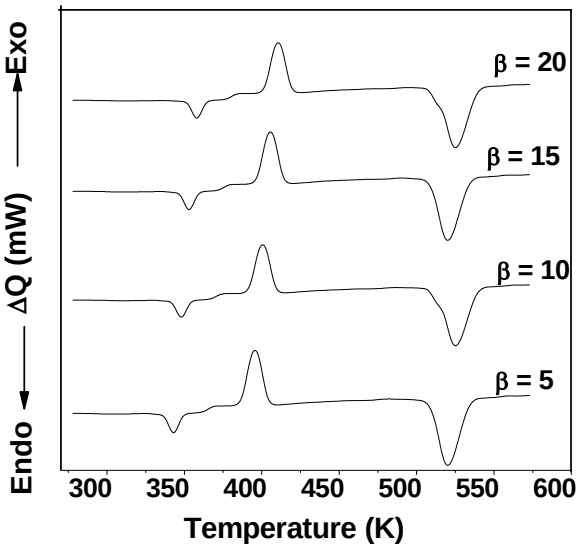

Figure 5.4 Plot of DSC thermograms for $Se_{85-x}Te_{15}Bi_x$ (x = 5) at different heating rates.

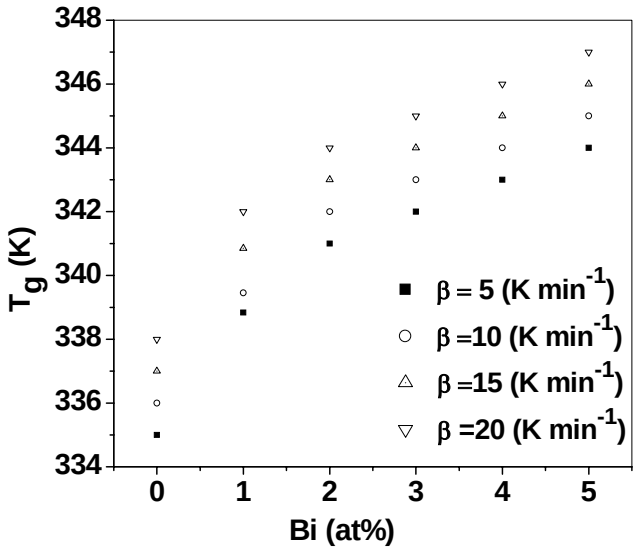

Figure 5.5 Plot of $\left(T_g\right)$ vs. Bi (at. %) for $Se_{85-x}Te_{15}Bi_x$ ($0 \leq x \leq 5$) alloy.

$$\ln\left[\frac{T_g^{\,2}}{\beta}\right] + const. = \frac{E_t}{RT_g} \tag{5.27}$$

where R is the gas constant and β is heating rate. Figure 5.6 shows the plot of $\ln\left(T_g^{\,2}/\beta\right)$ as a function of $1000/T_g$ and is found to be linear for all the samples. The slope of the plot gives the value of E_t and is reported in table 5.1. The glass activation energy is the amount of energy absorbed by a group of atoms in the glassy region so that a jump from one metastable state to another metastable state is possible. In other words the activation energy is involved in molecular motion and rearrangement of atoms around the glass transition temperature. In the present system under study, the activation energy for glass transition increases with Bi content. It implies that the probability of atoms to jump to the metastable state of lower internal energy decreases with increasing Bi concentration and hence the stability of system decreases with Bi content. Activation energy for crystallization E_c is calculated from modified Kissinger equation [42, 43]

$$\ln\left[\frac{T_p^{\,2}}{\beta}\right] + const. = \frac{E_c}{RT_g} \tag{5.28}$$

where E_c is determined from the slope of the plot of $\ln\left(T_p^{\,2}/\beta\right)$ vs. $1000/T_p$ as shown in figure 5.7. The calculated value of E_c for the studied composition using Kissinger formula is given in table 5.1. Now according to Matusita relation [44]

$$\ln[-\ln(1-V_F)] = -n\ln(\beta) - 1.052\frac{fE_c}{RT} + const \tag{5.29}$$

where V_F the volume fraction of crystals precipitated in the glass is heated at uniform rate

Table 5.1

Parameters determined from heating rate dependence of $Se_{85-x}Te_{15}Bi_x$ glassy system

x	A	B	$E_t(kJ/mol)$	$E_c(kJ/mol)$ (Kissinger)	n	f	$E_c(kJ/mol)$ (Matusita)
0	331	2.10	111.00	63.96	2.68	1.68	56.97
1	338	2.11	114.32	72.07	2.56	1.56	61.28
2	340	2.12	115.19	71.42	2.68	1.68	60.00
3	341	2.13	116.36	70.62	2.67	1.67	59.08
4	342	2.14	117.48	69.58	2.64	1.64	58.27
5	343	2.15	118.26	68.76	2.60	1.60	57.06

.

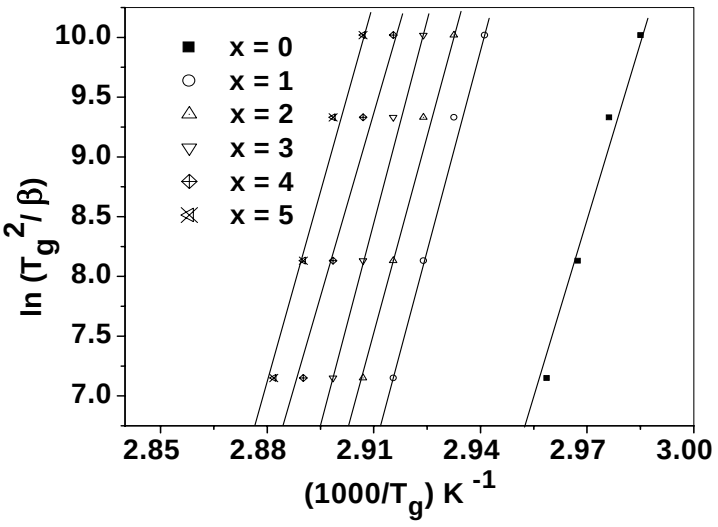

Figure 5.6 Plot of $\ln\left(T_g^{\,2}/\beta\right)$ vs. $1000/T_g$ for $Se_{85-x}Te_{15}Bi_x$ ($0 \le x \le 5$) alloy

.

Table 5.2

Values of $\left(T_P - T_g\right), \left(T_m - T_p\right), K_{gl}$ and T_{rg} calculated from DSC thermograms at 10 K/min heating rate for the system.

X	$T_g(K)$	$T_p(K)$	$T_m(K)$	$\left(T_P - T_g\right)$	$\left(T_m - T_p\right)$	K_{gl}	T_{rg}
0	335	376	519	41	143	0.29	0.645
1	339	399	526	60	127	0.47	0.645
2	341	398	527	57	129	0.44	0.647
3	343	397	528	54	131	0.41	0.649
4	344	396	529	52	133	0.39	0.65
5	345	395	530	50	135	0.37	0.651

and is calculated by the relation $V_F = S_T / S$ [45]. In this relation S is the total area of exothermal peak and S_T is the area between starting point of exotherm and peak crystallization temperature. *f* and *n* are constants depending upon the morphology of growth [46]. For the present system the value of kinetic exponent *n* is determined from the slope of $\ln[-\ln(1-V_F)]$ vs. $\ln(\beta)$ as shown in figure 5.8 (b). Mean value of *n* as obtained for the studied composition is 2.60 $\approx$ 3. From the mean value of *n* it is possible to postulate a crystallization mechanism. It has been shown that *n* may be 4, 3, 2 or 1 [47], depending upon the type of nucleation and growth of the system. Since quenched samples were used in the present study, the value of *f* is one less than *n*, i.e.; 2 indicating that bulk nucleation with two dimensional growth occurs in the system. The activation energy for crystallization is determined from the slope of $\ln[-\ln(1-V_F)]$ vs. $1000/T$ (see figure 5.8 (a)), and is stated in table 1. The behaviour of E_c is found to be similar from both the approaches. The difference between T_p and T_g which is an indication of the thermal stability of glasses against crystallization is maximum at Bi = 1 at. % and further it decreases with increases in Bi content. The glass forming ability K_{gl} is calculated from Hurby's parameter [48]

$$K_{gl} = \frac{T_P - T_g}{T_m - T_P} \tag{5.30}$$

The ease in glass formation is determined by calculating the reduced glass transition temperature, $T_{rg} = T_g / T_m$ [49]. The value obtained obeys the two third rule which states

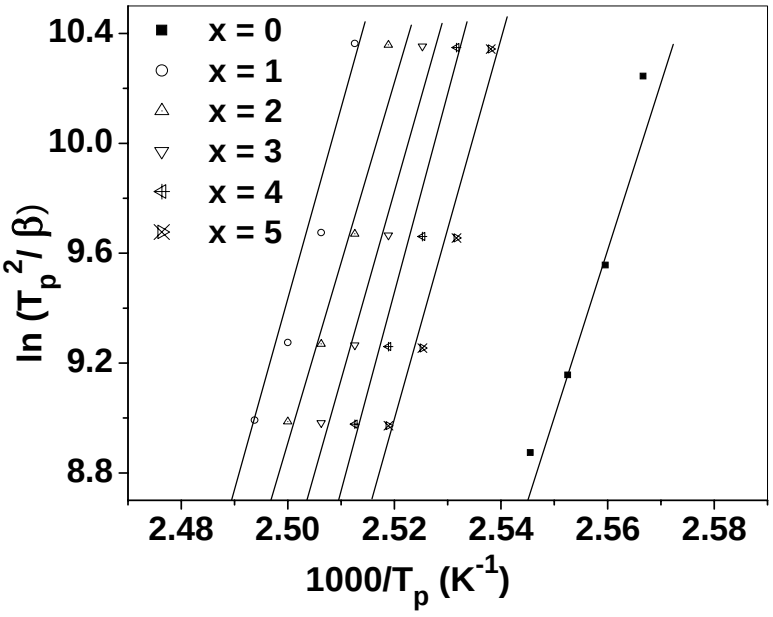

Figure 5.7 Plot of $\ln\left(T_p^{\,2}/\beta\right)$ vs. $1000/T_p$ for $Se_{85-x}Te_{15}Bi_x$ ($0 \leq x \leq 5$) alloy.

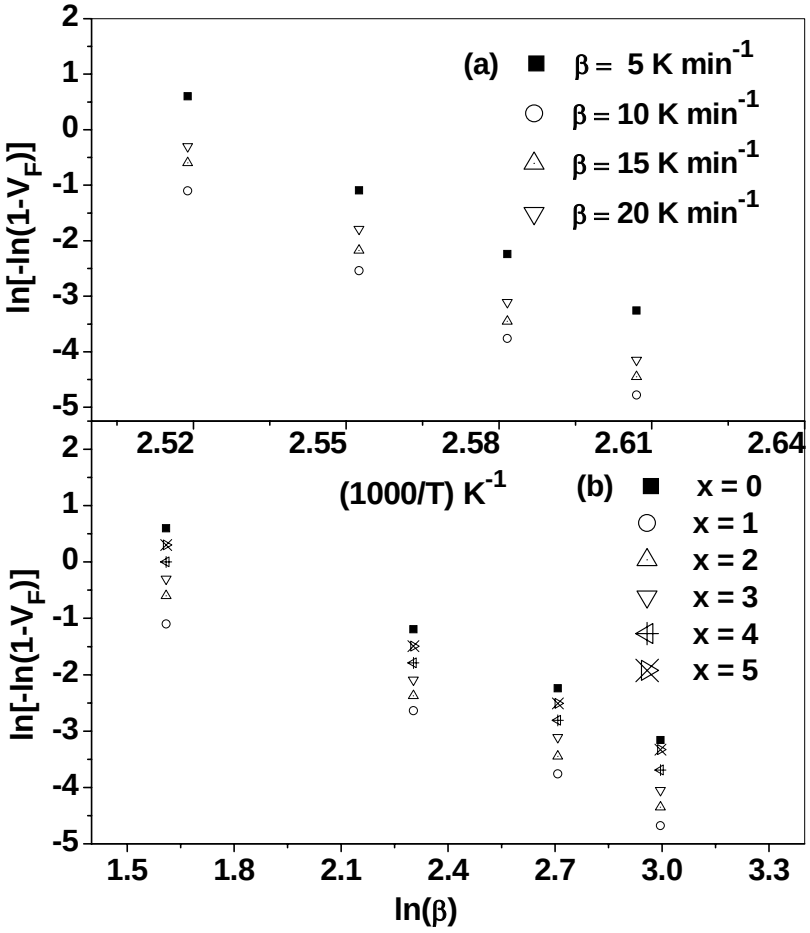

Figure 5.8 Plots of (a) $\ln[-\ln(1-V_F)]$ vs. ln (β) and (b) $\ln[-\ln(1-V_F)]$ vs. 1000/T for a $Se_{85-x}Te_{15}Bi_x$ ($0 \leq x \leq 5$) alloy at four heating rates, β

that $\frac{T_g}{T_m} = \frac{2}{3}$ and holds well for the studied composition. The value of K_{gl} and T_{rg} for the studied composition is reported in table 5.2.

5.4.1.2 Evaluation of specific heat

Specific heat is very sensitive to the way in which atoms or molecules are dynamically bound in a solid [50]. An abrupt change in specific heat at glass transition temperature is the characteristic of all chalcogenide glasses. The parameter detects sensitively the change in microstructure of glass which can be seen by the jump of specific heat close to Dulong and Petit value of $C_p = 3R$. Figure 5.9 shows typical C_p *vs.* T plot obtained for $Se_{83}Te_{15}Bi_{2.0}$ glass at 10 $Kmin^{-1}$ heating rate. It has been observed that below T_g, the C_p values agrees with the classical limit of Dulong and Petit for the vibrational heat capacity of solids. The observed increase in C_p at glass transition temperature is due to the addition of translational and/or rotational modes made available by the breakage of bonds forming the glass network [51, 52]. The value of C_p is found to decrease with increasing Bi content (table 5.3). This behaviour is may be due to the non availability of the larger number of degrees of freedom in the alloy which could absorb heat energy. The heat capacity jump (excess heat capacity at T_g) is expressed as

$$\Delta C_p = (C_{pl} - C_{pg})_{T=Tg} \qquad (5.31)$$

where C_{pl} and C_{pg} are the heat capacity of liquid and glassy states across the glass transition. ΔC_p reflects the amount of configurational change occurring in the network

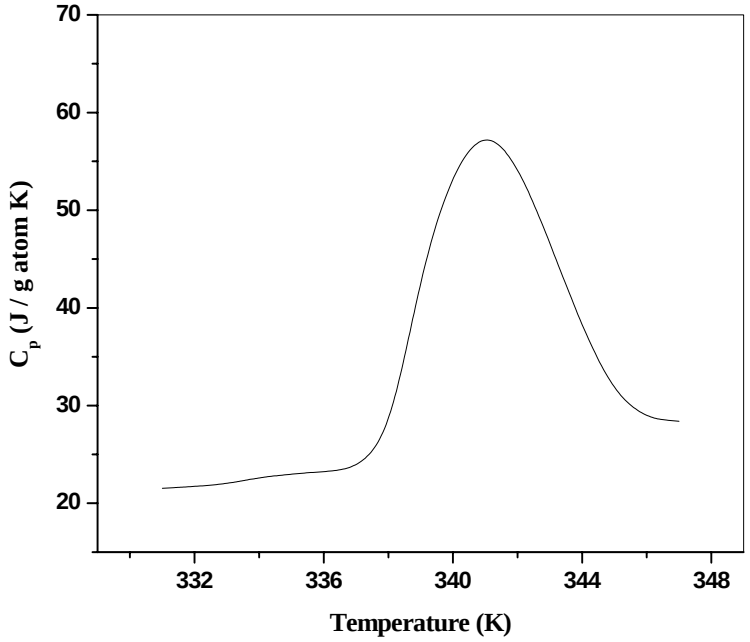

Figure 5.9 Plot of C_p *vs*. temperature (T) for $Se_{85-x}Te_{15}Bi_x$ (x=2) alloy.

Table 5.3.

Value of m, C_p and ΔC_p for $Se_{85-x}Te_{15}Bi_x$ glassy system.

Bi (at.%)	m	C_p (J/gatomK)	ΔC_p (J/gatomK)
0	2.00	74.60	0.270
1	2.01	68.27	0.261
2	2.02	62.73	0.248
3	2.03	54.93	0.239
4	2.04	49.20	0.223
5	2.05	42.81	0.131

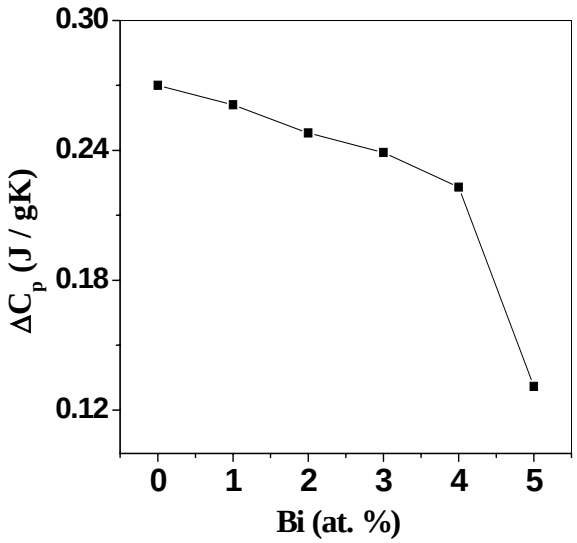

Figure 5.10 Plot of ΔC_p vs. Bi (at. %) for $Se_{85-x}Te_{15}Bi_x$ alloy.

Table 5.4

Value of ρ, ρ_{exp}, V_m, n_b and L for the system

Bi (at.%)	ρ (g/cm^3)	ρ_{exp} (g/cm^3)	V_m (cm^3)	n_b	L
0	5.07	5.57	17.01	$0.7790*10^{23}$	4.00
1	5.13	5.68	17.06	$0.7803*10^{23}$	3.99
2	5.20	5.70	17.09	$0.7828*10^{23}$	3.98
3	5.25	5.81	17.17	$0.7830*10^{23}$	3.97
4	5.31	5.96	17.21	$0.7851*10^{23}$	3.96
5	5.37	6.04	17.26	$0.7866*10^{23}$	3.95

during glass to liquid transition. The excess heat capacity ΔC_p, during glass transition is evaluated using the relation [53]

$$\Delta C_p = \frac{\Delta H}{\beta m} \tag{5.32}$$

where ΔH the change of heat flow through the investigated sample with mass m at glass transition and β is the heating rate. It has been observed that ΔC_p decrease with increasing Bi content as shown in figure 5.10 (and table 5.3). The observed decrease in ΔC_p may be due to the fact that with increasing Bi content the concentration of defect states increases. It leads to a decrease in structural relaxation time and hence further responsible for the fall in $\Delta C_{p.}$

5.4.1.3 Theoretical parameters

The rise in T_g with Bi and microscopic changes taking place in the system can be understood in the light of various physical parameters of the system. T_g can be related to

i) Density of the system which increases monotonically with Bi.

ii) Average number of bonds per unit volume and number of lone pair electrons.

iii) Average bond strength of the system.

Density is an important physical parameter and is a measure of rigidity of the system. It can be deduced by using formula [54]

$$\rho = \left(\sum m_i / d_i\right)^{-1} \tag{5.33}$$

where m_i is the fraction of weight and d_i is the density of i^{th} structural unit density. The density of above glassy system is also determined experimentally by Archimedes method and is tabulated in table 5.4. Using the value of density obtained from equation 5.33, the molar volume of the system is calculated by using the formula

$$V_m = \frac{1}{\rho}\left(\sum x_i M_i\right) \tag{5.34}$$

where x_i represents the atomic fraction of component i and M_i is its atomic mass. The molar volume is also found to increase with Bi content, which is a result of substituting Se atoms with the heavier and larger Bi atoms in the glass network. The theoretical density and molar volume calculated using above two relations is presented in table 5.4 for the mentioned glassy system.

In chalcogenide glasses the valence band originates from lone pair electron states whereas the conduction band arises from antibonding states. The energy of the conduction band edge is decided by the number of atoms per unit volume n_b and is determined by using the formula [54]

$$n_b = m\left(\frac{N_A}{V_m}\right) \tag{5.35}$$

where N_A is the Avogadro number and m is the coordination number. n_b is found to increase with Bi content (see table 5.4). In terms of Pauling view point [55], the chemical bonds with lone pair electrons decreases the strain energy in the system and structures with large number of lone pair electrons favor glass formation. The number of lone pair electrons is calculated by using following relation

$$L = V - m \tag{5.36}$$

where L is the number of lone pair electrons and V is the number of valence electrons. The results are also listed in table 5.4. It has been found that the number of lone pair electrons decrease with increasing Bi content. This behavior is caused by the interaction between the Bi ion and lone pair electrons of bridging Se atom. The interaction decreases the role of lone pair electrons in the glass formation. According to a simple criterion proposed by Zhenhua [56] for a binary system, the number of lone pair electrons must be larger than 2.6 and for a ternary system it must be larger than 1.

5.4.2 Thermal properties of Ge-Te-Bi glassy alloys

5.4.2.1 *Thermal studies*

DTA curves of $Ge_{20}Te_{80-X}Bi_x$ (x = 0, 1.5, 2.5, 5.0) glassy alloy are shown in figure 5.11 It is clear that the value of glass transition temperature (T_g) as well as peak crystallization temperature (T_p) increases with increase in Bi content (table 5.5). The effective increase in (T_g) is explained on the basis of coordination number of the system which increases with the increase in Bi content. Coordination number in $Ge_{20}Te_{80-x}Bi_x$ system has been calculated using the relation

$$m = \frac{\alpha N_{Ge} + \beta N_{Te} + \gamma N_{Bi}}{\alpha + \beta + \gamma} \tag{5.37}$$

where α, β and γ are the at. % of Ge, Te and Bi, respectively, and N_{Ge}= 4, N_{Te}= 2 and N_{Bi} = 3 are their respective coordination numbers. The value of coordination number (m) values lie in range 2 to 2.5. The calculated values of m (listed in table 5.5) indicate that it increases with increase of Bi content. In chalcogenide based glasses T_g represents the temperature above which an amorphous matrix can attain various structural configurations and below which the matrix is frozen into a structure which cannot easily change to another structure. Therefore, it is reasonable to assume that T_g must be related to the structural changes and hence coordination number of the network. The glass transition temperature T_g of chalcogenide glasses shows coordination number dependence. It increases linearly with increase in coordination number and follows the relation [57]

$$\ln(T_g^{th}) = 1.6m + C \tag{5.38}$$

where C = 2.3. The theoretically calculated values of T_g^{th} are tabulated in table 5.5. The dependence of T_g and T_P on composition for the present glassy system is also explained on the basis of deviation of stoichiometry, R of the system. It is expressed by the ratio of covalent bonding possibilities of chalcogen atom to that of non chalcogen atom. Values of R were found to be larger than unity for such glasses, which indicate chalcogen-rich materials and less than unity for the glasses which shows chalcogen poor material. For $Ge_xTe_yBi_z$ system, the quantity R is defined by [58, 59]

$$R = \frac{yCN(Te)}{xCN(Ge) + zCN(Bi)} \tag{5.39}$$

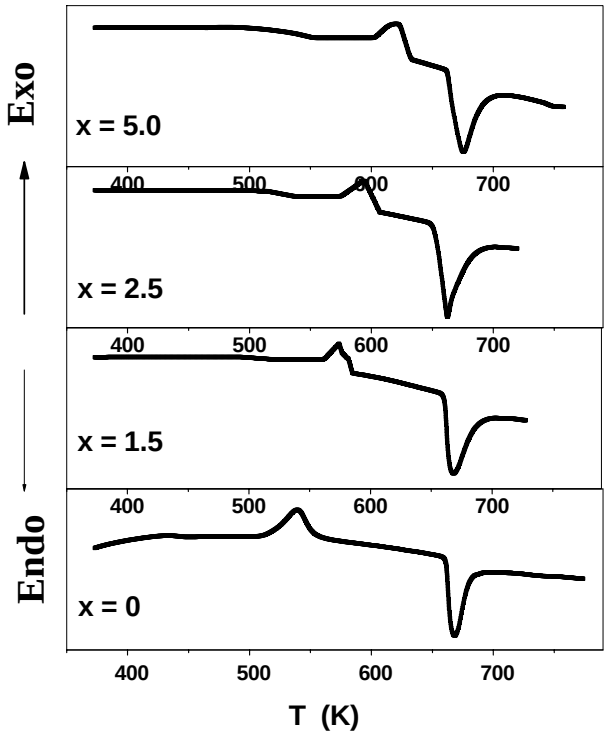

Figure 5.11 Plot of DTA thermograms for $Ge_{20}Te_{80-X}Bi_x$ glassy alloy at 20 ˚C/min heating rate.

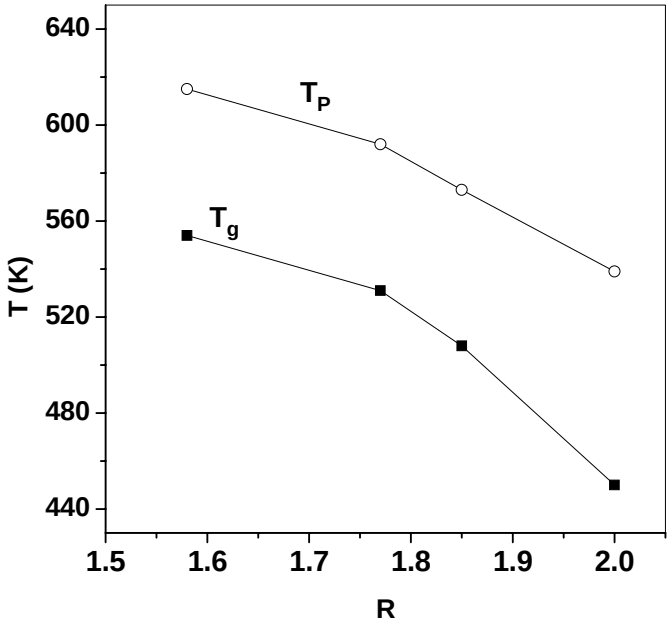

Figure 5.12 Plot of (T_g) and *(T_P)* vs *R* for $Ge_{20}Te_{80-X}Bi_x$ glassy alloy

Table 5.5

Values of T_g , T_c, T_m, ΔT, T_{rg} , *m, R* and T_g^{th} calculated from DTA thermograms at 10 K/min heating rate, for $Ge_{20}Te_{80-X}Bi_x$ system.

x	$T_g(K)$	$T_P(K)$	$T_m(K)$	ΔT *(K)*	T_{rg}	*M*	*R*	$T_g^{th}(K)$
0	450	539	667	89	0.45	2.40	2.00	267
1.5	508	573	669	65	0.59	2.42	1.85	270
2.5	531	592	665	61	0.66	2.43	1.77	273
5.0	554	615	674	61	0.70	2.45	1.58	279

where *x, y* and *z* are respectively, the atomic fractions of Ge, Te and Bi. The threshold occurs at $R = 1$ (the point of existence of only heteropolar bonds). For the present investigating system the values of *R* are greater than 1 (table 5.5).

leading the system to be chalcogen-rich region. Figure 5.12 shows the variation of T_g and T_P with *R*-value. Consequently the increase in T_g and T_P with decrease in *R*- value can be interpreted as approaching to chemical threshold [60]. The thermal stability of the glass is generally measured by the difference $\Delta T = T_P - T_g$. For the present system the value of ΔT is maximum for x = 0 (table 5.5), indicating the maximum thermal stability at chemical threshold. The reduced glass transition temperature is calculated as $T_{rg} = T_g / T_m$ and its value is nearly equal to 2/3 for all the samples (table 5.5).

5.4.2.2 Density (ρ) and molar volume (V_m)

Density (ρ) of the system is a measure of rigidity of the system and is deduced by using equation (5.33) [54]. The density of above glassy system is also determined experimentally by Archimedes method and the values are tabulated in table 5.6. It has been observed that both the experimental and theoretically calculated values of density increases with increase in Bi content. This may be due to the replacement of less denser Te (6.24 g/cm^3) by denser Bi (9.8 g/cm^3). Using the value of density obtained from equation (5.33), the molar volume (V_m) of the system is calculated by using the equation (5.34). The molar volume is also found to increase with Bi content (table 5.6), which is a result of substituting Te atoms with the heavier and larger Bi atoms in the glass network. In chalcogenide glasses the energy of the conduction band edge is decided by the number of atoms per unit volume (n_b) and is determined by using equation (5.35). The number of

lone pair electrons L is calculated by using following relation (5.36). The results are listed in table 5.6. It has been found that the number of lone pair electrons decrease with increasing Bi content. This behavior is caused by the interaction between the Bi ion and lone pair electrons of bridging Te atom. The interaction decreases the role of lone pair electrons in the glass formation. In chalcogenide glasses, chemically ordered networks are expected where the number of heteropolar bonds is maximized *i.e.* they are more favourably formed than homopolar bonds. Since bulk glasses are considered, a chemical bond ordering model is assumed. Based on this assumption mean bond energy is given by

$$<E> = E_S + E_{rm} \qquad (5.40)$$

where E_S is the overall contribution towards bond energy arising from strong heteropolar bonds and E_{rm} is the contribution arising from weaker bonds that remain after the strong bonds have been maximized *i.e.* the average bond energy per atom of the remaining

Table 5.6

Value of ρ, V_m, n_b, L and <E> for $Ge_{20}Te_{80-x}Bi_x$ glassy alloys.

x	ρ (g / cm^3)	V_m (cm^3)	n_b	L	<E> (eV/atom)
0	6.11	19.09	0.756×10^{23}	3.200	1.76
1.5	6.17	19.10	0.763×10^{23}	3.165	1.77
2.5	6.21	19.11	0.766×10^{23}	3.145	1.78
5.0	6.31	19.13	0.771×10^{23}	3,100	1.80

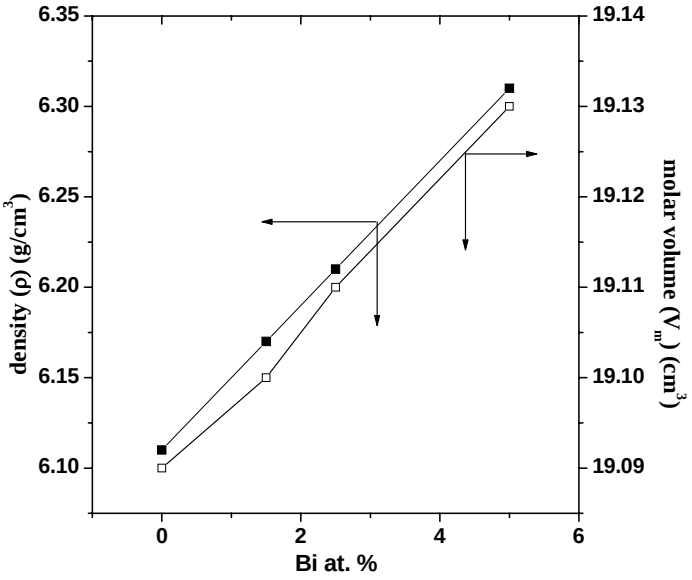

Figure 5.13 Density and molar volume versus Bi content (at. %) for $Ge_{20}Te_{80-x}Bi_x$ glassy alloys.

matrix. The values of mean bond energies for the compositions under investigation are stated in table 5.6.

4. Conclusion

DSC studies have been performed on the melt quenched $Se_{85-x}Te_{15}Bi_x$ chalcogenide glasses. The glass transition temperature has been found to increase from 335 to 345 K due to Bi addition. The stability is maximum for x = 1 and it decreases with Bi addition. It further leads to the conclusion that stable glasses are formed only with lower Bi concentration. DSC analysis also shows that bulk nucleation with two dimensional growth occurs in the system. It has been observed that Bi atom leads to the cross linking

of chains and increases the coordination number of the system. The specific heat capacity and change in heat capacity at glass transition is also evaluated and has been found that both the parameters decrease with increasing Bi concentration. This decrease is attributed to non availability of the larger number of degrees of freedom in the alloy which could absorb the heat energy. Various physical parameters are also calculated theoretically and were found that density, molar volume and number of atoms per unit volume increases, whereas the lone pair electrons decrease with Bi concentration.

DTA curves of $Ge_{20}Te_{80-X}Bi_x$ (x = 0, 1.5, 2.5, 5.0) glassy alloy are analyzed for T_g, T_c and T_m . T_g as well as T_c are found to increase with increasing Bi content. The results are explained on the basis of coordination number and stiochiometry of the system. T_g is also calculated theoretically and it is found to follow the similar trend as that of experimental values.

References

1. Mott N F and Davis E 1979 Electronic Processes in Non-Crystalline Materials (Oxford: Clarendon Press).

2. Hodge I M., Berens A J 1982 Macromolecules 15 762.

3. Gomez Ribelles J L, Monleon Pradas M, Vidaurre Garayo A, Romero Colomer F, Mas Estelles J and Meseguer Duenas J M 1995 Macromolecules 28 5878.

4. Kovacs A J, Aklonis J J, Hutchinson J M., Ramos A R 1979 J. Polym. Sci. B, Polym. Phys. Ed.17 1097.

5. Grenet J, Larmagnac J P, Michon P and Vautier C 1981 Thin Solid Films 76 53.

6. Dimarzio E A and Gibbs J H 1959 J. Polym. Sci. 60 121.

7. Gibbs J H and Dimarzio E A 1958 J. Chem. Phys. 28 373.

8. Saiter A, Hess M and Saiter J M 2001 Europeen Polym. J. in press.

9. Angell C A, 1984 'Relaxation in complex systems', Ed. Ngai K. L. and Wright G. B. (Washington D C: Naval Research Laboratory), p.3.

10. Saiter J M, Langevin D, Lebaudy P and Grenet J 1994 J. Non-Cryst. Solids 172/174 640.

11. Grenet J, Larmagnac J P and Michon P 1982 J. Therm. Anal. 25 539.

12. Grenet J, Saiter J M, Bayard J, Vautier C 1992 J. Thermal Anal. 38 557.

13. Saiter J M, Assou A, Grenet J and Vautier C 1991 Phil. Mag. B 64 33.

14. Hamou A, Saiter J M, Bayard J, Grenet J, Vautier C 1992 Mat. Letters 12 442.

15. Mehta N, Agrahari S K, Kumar A 2006 Phys. Scr. 74 579-583.

16. Saxena M and Bhatnagar P K 2003 Bull. Mater. Sci. 26 547-552.

17. Suri N, Bindra K S, Thangaraj R 2007 J. Non-Cryst. Solids 353 2079–2083.

18. Fukui K 1992 J. Phys. Soc. Jpn. 61 1084.

19. Kaban I., Halm Th, Hoyer W, Jovari P, Neuefeind J, 2003 Journal of Non-Crystalline Solids, 326-327 120.

20. Varshneya A K, Mauro D J 2007 J. Non-Cryst. Solids 353 1291.

21. Micoulaut M, Phillips J C 2003 Phys. Rev. B 67 104204.

22. Boolchand P, Feng X, Bresser W.J 2001 J. Non-Cryst. Solids 293–295 348.

23. Frade J R 1998 J. Am. Ceram. Soc. 81 2654.

24. Avrami M 1941 J. Chem. Phys. 9 177.

25. Kasap S O and Juhasz C 1995 J. Chem. Soc., Faraday Trans. 2 (81) 811.

26. Weinberg M C and Kapral R 1989 J. Chem Physics, 91 7146.

27. Cahn J W 1996 Acta Metall, 4 572.

28. Christian J W 1975 The theory of Transformation in Metals and Alloys (Pergamon: Oxford).

29. Kolomogoroff A N 1937 Izvestiya Akad, Nauk USSR, Ser. Math.1 355.

30. Kissinger H E 1957 Anal Chem 29 1702.

31. Vazquez J, Wagner C, Villares P, Jimenez-Garary R 1996 Acta Mater. 44 4807.

32. Yinnon H and Uhlmann D R, 1983 J. Non-Cryst. Solids 54 253 .

33. Starink M J, Zahra A M 1997 Thermochim Acta 292 159.

34. Handerson D W 1979 J. Non-Cryst. Solids 30 301.

35. Yannacopoulos S, Kasap S O, Hedayat A, Verma A 1994 Can. Metall. Q. 33 51.

36. Moynihan C T, Easteal A J, Wilder J and Tucker J 1974 J. Phys. Chem. 78 267.

37. Kasap S O, Juhaz C 1986 J. Mater. Sci. 24 1329.

38. Larmagnac J P, Grenet J and Michon P 1981 J. Non-Cryst. Solids 45 157.

39.Colemenero J, Barandiaran J M, 1978 J. Non-Cryst. Solids 30 263.

40. Kasap S O and Yannacopoulos S 1990 Phys. Chem. Glasses 31 71.

41. Kissinger H E 1956 J. Res. Nat. Bur. Stand. 57 217.

42. Matusita K, Saka S 1979 Phys. Chem. Glasses 20 217.

43. Macfarane D R, Maecki M and Paulain M 1984 J. Non-Cryst. Solids 64 351.

44. Matusita K, Komatsu T and Yokata R 1984 J. Mater. Sci. 19 291.

45. Shiryaev V S, Adam J L and Zhang X H 2004 J. Phys. Chem. Solids 65 1737.

46. Suri N, Bindra K S and Thangaraj R 2007 J. Non-Cryst. Solids 353 2079.

47. Mahadevan S, Giridhar A and Singh A K 1986 J. Non-Cryst. Solids 88 11.

48. Hurby A, Czech 1972 J. Phys B 22 1187.

49. Kauzmann W 1948 Chem. Rev. 43 219.

50. Ma H L, Zhang X H, Lucas J, Moynihan C T 1992 J. Non Cryst. Solids 140 209.

51. Thornburg D D, Johnson R J 1975 J. Non Cryst. Solids 17 2.

52. G.O. Jones, Glass, Chapman and Hall, London, 1971.

53. Narasimham P S L, Giridhar A, Mahadevan S 1981 J. Non Cryst. Solids 43 301.

54. Fayek S A, Balboul M R and Marzouk K H 2007 Thin Solid Films 515 7281- 7285.

55. Pauling L 1960 The Nature of the Chemical Bond. 3rd Ed. (Cornell University Press, Ihica NY).

56. Zhenhua L 1981 J. Non Cryst. Solids 127 298.

57. Kasap S O and Yannacopoulos S 1989 J. Mater Res. 4 893.

58. Tichy L and Ticha H 1994 Mater. Lett. 21 313.

59. Tichy L and Ticha H 1995 J. Non-Cryst. Solids 189 141.

60. Saffarini G 2002 App Phys A 74 283-5.

CHAPTER 6

Summary

Chalcogenide glasses form an important class of materials which are used in various infrared optics and technological applications. Here we have studied two chalcogenide glassy systems *viz*. $Se_{85-x}Te_{15}Bi_x$ (x = 0, 1, 2, 3, 4, 5) and $Ge_{20}Te_{80-X}Bi_x$ (x = 0, 1.5, 2.5, 5.0). These two glassy systems were studied for their optical, electrical and thermal properties

Thin films of $Se_{85-x}Te_{15}Bi_x$ glassy alloys have been analyzed by using the transmission spectra taken at normal incidence in the spectral range 400-1500 nm and the various optical parameters are calculated. The refractive index and film thickness are calculated by using envelope method proposed by Swanepoel. The results indicate that n increases with the increasing Bi content which is related to the increased polarizability of the larger Bi atomic radius 1.46 Å compared with the Se atomic radius 1.16 Å. The dispersion parameters E_d, E_0 and n_0 are discussed in terms of WDD model. It has been observed that E_d and n_0 increases while E_0 decreases with increase in Bi content. The optical absorption in the given system seems to be of non direct type and the optical band gap determined in the strong absorption region by Tauc's extrapolation is found to decrease from 1.46 to 1.24 eV by the addition of Bi content. The decrease in average bond energy and hence optical band gap is interpreted in terms of cohesive energy and electronegativity difference of the atoms involved. The dielectric constants and optical conductivity are determined for the system and they are found to follow the similar trend as that of refractive index.

In the electrical study of $Se_{85-x}Te_{15}Bi_x$ (where x = 0, 1, 2, 3, 4, 5) thin films the *I-V* characteristics have been discussed and the conduction is explained qualitatively in terms of Poole Frenkel conduction mechanism for higher voltage range. The mechanism is

further confirmed by the dependence of *I* on square root of *V*. The study of dark and photoconductivity of $Se_{85-x}Te_{15}Bi_x$ thin films as a function of temperature (303-333 K) reveals that the conduction is through an activated process with single activation energy. Activation energy for photoconduction is found to be much smaller than its value for dark conduction. Dark as well as photo conductivity (at 1085 lux) is found to decrease as Bi is introduced to the host $Se_{85}Te_{15}$ glassy alloy whereas its further addition (> 1 Bi at. %) causes the conductivity to increase. Intensity dependent photoconductivity has also been studied and it shows the existence of bimolecular recombination in the thin films. The values of σ_{Ph}/σ_d and n_σ are calculated for $Se_{85-x}Te_{15}Bi_x$ thin films at absolute temperature (303 K) within the intensity range 20-1085 lux. It is observed that at a particular intensity, photosensitivity increases as Bi is introduced to host $Se_{85}Te_{15}$ glassy alloy and then decreases with the further addition of Bi (≥ 2 at. %) however, exactly opposite trend has been observed in case of n_σ. The results were successfully explained on the basis of density of defect states. The transient photoconductivity measurements for investigating thin films at room temperature and 1035 lx intensity shows that the photocurrent rises in a monotonic manner up to a steady state value, and after cessation of illumination, it follows a non-exponential decay. An increase in the differential lifetime is also observed with time (for all compositions) as well as with the increase in the Bi concentration.

Differential scanning calorimetric technique (DSC) has been employed for thermal studies of $Se_{85-x}Te_{15}Bi_x$ chalcogenide glasses. The glass transition temperature has been found to increase from 335 to 345 K due to Bi addition. The stability is maximum for x = 1 and it decreases with Bi addition. It further leads to the conclusion that stable glasses

are formed only with lower Bi concentration. DSC analysis also shows that bulk nucleation with two dimensional growth occurs in the system. It has been observed that Bi atom leads to the cross linking of chains and increases the coordination number of the system. The specific heat capacity and change in heat capacity at glass transition is also evaluated and has been found that both the parameters decrease with increasing Bi concentration. This decrease is attributed to non availability of the larger number of degrees of freedom in the alloy which could absorb the heat energy. Various physical parameters are also calculated theoretically and were found that density, molar volume and number of atoms per unit volume increases, whereas the lone pair electrons decrease with Bi concentration.

The transmission and reflection spectra of vacuum evaporated $Ge_{20}Te_{80-x}Bi_x$ thin films taken at normal incidence have been analyzed in the spectral range 900-2400 nm and the various optical parameters are calculated. The results indicate that n increases with the increasing Bi content which is related to the increased polarizability of the larger Bi atom compared to Te. The dispersion parameters E_d, E_0 and n_0 are discussed in terms of WDD model. It has been observed that E_d and n_0 increases while E_0 decreases with increase in Bi content. The optical absorption in the given system seems to be of non direct type and the optical band gap determined in the strong absorption region by Tauc's extrapolation is found to decrease from 0.86 to 0.74 eV with the addition of Bi content. The decrease in average bond energy and hence optical band gap is interpreted in terms of cohesive energy and electronegativity difference of the atoms involved.

The *I-V* characteristics of $Ge_{20}Te_{80-X}Bi_x$ thin films have been discussed and the conduction is explained qualitatively in terms of Poole Frenkel conduction mechanism

for x = 2.5 and 5.0. The mechanism is further confirmed by the dependence of *I* on square root of *V* for these samples. The study of dark and photoconductivity of $Se_{85-x}Te_{15}Bi_x$ thin films as a function of temperature (303-333 K) reveals that the conduction is through an activated process with single activation energy. Activation energy for photoconduction is found to be much smaller than its value for dark conduction. Dark as well as photoconductivity (at 1085 lux) is found to increase as Bi is introduced to the host $Ge_{20}Te_{80}$ glassy alloy. Intensity dependent photoconductivity has also been studied and it shows the existence of bimolecular recombination in the thin films. The values of σ_{Ph}/σ_d and n_σ are calculated for $Se_{85-x}Te_{15}Bi_x$ thin films at absolute temperature (303 K) within the intensity range 20-1085 lux. It is observed that at a particular intensity photosensitivity decreases with the addition of Bi but exactly opposite trend has been observed in case of n_σ. The results were successfully explained on the basis of density of defect states. The transient photoconductivity measurements for investigating thin films at room temperature and 1035 lx intensity shows that the photocurrent rises in a monotonic manner up to a steady state value, and after cessation of illumination it follows a non-exponential decay. An increase in the differential lifetime is also observed with time (for all compositions) as well as with increase in Bi concentration.

Differential thermal analysis (DTA) curves of $Ge_{20}Te_{80-X}Bi_x$ (x = 0, 1.5, 2.5, 5.0) glassy alloy are analyzed for T_g, T_c and T_m . T_g as well as T_c are found to increase with increasing Bi content. The results are explained on the basis of coordination number and stiochiometry of the system. T_g is also calculated theoretically and it is found to follow the similar trend as that of experimental values. Density and molar volume both are fond to increase with increase in Bi. Number of lone pair electrons is calculated for the system

and are found to decrease with Bi at. %. Using the data for coordination number the glass transition has been calculated and is found to follow the same trend as that of density and molar volume. Mean bond energy is calculated using chemically ordered network model and is found to increase with increasing Bi content.